Integrated tilt and active lateral secondary suspension control in high speed railway vehicles

Ronghui Zhou

A Doctoral Thesis submitted in partial fulfilment of
the requirements for the award of

Doctor of Philosophy

Loughborough University

September 2010

Abstract

The use of tilting bodies on railway vehicles is increasingly widespread with a number of well-established services using tilt technology already existing around the world. The motivation for tilting railway vehicles is that they give a cost-effective means of achieving a substantial reduction in journey time by increasing the vehicle speed during curves, without the need of building new high speed railtrack infrastructure.

A tilting railway vehicle is a dynamically complex structure. Many of the dynamic modes of the system are coupled and the coupling in certain situations, i.e. coupling between the vehicle lateral and roll modes, is very significant which unavoidably causes difficulties in control system design, especially for the local vehicle control strategies. Meanwhile, the high speed results in the worse ride quality on straight track, and an effective solution is to use the active secondary suspension. This research investigated control strategies for the integration of tilt and active lateral secondary suspension. The simulation results showed the efficiency of this research on enhancing local tilting control performance both on straight and curved track.

Furthermore, Multi-input and Multi-output system configuration, control and optimization, as well as model-based estimation are also investigated for this tilt and lateral actuators control system aiming to further improve the control system robustness and performance. Finally, a FPGA-based Hardware-In-the-Loop simulation system is set up with the considersion of the controller practical implementation.

Acknowledgments

I would like to express the profound gratitude to my supervisors, Prof. Roger Goodall and Dr. Argyrios Zolotas, for their invaluable support, encouragement, supervision and useful suggestions throughout this research work. One simply could not wish for better or friendlier supervisors. The Department of Electronic and Electrical Engineering in Loughborough University must be greatly acknowledged for the award of my scholarship.

I also had the pleasure of working with my good friends in Control Systems Group of Loughborough University: Dr Roger Dixon, Dr Christopher Ward, Dr Yimin Zhou, Dr Thomas Steffen, Dr Samir Khan, Dr Karmjit Grewal, Hazlina Yusof, Xiang Zheng, Alejandra Matamoros-Sanchez, Andrew Stanley, as well as former colleagues: Dr Jessica Davies, Dr Konstantinos Michail, Dr Hairi Zazuri and Dr Xinli Du, to whom I am very grateful for giving me so much help and suggestions with my research and my life in the past three years. I sincerely hope we can keep this good friendship forever no matter where we stay.

Finally, I would like especially to dedicate this thesis to my parents and my elder sister for their unconditional love, care, education, and support through all my life. Like a grass-blade owes sunshine, I owe them a debt of gratitude that I shall never be able to repay.

Contents

List of Figures

List of Tables

List of Symbols and Acronyms

D	Cant deficiency
v	Vehicle forward speed
δ	δ operator
θ_r	Airspring reservoir roll defection
y_v, y_b, y_0	Lateral displacement of body, bogie and track
θ_v, θ_b	Roll displacement of body and bogie
θ_0, R	Track cant, curve radius
δ_a	Anti-roll bar actuator roll angle
θ_m	Actuator roll angle in tilting bolster
F_a	Lateral actuator force
θ_{dm}	Effective cant deficiency
y_{vm}	Measured body lateral acceleration
ζ_{m0}	Front tilting bolster actuation system damping ratio
ζ_{m1}	Rear tilting bolster actuation system damping ratio
w_{cm0}	Front tilting bolster actuation system cut-off frequency
w_{cm1}	Rear tilting bolster actuation system cut-off frequency
DOF	Degree Of Freedom
PID	Proportional-Integral-Derivative
LQG	Linear Quadratic Gaussian
LQR	Linear Quadratic Regulator
RGA	Relative Gain Array
MIL	Model-In-the-Loop
SIL	Software-In-the-Loop
HIL	Hardware-In-the-Loop
KBF	Kalman-Bucy Filter
ICD	Individual Channel Design
MIMO	Multi-input and Multi-output
FPGA	Field Programmable Gate Array

e.c.d.	Effective cant deficiency
t.c.d.	True cant deficiency
R.M.S.	Root Mean Square
GA	Genetic Algorithm
S	Sensitivity
T	Complementary Sensitivity
KS	Control Sensitivity
PT	Precedence Tilting (tilt-only)
NT	Nulling Tilting (tilt-only)

****

Other symbols and acronyms are defined as they appear

****

Chapter 1

Introduction

1.1 Background and Overview

High speed trains which are able to operate at $200km/h$ and faster are nowadays widely spread in the world, i.e. France, Germany and United Kingdom in Europe, Japan and China in Asia. The recent world rail speed record is $578km/h$ achieved by the French V150 TGV (Alstom (2007)), and the TGV service also holds the record for the fastest scheduled rail journey with an average speed of $279.4km/h$. However, in order to develop the TGV, new rail infrastructures are needed, i.e. new rail tracks.

In the UK, British Rail opted instead to develop a train capable of running on its existing rail infrastructure based on the car body tilting technology. The Advanced Passenger Train (APT) developed in the 1970s used active roll suspension to tilt the vehicle body in curves to compensate the large lateral acceleration at higher speed, which ran in service beyond $200km/h$. Compared with improving or upgrading the rail infrastructures, tilting technology is an economical, environmental and sustainable solution to decrease the journey time while maintaining a good passenger comfort.

The idea of introducing tilting to the train comes from 1930s. It was based on the nature pendulum motion laws responding to the track profile. Active tilting, most commonly using a tilt mechanism in conjunction with an actuator to tilt the vehicle body, was introduced in 1965 by Deutsche Bahn. After being progressively developed

for several decades, now it becomes a standard technology in world wide, e.g. the Swedish X2000, the Italian Pendinolio tilting trains.

In addition to tilt suspensions, the active lateral secondary suspension is successfully applied in service for Japanese high speed trains (i.e. Series E2-1000 Shinkansen rail cars and Series E3 fifth type Shinkansen rail cars (Tahara et al. (2003))), which also improves the passengers' lateral comfort with no need to upgrade the rail infrastructure.

The use of active components in railway vehicles has been studied for decades, and the benefits have been demonstrated by the experimental research and operational train service. In this research, the combination of tilting technology and active lateral secondary suspension control is studied.

1.2 Active suspension technology

Figure 1.1 illustrates the complex structure of a conventional railway vehicle. The passive primary suspensions fitted between wheelsets and vehicle bogies help with guidance (running stability) of the vehicle, while the passive secondary suspensions (airspring) fitted between vehicle bogies and vehicle body provide passenger ride quality (high frequency irregularity isolation).

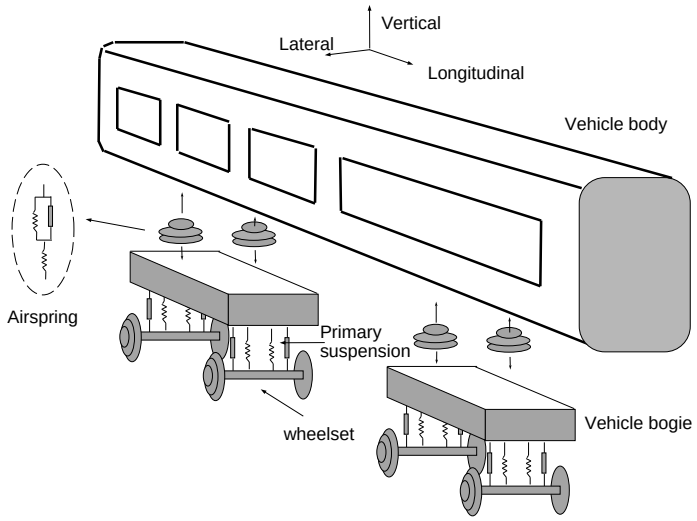

Figure 1.1: Mechanical arrangement of conventional railway vehicles (Goodall (1999a))

Conventional passive suspensions are usually configured by coil or leaf springs and viscous dampers, also, there have been springs using rubber, liquids or gases or combinations of these media. The performance of passive suspensions is determined solely by the values of parameters (damping, spring, mass) and the geometrical arrangement, which introduces a design trade-off between low frequency resonance attenuation and reduction in the high frequency transmissibility when they respond to rail track profiles (Pratt (1996)).

Active suspensions differ from passive suspensions by utilizing sensors, electronic controller and actuators with an existing mechanical system, as shown in Figure 1.2(a, b). The response of the active suspension system is mainly governed by the control law embedded in the controller (Goodall (1997)).

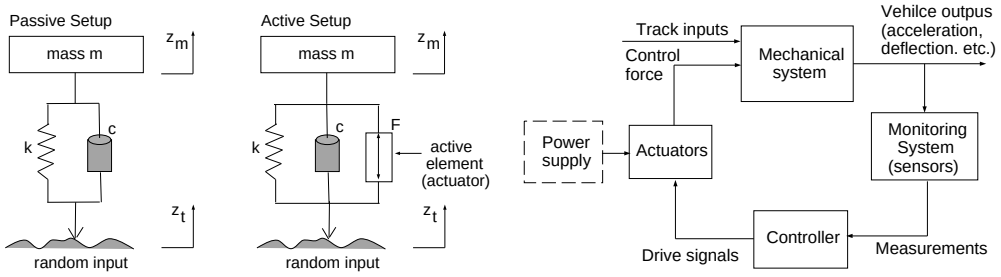

(a) Suspension configuration (b) General active suspension scheme

Figure 1.2: Active suspension

1.2.1 Active suspension categories and control

Active suspensions can be applied in vertical, lateral, roll, yaw and longitudinal direction to improve the vehicle dynamics response on the deterministic (curved track/gradient) and stochastic (straight track) excitations. The main active railway suspension categories and control are summarised below:

• Active primary suspension is located between the wheelsets and vehicle bogies to enhance the bogie stability and its curving performance. The critical problem for the wheelset dynamics is called "Hunting", which is caused by the combination of the profiled wheels and the creep forces, also the strong coupling between wheelsets' yaw and lateral dynamics. The normal solution is to connect two wheelsets to a bogie frame with lateral and longitudinal springs, but a trade-off arises for the design of longitudinal springs with the consideration of both the straight track and curving performance. The combination of four longitudinal actuators and lateral springs is the most basic scheme to solve this issue. The actuators are controlled in a differential sense to apply a yaw torque to each wheelset, as shown in Figure 1.3(a) (Goodall (1999b)). Also, there are various strategies for active primary suspensions control, e.g. Actuated Independently Rotating Wheels (AIRW) and Robust H_∞ control, see Mei and Goodall (2001, 2003). The world first demonstration of active stability system for a high speed bogie is described in Pearson et al. (2004).

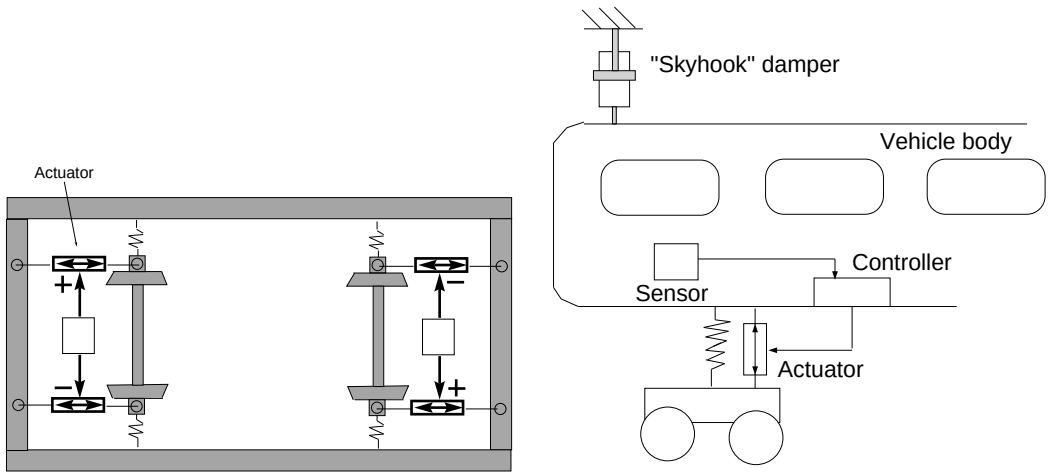

(a) Active primary suspension concept (b) Active secondary suspension concept

Figure 1.3: Active railway suspension

• Active secondary suspension is located between vehicle bogies (bolster in some tilting trains) and vehicle body to improve the ride comfort of passengers. The most used control law for active secondary suspension is called "Skyhook Damping", as shown in Figure 1.3(b). Theoretically, a virtual damper is hooked into the sky to provide extra damping to system dynamics modes, without degrading their responses to higher frequency. In reality, the vehicle body acceleration is measured and processed by a controller to determine the required actuator force. It has been proven to provide 50% ride quality improvement but with the expense of increasing the suspension deflection. Several control strategies have been designed to accommodate this design trade off, i.e. intuitive skyhook damping control, complementary filter skyhook damping control, optimal control and non-linear dual-Kalman filter control (Li and Goodall (1999)). However, the industrial emphasis is mostly upon active lateral suspensions since with using airspring vertical ride quality is less of a problem (Bruni et al. (2007)).

• Active roll suspension: equivalent to tilting, which is a special secondary suspension used to tilt the vehicle body inwards of the curve to compensate the large lateral acceleration perceiving by passengers, hence to improve the passengers' ride comfort in curves, which is now a standard technology used in operation trains world wild.

Active suspensions also can be subdivided into semi-active damping control and fully-active categories. Semi-active damping is based on passive components and its implementation modifies the stiffness and the damping characteristics of the suspension system without the need to supply a substantial amount of external energy (Karnopp (1974)). Most commonly used are switched or variable damper coefficients. However, semi-active damping can only dissipate the energy, because the force generated by the semi-active damping can only be in the opposite direction as the relative damper velocity. Only fully-active suspension control is addressed in this research.

1.3 Tilting technology

Tilting trains can run at higher speeds in curves compared to conventional trains by tilting the vehicle body inwards to compensate the large lateral acceleration perceived by the passenger. The idea of railway vehicle body tilting is first introduced by Deischl and Van Dorn and Beemer in 1938. Then the tilting technology has been developed from passive tilting to active tilting. ETR450 tilting train in Italy and X2000 tilting train in Sweden have been sucssesfully used in the service since 1990. In 2007, the Japanese Shinkansen Series N700 became the first high-speed tilting train in services. A full survey on the development history of tilting trains can be found in Persson et al. (2009).

1.3.1 Concept of tilting

A large centrifugal force acts on the vehicle when the train negotiates the curve at higher speed, and passengers experience a large lateral acceleration which causes the decreased ride quality and might result in nausea and similar health issues (Persson (2008)). Figure 1.4 gives the basic concept of tilting. In Figure 1.4(a), the vehicle body rolls out without the tilting action due to the centre of gravity being located above the lateral secondary suspension, while Figure 1.4(b) shows the situation of tilting train negotiating a curve (θ_v is the body roll angle (rad), θ_0 is the track cant angle (rad), R is the curve radius (m) and v is the vehicle forward speed (m/s)).

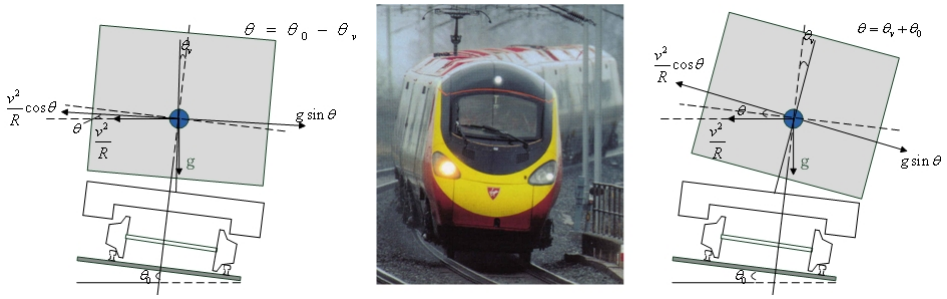

(a) No tilt action, roll out of curve (b) Active tilt, roll into curve

Figure 1.4: Non-tilt and tilting train

The curved sections on railway tracks are "canted" inward towards the centre of the curve, which reduces the lateral (curving) acceleration experienced by the passengers. The resultant lateral acceleration is defined as cant deficiency (D, m/s^2), and is given by (1.1) in the non-tilt case.

$$D = \frac{v^2}{R} \times cos(\theta_0 - \theta_v) - g \times sin(\theta_0 - \theta_v) \tag{1.1}$$

However, cant deficiency is most often espressed as an angle (D in (1.1) divided by g) presenting the difference between the existing cant angle (θ_0 in (1.1)) and the angle required to fully eliminate the effect of centrifugal force at maximum allowable speed. Based on (1.1), building the track with larger cant angle and curve radii can decrease the cant deficiency, hence to maintain the vehicle forward speed during curve. However, the amount of cant angle is limited due to safety and technical reasons (i.e. slow freight trains on curves, switching). Also, it needs to invest money into building new tracks which is not an economical and environmental friendly way especially in the hilly sections. Alternatively, tiltings effectively reduces the cant deficiency by leaning the vehicle bodies further towards the curve centre. The passenger curving acceleration in tilting trains now can be calculated by (1.2).

$$\ddot{y} = \frac{v^2}{R} \times cos(\theta_0 + \theta_v) - g \times sin(\theta_0 + \theta_v) \tag{1.2}$$

Generally, the vehicle speed can increase 30% by tilting the vehicle body to 6 deg, meanwhile maintaining the same curving performance (Goodall et al. (2000)). Also, the running time benefit is 10% between a non-tilting train and a tilting train on Stockholm-Gothemburg (Persson et al. (2009)).

1.3.2 Mechanical configuration of tilting

The early passive tilting trains completely relied on the nature pendulum motion laws which caused safety issues, e.g. vehicle body overturning, while active tilting trains use active mechanisms to tilt the vehicle body according to the track profile information. There are three basic active tilting mechanical configurations:

- Tilt across the secondary suspension
- Tilt above the secondary suspension
- Tilt below the secondary suspension

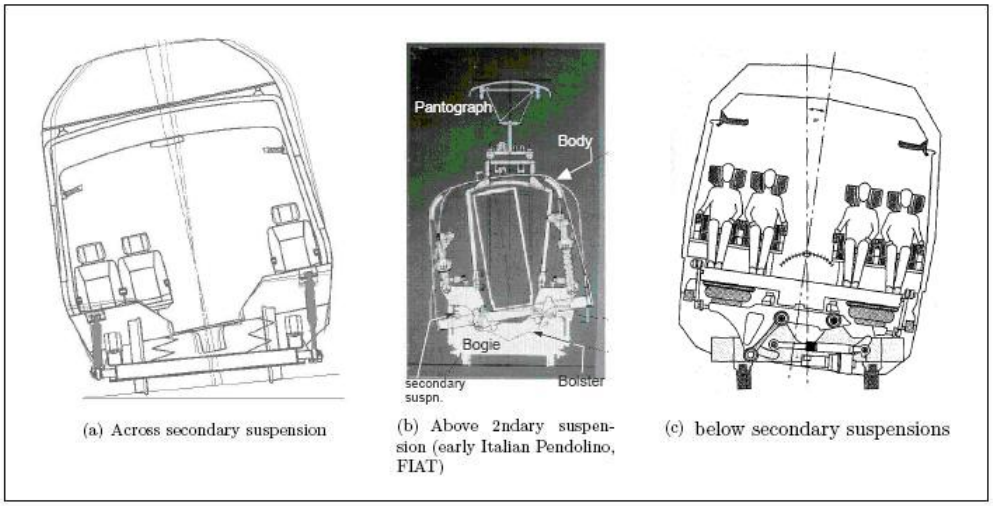

(a) Across secondary suspension

(b) Above 2ndary suspension (early Italian Pendolino, FIAT)

(c) below secondary suspensions

Figure 1.5: Tilting mechanical configuration (Goodall (1999a))

The first approach is to apply the active control to the secondary roll suspension. There are two methods: (1) Apply the differential control to the airsprings. It is being used to give 2 deg of tilt, i.e. Japnese Series 201 diesel trains of JR-Hokkaido (Goto (1997)). (2) Direct control of roll suspensions via the active anti-roll bar (stabiliser), which is applied in Bombardier's regional Talent train (Persson et al. (2009)), as shown in Figure 1.5(a). This has a transversely-mounted torsion tube installed through the bogie with vertical links to the vehicle body, except that one of the links is replaced by a hydraulic actuator, and thereby applies tilt via the torsion tube, which provides a relatively small tilt angle of around 4 deg. The second approach is to use the tilting bolster. The tilting bolster above the secondary suspension is employed in the early

Italian Pendolino FIAT, as shown in Figure 1.5(b). However the lateral suspension deflection is increased with the increase of the tilting angle, and in practice an extra centering device is needed. The most common configuration is to use the tilting bolster below the secondary suspension, as shown in Figure 1.5(c), which avoids the increased curving forces on the lateral suspension. An inclined swing link or a circular roller beam is employed. In this configuration, the tilting bolster is able to provide a maximum tilt up to 10 deg with the effective tilt center is above the vehicle body floor level.

There are several subsystems for the tilt technology, such as: tilt authorisation and speed supervision system, tilting mechanism of bogie, pantograph system, tilting control and actuation system. In this research, we mainly focus on the tilting control and actuation system which is the "heart" of the tilting train.

1.3.3 Tilting control systems

Control system based only upon local vehicle measurements (local tilting) was used in the early tilting trains, and the term, "nulling control" has been used to describe this approach (Goodall (1999a)). The body lateral acceleration is measured and used to drive the tilt actuator in a direction which will bring it to zero. However, full compensation of the lateral acceleration experienced by the passenger has been found to cause motion sickness. Thus, the basic nulling strategy has been modified by introducing a proportion of secondary suspension roll angle to give partial tilt (60%-70% compensation). But it proved difficult to achieve the trade-off between straight track ride comfort and curving performance even with advanced control strategies (Zamzuri (2008); Zolotas (2002a)). The more profound problem is the interaction with the lateral suspension, because the roll and lateral modes of the vehicle body are strongly coupled in a dynamic sense. If the tilting control loop bandwidth is low enough not to interfere with the lateral suspension, it is then too slow acting when entering or leaving curves.

The industries most use the so-called "precedence" control approach which is based upon providing tilt command from the vehicle in front (Goodall (1999a)). In this strategy, the lateral accelerometer on a non-tilting part (vehicle bogie) of the previous vehicle indicates the required tilting angle (avoid the modes coupling), with the body

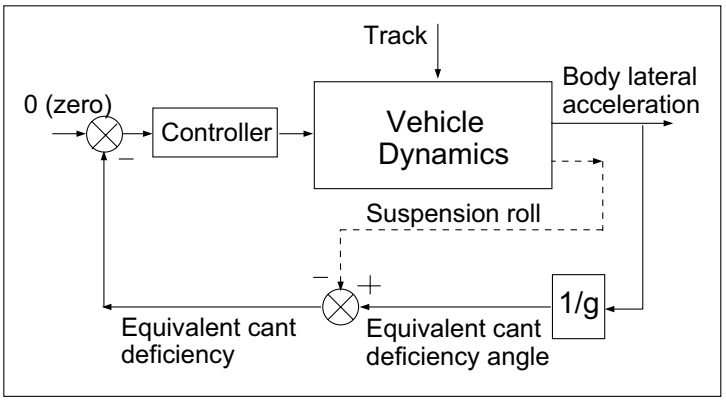

(a) Intuitive nulling control (modified)

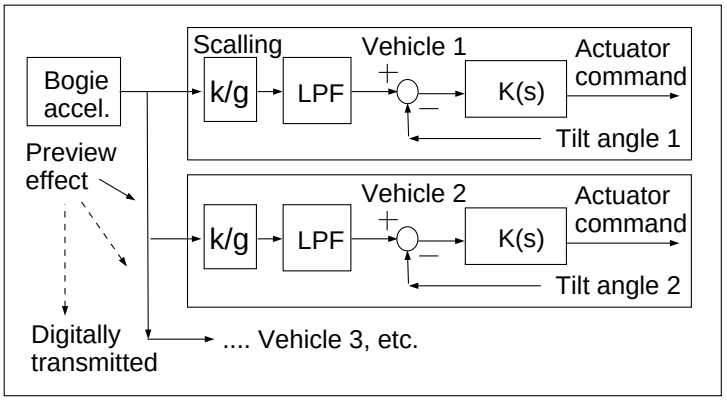

(b) Precedence command driven control

Figure 1.6: Tilting control system

tilt angle feedback controller locally ensuring that each vehicle tilts to the commanded angle, the advanced information enables a sufficient level of filtering to be applied to remove the effect of track irregularities (introduced by the bogie-mounted accelerometer) on the tilt command signal. But there are two issues for this approach:

(1) The performance of the leading vehicle is worse than the trailing vehicle due to having no precedence command for it, which means the tilt lag can not be avoided.

(2) The fast reaction of tilting control is needed in curve transitions but the low pass filter used to attenuate the high frequency disturbance signal caused by the track irregularity results in the reaction delay of the tilt actuation system, which is a trade-off for the precedence control.

More recently, ALSTOM developed a command driven controller named "Anticipative Tilt Control" (Hauser (2006)) which integrates the vehicle measurement with information from an onboard track database then provides the track information to the tilt controller. Therefore, as long as the location of the train is determined, the system can generate the tilt command using track data in the database. However, both the position of each vehicle along the track and the curve data contained in the database need to be known accurately and reliably for this approach to work effectively.

1.4 Actuators used in active suspensions

Various kinds of actuator have been designed and tested within active railway suspensions (Goodall (1997); Pratt (1996)). The most common three types of actuators for railway suspensions are: Electromechnical, Electrohydraulic and Electromagnetic actuator.

An electromechanical actuator consists of an electrical part and a mechanical part. A motor (AC/DC) in the electrical part rotates a screw mechanism (e.g. a roller or a ball screw in the mechanical part) to transfer the rotational motion of the screw to a translational motion. The force is produced by the motion on the body that the actuator is connected to. Figure 1.7 shows a typical electromechanical tilting actuator (ESW (2006)), which also can be modeled as shown in Figure 1.8.

The angular rotations generated by the DC motor are transformed by a gearing system to provide a linear motion to the screw. The output of the actuator is the force which is generated by compression of the screw as the motor is turned. In the electric circuit, the electrical power applied with a voltage (v) is opposed by a resistance of the conducting path (R_{arm}), the machine inductance (L_{arm}) and an e.m.f.

Figure 1.7: Electromechanical tilt actuator

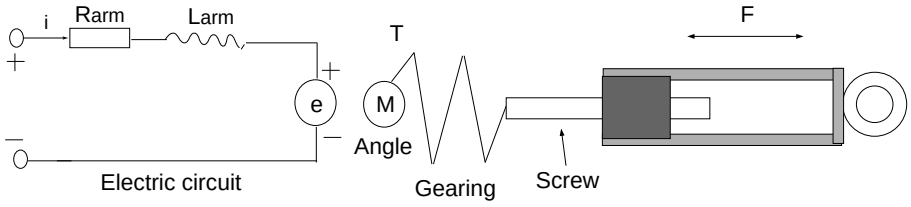

Figure 1.8: Equivalent electromechanical actuator model

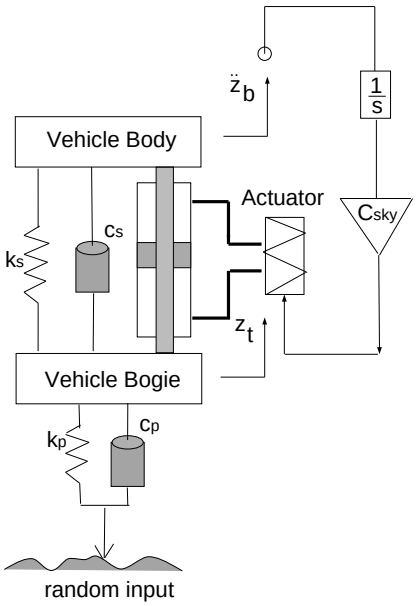

Figure 1.9: Electrohydraulic actuator implementing skyhook damping

Figure 1.9 shows an electrohydraulic actuator implementing the skyhook damping control. The general concept of hydraulic actuator is based on the idea that a control

signal to a valve or an electrically-driven pump to give a pressure difference between the two chambers of the actuator cylinder, hence generating the actuator force.

An electromagnetic actuator can provide the large frequency bandwidth up to $50Hz$. The experimental test carried by Pratt (1996) showed the internal dynamics of the electromagnetic actuator does not affect the actuator performance. The configuration of the electromagnetic actuator is based on two pairs of electro-magnets mounted back to back operating in attraction mode. The force can be generated in both directions between two masses connected via the actuator. However, feedback control is needed because the actuator itself is an unstable system (the air gap between the magnets has to be maintained within a limit) (Goodall et al. (1993); Michail et al. (2008)).

1.5 Hardware-In-the-Loop technology

Hardware-In-the-Loop (HIL) simulation is also investigated in this research with the consideration of the controller practical implementation. HIL technology is widely used in the automotive engine and aircraft control system design process to evaluate the controllers, which is a well-established techonogly, i.e. dSPACE system (dSPACE (2008)). Differing from pure real system, HIL has a real electronic control unit in the system, while the controlled plant is simulated (Rapid Control Prototyping is defined in the opposite way: the plant is real but the controller is simulated). The design process for a HIL system is presented below:

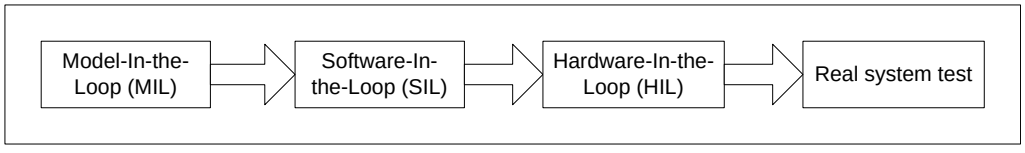

Figure 1.10: HIL design process

(1) Model-In-the-Loop (MIL): the controller and the system dynamic model are both developed and simulated in non-real time software tools, i.e. MATLAB/SIMULINK.
(2) Software-In-the-Loop (SIL): the functional model of the controller in MIL is replaced by C-code.
(3) Hardware-In-the-Loop (HIL): the model runs in a real time environment and the

control strategies (C-code) are downloaded into the electronic control device.
(4) Rapid prototyping or real system test.

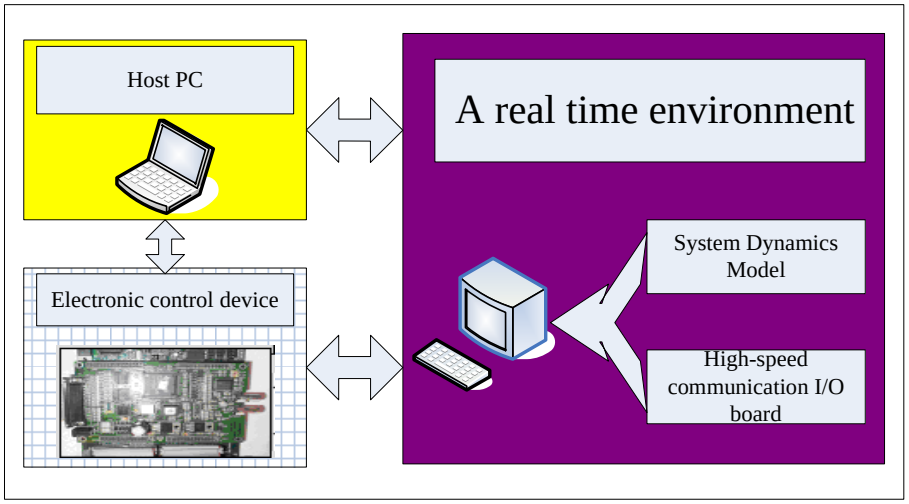

Figure 1.11: General HIL configuration

A general architecture of a HIL system is presented in Figure 1.11. The host PC has the function to monitor and manage system overall performance, perform MIL simulation and SIL simulation, compile the system dynamic model and download executable code into the target-PC with real time environment. The system dynamic model runs in a PC with real time environment and connects to an electronic control device via the high speed communication I/O (USB/RS232/GPIB/Ethernet, etc.). The electronic control device is designed with microcontroller, Digital Signal Processor (DSP) or Field Programming Gate Array (FPGA). Note that, the Design of HIL system with microcontroller and DSP is a rather mature technology, in this research, a FPGA-based HIL system is investigated.

1.6 Problem statement and research objectives

As presented in Section 1.3.3, although commercial solutions for the tilting control have been tested and successfully applied to service operation trains, research on a local control strategy still has the practical benefit which makes system simpler and

more straightforward for detecting sensor failures. Previous research studied issues on advanced control strategies for tilting trains as well as concepts related to intelligent control approaches, such as H_∞ and Fuzzy logic control, using conventional tilt mechanisms which gives the benefit we may obtain from the local controller. The overall performance on the curve is almost the same as the precedence control strategies. However, there are still some issues needed to be solved and improved.

(1) The tilting train runs at higher speed on the same rail infrastructure compared with non-tilting train which deteriorates the ride quality on straight track. One effective solution is to improve vehicle suspension such as using the active secondary suspension to replace the passive suspension.

(2) Based on the test on the service tilting train about the motion sickness carried out by Persson (2008), vehicle body lateral motions combined with the roll motions increases the incidence of motion sickness which particularly occurs when the train negotiates the curve transition.

(3) Moreover, the interaction between the roll and lateral motion makes the local and single vehicle controller design more difficult (Goodall (1999a)).

In this thesis, a lateral suspension actuator is integrated into the tilting train, the main objectives are:

(1) to improve the straight line ride quality of the tilting train

(2) to attenuate the dynamics interaction between lateral and roll modes of the vehicle body in order to provide high performance local tilting control

Futhermore, multi-variable control strategies, MIMO system analysis and HIL system design are also investigated.

1.7 Thesis structure

The thesis is organized into 8 chapters with its structure and contents summarized as follows:

Chapter 2 contains the literature survey on tilting control, active lateral secondary suspension control, MIMO system decoupling control and system configuration methods (particularly for the decentralised control), embedded digital control technology. According to the survey, although both tilt technology and active lateral secondary suspension have been developed and the tilting suspension has been combined with a lateral centering device and semi-active damping, full integration of tilt and active lateral suspension has not been studied, which is the main addressed aspect in this research.

Chapter 3 studies the railway track geometry, active suspension design requirements and its assessment methods. The lateral rail track is modeled by deterministic (curved track features) and stochastic (straight track features) signals respectively. Furthermore, the design requirements of the active railway suspension are presented. The controller design for the integrated tilt and active lateral secondary suspension needs to meet both tilting performance and active lateral suspension design requirements.

In Chapter 4, the end-view modeling and control of integrated active anti-roll bar with active lateral secondary suspension is introduced. Classical decentralised control, H_∞ based decentralised control as well as the MIMO LQG control are studied and designed for this dual-actuator system. Genetic Algorithm is used to optimize the controller parameters. The simulation results show the benefits we can obtain from this active suspension integration strategy.

Tilting trains most commonly use tilting bolster to provide the tilting action. In Chapter 5, the end-view modeling and control of integrated tilting bolster with active lateral secondary suspension is introduced. The active suspension integration strategy gives the improvement for this type of tilting train as well. It can further improve the tilting performance when the lateral actuator control is combined with precedence tilting

configuration. The comparison between integrated active anti-roll bar with active lateral secondary suspension and integrated tilting bolster with active lateral secondary suspension is addressed at the end of this chapter.

The work summarized in previous chapters is based on a 4 Degree Of Freedom (DOF) end-view model which only includes lateral and roll dynamics of railway vehicle body and bogie. In Chapter 6, a 9 DOF full vehicle model is presented including the dynamics of two bogies and vehicle body, the yaw dynamics is taken into account. Control strategies designed based on the end-view model can be directly implemented into this full vehicle model. Furthermore, modal control approach is employed to control the lateral and yaw dynamics to enhance the ride quality on straight track. Also, the actuator dynamics are discussed.

Chapter 7 considers some of the issues that will be encouterd when the controllers are implemented in practice. A SIL test strategy is presented to validate the C based digital controller. Further, a FPGA-based HIL system is designed with the classical control strategy for the 9 DOF model. Issues related to embedded FPGA-based controller design are discussed.

Chapter 8 presents final conclusions and future steps.

1.8 Thesis contribution and Publications

1.8.1 Thesis contribution

This thesis makes contributions in the following areas :
(1) The first investigation (world wide) on the integration of tilt and active lateral secondary suspension control with the objective to enhance tilting control system performance in high speed trains. The simulation results show the integration strategy not only improves the straight track ride quality of the tilting train, but also attenuates the dynamics interaction between lateral and roll modes of the vehicle body, hence providing a high performance local tilt control.

(2) Intensive study on the decentralized and centralized control on the integrated tilt (both active anti-roll bar tilting and tilting bolster) with active lateral secondary suspension system. The applied control strategies and methodologies cover:

• Active secondary suspension control: Skyhook damping, Complementary filter, Centering control, Modal control
• Model-based control: H_∞ and LQG control
• Model-based estimation: H_∞ filter and estimator-based decoupling control
• System dynamics interaction analysis based on Relative Gain Array (RGA)
• Genetic Algorithm based control optimisation

(3) Modeling of 9 DOF full vehicle for the integrated tilting bolster and active lateral secondary suspension control. Modal control approach for the lateral and yaw dynamics is investigated as well as the actuator dynamics responses.

(4) HIL system design for active railway suspensions. The issues related to FPGA based real-time control and HIL system design are discussed and presented.

1.8.2 Publication

Accepted and published:

- [1] Ronghui Zhou, Argyrios Zolotas, Roger Goodall. *9 DOF railway vehicle modeling and control for the integrated tilting bolster with active lateral secondary suspension*, accepted by UKACC 2010.

- [2] Ronghui Zhou, Argyrios Zolotas, Roger Goodall. *LQG control for the integration of tilt and active lateral secondary suspension in high speed railway vehicles*, proceedings of the 8th IEEE international conference on control & automation (ICCA'10), Xiamen, China, 9-11 June 2010.

- [3] Ronghui Zhou, Argyrios Zolotas, Roger Goodall. *Enhancing tilt system performance by integrating with active lateral suspension control*, proceedings of the 21st International Symposium on Dynamics of Vehicles on Roads and Tracks (IAVSD09), Sweden, 17-22 August 2009.

- [4] Ronghui Zhou, Argyrios Zolotas, Roger Goodall. *Integrated tilt and active lateral secondary suspension control*, proceedings of the 5th international symposium on speed-up, safety and service technology for railway and maglev systems (STECH'09), Japan, 11-15 June 2009.

- [5] Ronghui Zhou, Argyrios Zolotas, Roger Goodall. *Model-Based integrated tilt and active lateral secondary suspension control*, proceedings of the 23rd IAR Workshop on Advanced Control and Diagnosis, Coventry, UK, 27-28 November 2008.

Submitted:

- [6] Ronghui Zhou, Argyrios Zolotas, Roger Goodall. *Integrated tilt and active lateral secondary suspension control in high speed railway vehicles*, submitted to Mechatronics.

Chapter 2

Literature study and survey

This chapter presents a detailed literature survey of the following aspects:

- Tilting control system, particularly tilting control systems based on local vehicle sensor measurements
- Active lateral secondary suspension control
- Multi-input and Multi-output (MIMO) system control and configuration methods, particularly the inputs/outputs selection methods for decentralized control systems
- Recent applications of Genetic Algorithms (GA) in railway engineering
- Digital control technology

2.1 Tilting control systems

Full details of tilting trains and tilting control can be found in Bruni et al. (2007); Goodall (1997); Persson et al. (2009). Contemporary industrial tilting control systems mainly adopt a precedence tilting control scheme, i.e. ALSTOM $TILTRONIX^{TM}$ (Hauser (2006)). Further advanced precedence tilting schemes are combined with a track database or GPS device to provide information of track and train location (Enomoto et al. (2005); Hauser (2006)). Also, there are some advanced tilting control designs based on the precedence configuration, e.g. adaptive control (Shu (1999))

and predictive neural-network control (Dai and Zhang (2005)). Dai and Zhang (1999) applied a H_∞ strategy to a tilting test rig. Different from the local and conventional precedence tilting control configuration, Suescun (1996) introduced the inverse dynamics method via a simple example and simulation using real track data which demonstrated the effectiveness of the method in the design of the tilt control system. Most recent work on advanced precedence tilting control is described in Zeng and Luo (2009). A nonlinear mathematical model for the titling train composed of three cars is built. Moreover, Proportional control and robust H_∞ control are designed. Neural network forecast method is adopted to compensate the time delay caused by the filters. The survey here however is limited within the local tilting control system.

2.1.1 Local tilting control systems

A good tilting control system needs to provide a comfortable response to the passengers during curve transitions, whilst maintaining the straight track ride quality within acceptable limits. However, a design trade-off always exists between these two requirements. With the local tilting control, it is difficult to achieve this trade-off due to the dynamic interaction within the lateral suspension between the roll and lateral modes.

The research work in Pearson et al. (1998) described the control system design for tilting trains with an active anti-roll bar, in which the design requirements for the active anti-roll bar in railway vehicles is introduced. Classical and optimal controllers are designed based on 4 DOF end-view and 9 DOF full vehicle models. The simulation results showed the efficiency of optimal control on the improvement of the local tilting control performance, also the trade-off for the tilting control between curving performance and straight track ride quality is presented. It suggested that the integration of tilt with active lateral secondary suspension control could be a further solution to optimize this design trade-off.

Zolotas (2002a) conducted research on advanced tilting control, in which, a 4 DOF end-view model for the tilting train with active anti-roll bar and tilting train with tilting bolster were presented. In the control system design, modified nulling control and commercial precedence control were studied firstly which provide a benchmark

for the further advanced control system design. Optimal control and H_∞ control are addressed afterward, more details can be found in Zolotas and Goodall (2007a); Zolotas et al. (2002b). For the tilting train with active anti-roll bar, it was found that with a mixed sensitivity H_∞ control, it is difficult to achieve the design trade-off with one set of weighting filters. Hence the mixed $H_2\&H_\infty$ multi-objective design is proposed. Moreover, the H_∞ loop shaping design is proposed and simulated for the tilting train with tilting bolster (Zolotas et al. (2007b)). Note that, the above control systems are all based on the effective cant deficiency (e.c.d.), e.c.d.(θ_{dm}) is defined as:

$$\theta_{dm} = -k_1 \ddot{y}_{vm}/g - k_2 \theta_{2sr} \tag{2.1}$$

where $\ddot{y}_{vm}$ is the measured body lateral acceleration, θ_{2sr} is the secondary suspension roll angle (for tilting trains with ARB).

$$\ddot{y}_{vm} = \frac{v^2}{R} - g(\theta_0 + \theta_v) + \ddot{y}_v; \quad \theta_{2sr} = \theta_v - \theta_b \tag{2.2}$$

Actuator roll angle θ_m replaces θ_{2sr} in (2.1) for the tilting bolster scheme which gives a more direct measurement of vehicle tilt. k_1 and k_2 in (2.1) are set to 0.60 and 0.40 for 60% partial tilt compensation (for tilting trains with ARB), while k_1 and k_2 are changed to 0.75 and 0.25 in the tilting bolster case for 75% partial tilt compensation.

Another way to drive the tilt action is to use true cant deficiency (t.c.d., θ_{tdm}),

$$\theta_{tdm} = \frac{v^2}{gR} - (\theta_0 + \theta_v) \tag{2.3}$$

which is unaffected by the suspension dynamic interactions. However, the information about track cant angle is needed to obtain the t.c.d., which is impossible to measure in practice. A Kalman-Bucy Filter (KBF) is designed to estimate the t.c.d. in Zolotas et al. (2007b), and classical control can be applied based on the estimator.

Zamzuri (2008) applied Fuzzy logic control to the tilting train with active anti-roll bar, still based on body-mounted sensor (i.e. e.c.d.), aimed to further optimize the local tilting design trade-off. Genetic Algorithms are employed to optimize the controller parameters and Fuzzy membership functions (Zamzuri et al. (2006a)). A 9 DOF vehicle model is presented and it is used to validate the proposed Fuzzy PID (Zamzuri et al.

(2006b)) and Fuzzy LQG controllers (Zamzuri et al. (2007)). The simulation results with 9 DOF model are similar to the results with 4 DOF model.

All the research described above show their efficiency on enhancing local tilting control system performance, but due to the dynamic interaction between roll and lateral modes of the railway vehicle body, there is a limit to what can be achieved in terms of improving the transition performance. Integrated tilt and active lateral secondary suspension is suggested to be an alternative solution, which also can improve the passenger ride quality on straight track.

2.2 Active lateral secondary suspension control

Detailed surveys about lateral active secondary suspension control can be found in Bruni et al. (2007); Goodall (1997). Based on these survey papers and recent development, three main aspects of active lateral secondary suspensions and their control strategies are summarized as follows:

(1) Semi-active damping concepts
Semi-active damping can improve passenger ride comfort on straight track. O'Neill and Wale (1994) presented details about semi-active damping concepts and the associated control strategies. Tanifuji et al. (2002) gave details about the application of semi-active damping control in Japanese high speed trains. Switching of damper coefficients is adopted because a small damping coefficient in the secondary suspension is desirable for the high frequency vibration caused by track irregularities, while a large damping coefficient is effective to the direct low frequency larger car body excitation, e.g. the aerodynamic force in the tunnel. Semi-active damping with the sky-hook control law reduced the lateral vibration by about 30% at a speed of 300km/h. It has been applied to the semi-active system of Series 500 EC trains for the commercial use since 1996, and in Series 700 Shinkansen EC trains since 1999. However, Semi-active damping can just dissipate the energy. The force generated by semi-active damping can only be in the opposite direction to the relative damper velocity, and cannot be used to give satisfactory curving transition performance in railway vehicles.

(2) Active lateral centring (hold-off) devices

This is a low bandwidth full active lateral suspension which actively moves the vehicle body laterally and is installed to compensate for quasi-static lateral force due to residual cant deficiency. The control can be fulfilled by introducing a displacement sensor fitted to the bogie (Goodall (1997)). It has been used on the service vehicle, such as: Virgin Class 390 tilting trains for the UK west coast main line, for which pneumatic cylinders are used (HAUSER (2002); O'Neill (2008)). A mainline test was also carried out by Siemens SGP (Stribersky et al. (1998)) which combined semi-active damping, tilt active suspension control and Hold-off device, also the lateral displacement is measured to configure the hold-off device controller. Moreover, numerical model and field test result of Italian 'Pendolino' train combined with an active lateral suspension (centering device) can be found in Cheli et al. (2001).

(3) Full active lateral secondary suspension control

The implementation of active lateral secondary suspension is more difficult than in the vertical direction because of sustained curving forces that have to be accommodated during curving; and those which limit the possibilities for reducing the lateral spring rate (Bruni et al. (2007)). The world first fully active lateral secondary railway suspension demonstration was carried out by the British Rail in 1978 (Goodall et al. (1982)). A hydraulics actuator was fitted in parallel with the lateral secondary air suspension at each end of the vehicle. Results obtained from a series of field tests showed 50% passenger ride comfort improvement compared to the passive suspension. The first commercial use of an active suspension however was developed by Sumitomo for the East Japan Railway Company in 2002, which is used in Series E2-1000 Shinkansen and Series E3 fifth type Shinkansen high speed trains (Tahara et al. (2003)). A pneumatic actuator system is installed in parallel with the secondary suspension damper, and H_∞ controller is applied using measurements from body-mounted accelerometers. Also, it provides 44-64% improvement in the passenger lateral ride comfort on straight track. Major research on full-active lateral suspension control systems world wide is summarized in Table 2.1. The details of each case can be found in the reference papers.

Table 2.1: Summary of major full-active lateral secondary suspension control systems

No.	Country	Manufacturer	Status	Actuator	Measurements	Controller	References
1	UK (1970s-1980s)	British Rail	Experiment	Servo-hydraulic Electro-mechanical		Classical Optimal control	Goodall (1997)
2	Japan (1980s)	Japanese National Railways	Field test	pneumatic	Lateral acceleration	Classical	Okamoto (1987)
3	Japan (1991-1993)	Privatized JR-East	Field test	pneumatic	Lateral acceleration	H_∞	Koizumi (1992, 1993)
4	UK (1996)	Loughborough University	Lab experiment	Electrohydraulic Electromechanical Electromagnetic	Body lateral acceleration Body lateral displacement	Modified skyhook damping Complementary filter control Optimal control	Pratt (1996)
5	Japan (1996)	RTRI	Experiment	Hydraulic Pneumatic	Body and bogie lateral vertical and roll accelerations	Modern control	Goodall (1997)
6	Japan (1997)	Hitachi	Field test	Hydraulic	Lateral acceleration	H_∞	K. Kanbayashi (1997)
7	China (1998)	Southwest Jiao Tong University	Lab experiment				Jin and Zhang (1998)
8	UK (2001)	DaimlerChrysler AG	Filed test	Hydro-pneumatic	Car body inertial lateral and yawing, Relative Car body lateral displacement in relation to the two bogies, and also their relative yawing and rolling angles	Classical control	Streiter et al. (2001)
9	Japan (2003)	East Japan Railway company	Operation	pneumatic	Lateral acceleration Lateral displacement Roll angular acceleration	H_∞	Tahara et al. (2003)

2.3 MIMO system control and configuration methods

2.3.1 MIMO system control

Loop interactions exist in many MIMO systems, such as industrial process control systems (distillation columns (Luyben (1970))), flight systems (helicopter control system (Liceaga-Castro et al. (1995)), missile STT (Skid To Turn) control systems) and submarine systems (Liceaga-Castro and Liceaga-Castro (1998)). Some loop interactions cause the system instability and affect the controller performance. In this section, a survey on MIMO system control is presented first followed by the study on the system structure configuration methods.

2.3.1.1 Classical decoupling control strategies

The objective of classical decoupling control is to separate a MIMO dynamics control system into a series of independent SISO sub-systems. Simple strategies including the decoupling network of Boksenbom and Hood, and the method of Zalkind and Luyben are presented in Boksenbom and Hood (1949); Luyben (1970); Tham (1998). Zheng et al. (2004) treated the interaction as a disturbance and used feedforward decoupling control to compensate for the interaction.

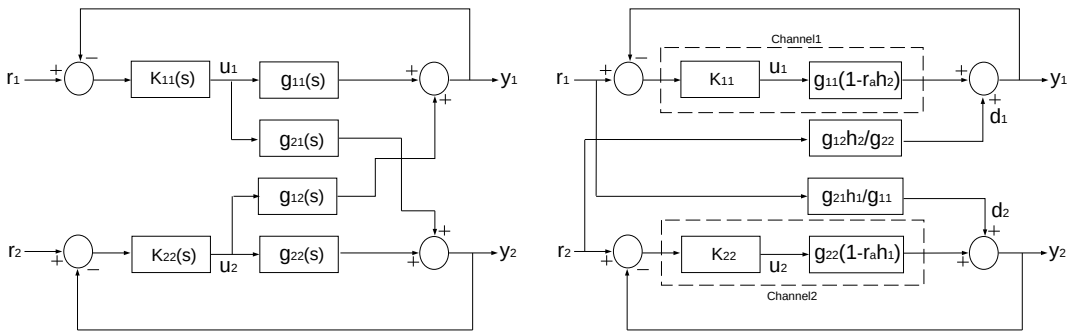

(a) 2X2 multivariable system with diagonal controller

(b) Equivalent channels of 2X2 control system

Figure 2.1: ICD concept

Individual Channel Design (ICD) is a novel analytical framework that allows the analysis and synthesis of multivariable control systems under the context of the multivariable structure function by applying classical techniques based on the Bode and Nyquist plots (Leithead and O'Reilly (1991)). It can decouple the MIMO system without losing the interaction information of the system. Figure 2.1 shows the basic concept of the ICD for the 2×2 system. The original plant (Figure 2.1(a)) is maintained in the equivalent SISO system (Figure 2.1(b)) through the Mutivariable Structure Functions (r, MSF) with no loss of interaction information, where

$$G = [g_{11} \;\; g_{12};\;\; g_{21} \;\; g_{22}]; \qquad r = \frac{g_{12}g_{21}}{g_{11}g_{22}}; \qquad h_i = \frac{k_{ii}g_{ii}}{1 + k_{ii}g_{ii}} \tag{2.4}$$

k_{ii} is the controller for the channel i. The design process includes controller design for each channel and structural robustness assessment (via analysis of the Nyquist stability of $r \times h$) (Carlos et al. (2005)). The application of ICD can be found in Leithead and O'Reilly (1991, 1992); Liceaga-Castro et al. (1995). However, the framework can guarantee the system robustness but without consideration of the system performance, and a great effort is needed for the controller design when it is applied to a complex system, particularly when the system has strong coupling and non-minimum phase characteristics.

2.3.1.2 Modern control strategies

Modern design techniques allow for direct use of MIMO state space models in control system design algorithms. There is no need to break down the coupled system into SISO subsystems. Thus all the control state relationships, including cross couplings, are considered in the design process. Methods of Eigenstructure assignment, Linear Quadratic Regulator (LQR) and H_∞ control are summarized here.

Eigenstructure assignment allows control system designers to prescribe desired closed loop eigenvalues and eigenvectors for a given system, thus achieving desired performance characteristics. Two extensions can be used to do the decoupling control: state feedback eigenstructure assignment decoupling strategy and output feedback eigenstructure assignment decoupling strategy (Zheng (2002)).

LQR is an optimal control design method that yields a full state feedback controller which minimizes the quadratic performance index (using output regulation):

$$J = \int_0^\infty [x^T Q x + u^T R u] d\tau \tag{2.5}$$

where Q is the symmetric, positive semi-definite state weighting matrix and R is the symmetric, positive definite control weighting matrix. The controller design process involves selecting the outputs to be weighted (x in (2.5)), and tuning the system output and control input weighting factors (Q, R). In the case where all required system states are not available for feedback, which may be difficult or even impossible to measure, a Kalman filter can be combined with the optimal controller to provide the necessary state estimate for state feedback. This is known as the Linear Quadratic Gaussian or LQG control (Skogestad and Postlethwaite (2000)) which has been applied to many problems inculding Gas Engine control (Hofbauer et al. (2006)) and High Redundancy Actuator control (Du et al. (2007)), etc..

The research on H_∞ control started from 1980s with the objective to compensate the weakness of LQG control to deal with good robustness properties (Zames (1981)). The design process involves the minimization of the H_∞ norm of the transfer function from exogenous signals (such as disturbances and input commands) to the signals which are to be minimized to meet the control objectives (Skogestad and Postlethwaite (2000)). Mixed-sensitivty H_∞ control, signal-based H_∞ control and H_∞ loop-shaping are the three basic types of H_∞ control. However, H_∞ control is criticised due to the complexity of selecting the frequency-dependent weighting filters. Although weighting filters can be designed based on the system frequency features (i.e. bandwidth), and Beaven et al. (1996); Ortega and Rubio (2004); Postlethwaite et al. (1990) provided several methods for the weighting filters design, the selection of weighting filters sometimes still presents difficulty, particularly for MIMO multi-objective design problem. Miranda et al. (2007) described a hierarchical approach for H_∞ robust control design for a real pilot-scale plant, in which H_∞ mixed-sensitivity constitutes the bottom level optimisation to guarantee the system robustness and stability. Genetic Algorithms are employed for tuning the parameters of the H_∞ controller, searching for the solutions that satisfy the high-level practical control constraints. More recently, Michail et al. (2008) also utilised Genetic Algorithms to tune weighting filters for H_∞ loop-shaping

design subject to the given performance indices for a Maglev suspension control system.

There are some other control strategies such as: Adaptive control (Li and Bayoumi (2007)), Intelligent Fuzzy logic control (Zhang et al. (2003)) and Model Predictive Control (Keviczky et al. (2004); Ruth et al. (2008)) also can be applied to the MIMO control system.

2.3.2 MIMO system configuration methods

A good control system structure can simplify the controller design process, i.e. a complex plant with a good system structure can be well controlled only by a simple PID controller. Based on van de Wal and de Jager (2001) and Skogestad and Postlethwaite (2000), the system structure includes two aspects: Input-Output Selection (IO Selection) and Control Configuration (CC).

IO Selection and CC are generally misunderstood by most researchers as being the same concept, where these are really exclusive processes. Figure 2.2 classifies the main conventional aspects of the control structure selection. The IO Selection can rely on investigation of the system relative degree, Hankel singular values, LQG cost function and H_∞ norm, etc.. The control configuration can be divided into cascade control, decentralized control, decoupling control, selectors and feedforward control. Independent design and sequential design are two basic design methods for the decentralized control, Relative Gain Array (RGA), Decentralized integral controllability (DIC) as well as Performance Relative Gain Array (PRGA) and Closed-Loop Disturbance Gain (CLDG) can be applied to analyze the robustness and performance of the control configuration. The study here mainly focuses on the IO selection for the decentralised control. Relative Gain Array (RGA) and their recent extensions are mainly addressed.

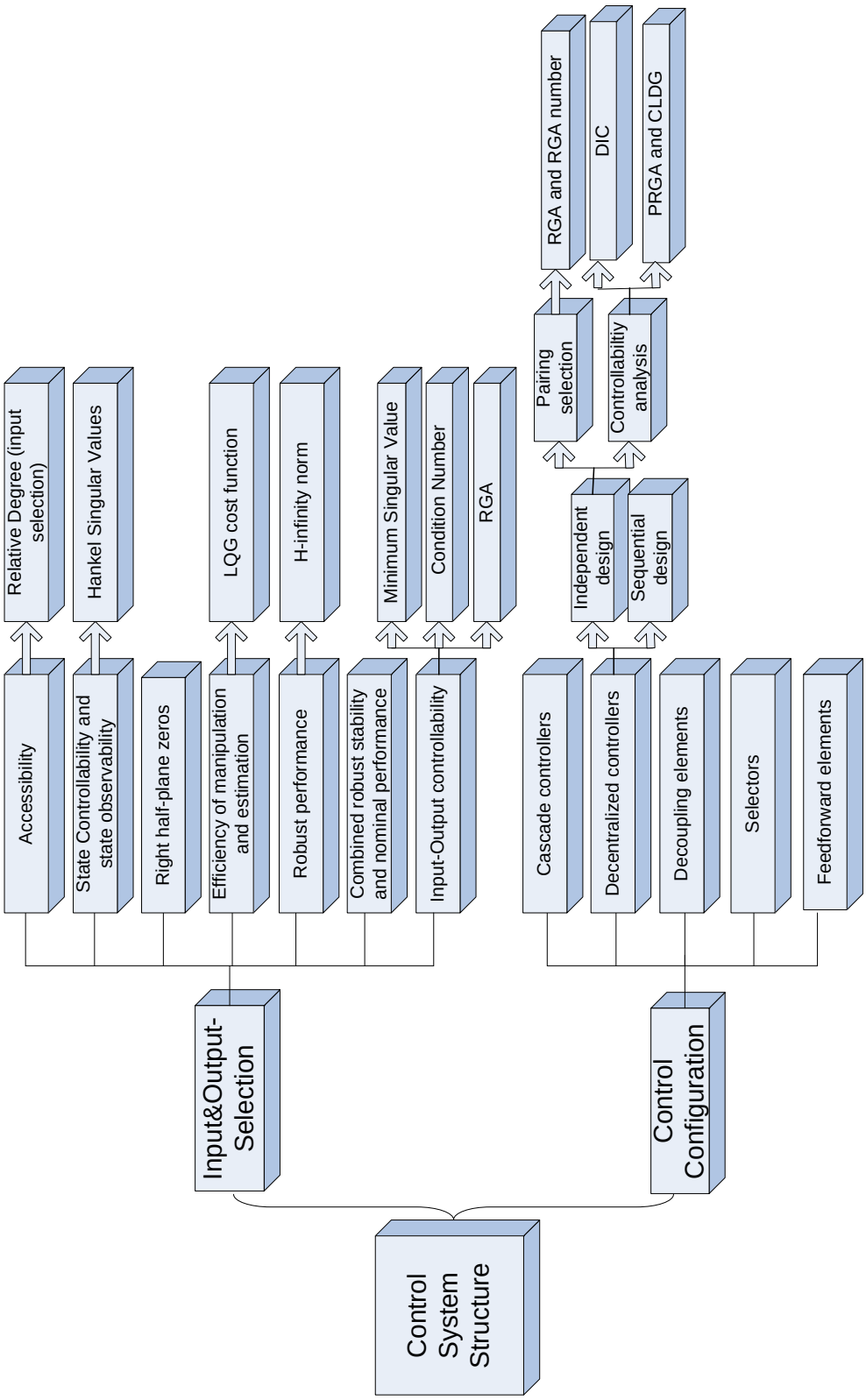

Figure 2.2: Conventional aspects of the control structure selection

2.3.3 Relative Gain Array (RGA) and RGA number

The RGA is first introduced by Bristol (1966). It is a non-singular square complex matrix defined as the ratio between the gain of an element G_{ij} in the transfer matrix G when all loops are open and the gain of the same element when all the other loops are perfectly controlled. It can be expressed as:

$$\Lambda(s) = G(s) \times (G^{-1}(s))^T \tag{2.6}$$

where G(s) is the system transfer function, $\times$ denotes element-by-element multiplication. There are some useful control properties:
(a) Large RGA elements (typically, more than 5 or larger) at frequencies important for control indicate that the plant is fundamentally difficult to control due to strong interactions and sensitivity to uncertainty.

- Uncertainty in the input channels (diagonal input uncertainty). Plants with large RGA elements (at crossover frequency) are fundamentally difficult to control because of sensitivity to input uncertainty, e.g. caused by uncertain or neglected actuator dynamics. In particular, decouplers or other inverse-based controllers should not be used for plants with large RGA elements.
- Element uncertainty. As implied by algebraic property above, large RGA elements imply sensitivity to element-by-element uncertainty. However, this kind of uncertainty may not occur in practice due to physical couplings between the transfer function elements. Therefore, diagonal input uncertainty (which is always present) is usually of more concern for plants with large RGA elements.

(b) RGA and RHP-zeros. If the sign of an RGA element changes as the frequency goes from $w = 0$ to $w = \infty$, then there is a RHP-zero in G or in some subsystem of G.

(c) RGA and decentralised control. The usefulness of the RGA for control design is summarized by the two pairing rules:

- Prefer pairings such that the rearranged system, with the selected pairings along the diagonal, has an RGA matrix close to identity at frequencies around the closed-loop bandwidth. It addresses the subsystem closed-loop performance.
- Pairing on negative steady-state RGA elements may cause the stability issues which

should be avoided.

(d) RGA number. The RGA number can be used to measure diagonal dominance, by the simple quantity:

$$RGA_{number} = ||\Lambda(s) - I||_{sum} \tag{2.7}$$

where $||A||_{sum} = \sum_{i,j} |a_{i,j}|$ (The sum norm) (Skogestad and Postlethwaite (2000)). For decentralized control we prefer pairings for which the RGA-number at crossover frequencies is close to 1 and we first rearrange the inputs and outputs to make the plant diagonally dominant with a small RGA-number.

There are many successful applications using the RGA to guide controller design for the MIMO system (Havre and Skogestad (1996); Hovd and Skogestad (1992); Skogestad and Havre (1996)). However, RGA is criticized by the assumption of the perfect control of the subsystem (for frequencies up to the desired bandwidth) (Balestrino and Landi (2006); Haggblom (1997); Schmidt (2002)). Haggblom (1997); Schmidt (2002) also indicated that the RGA is an acceptable tool only for 2×2 system. The alternative methods, i.e. Partial Relative Gain (PRG) and decentralised Relative Gain (dRG) can be used for the system with the order higher than 2.

In addition to RGA, Table 2.2 illustrates several methods which can be used for IO selection of decentralised control system, more details about each method can be found in coresponding references. Note that, they are grouped by three different approaches. The first approach is to pair the IO based on stability considerations, the second one is to focus on the performance of the closed loop system, and the last approach is to consider the disturbance rejection. The methods can be combined together to achieve all three objectives, i.e. a first analysis can be performed using the classical RGA method, then the Niederlinski Index (NI) can be applied, after discarding the negative pairings, if necessary Performance Relative Gain Array (PRGA) can be used to assess the closed-loop performance with the selected pairing. Relative Omega Array (ROMA) is different from the other method, it maintains all properties of static RGA index, but it considers dynamics of the process under test with simple autotuning. All critical frequencies can be measured from autotuning tests, it may be easily performed on line and the knowledge of the model of the process is unnecessary.

Table 2.2: System configuration method for the decentralized control

No.	Method	System Stability	Closed-loop performance	Disturbance rejection	Model free	References
1	Niederlinski Index (NI)	V				Chiu and Arkun (1991); Niederlinski (1971)
2	Relative Gain Array (RGA) and RGA number	V				Bristol (1966) Skogestad and Postlethwaite (2000)
3	Partial Relative Gain (PRG)	V				Haggblom (1997)
4	Iterative RGA	V				Wolff (1994)
5	Decentralized Integral controllability (DIC)	V				Skogestad and Morari (1998)
6	Performance Relative Gain Array (PRGA)		V			Hovd and Skogestad (1992)
7	Closely Related Closed Loop Disturbance Gain (CLDG)			V		Hovd and Skogestad (1992)
8	Block Decentralized Performance Degradation (BDPD)	V	V			Reeves (1991); Schmidt (2002)
9	The Block Relative Gain (BRG)	V				Manousiouthakis et al. (1986)
10	Dynamic Block Relative Gain (DBRG)	V	V			Arkun (1987)
11	The SSV interaction measure ($\mu - measure$)	V				Grosdidier and Morari (1986)
12	Direct Nyquist Array (DNA)	V				Rosenbrock (1970) Maciejowski (1989)
13	Decentralized Relative Gain (dRG)	V	V			Schmidt (2002)
14	Ratio X and $\xi - measure$		V			Schmidt (2002)
15	Ratio $X_d and \xi_d - measure$			V		Schmidt (2002)
16	Relative Omega Array (ROMA)				V	Balestrino and Landi (2006)

2.4 Genetic Algorithm optimisation

The Genetic Algorithm (GA) is a stochastic global search method that is based on the principles of the natural evaluation and population genetics, aiming to find the best solution for the given problem. The searching process works with a group of individuals, each coded either in a set of binary strings or using real numbers representing a possible solution to the given problem. The group is called a population. A fitness value is assigned to each individual according to the suitability of that individual to the solution, and the suitability is assessed by the fitness function of the given problem. The individuals with the highest fitness value survives to reproduce, crossbreed and mutate to produce a new offspring. Then after many generations, a wide space will converge to one optimal solution (Goldberg (1989); Goldberg and Richardson (1987)). GA also provides a way for the multi-objective optimization in which the objectives conflict with each other, trade-offs exist between these objectives. In this case, the optimization results from GA consist of multiple non-dominated solutions (Coello and Fleming (1999); Deb (2001); Fonseca and Fleming (1993); Srinivas and Deb (1994)).

The Department of Automatic Control and Systems Engineering at the University of Sheffield produced a toolbox for the single and multi-objective GA application (Chipperfield et al. (1994a,b). Also, a toolbox for the Nondominated Sorting Genetic Algorithms II ($NSGA_{II}$) is available in Seshadri (2009), which shorts the design cycle for a variety of applications. The work left for the GAs application are the set of search spaces, number of generation and population, design of the objective functions and constraints based on the requirements of the given problem.

GA has been widely used in a variety of problems. In railway engineering, there are a number of published work related to GA optimization. Mei and Goodall (2000) applied LQG control to the active steering of solid axle railway vehicles, and GA is adopted to compromise the parameters of the controller to stabilize the vehicle without interfering with the natural curving/centering actions of the solid axle wheelset and with minimum control effort. Also, Mei and Goodall (2002) presented a GA optimization process for the design of inter-vehicle vertical active suspension controllers. The optimization results achieved the best compromise between ride-quality and suspension deflection

for active suspensions. Persson and Iwnicki (2004) used GA to produce optimized wheel profiles. More recently, Zamzuri et al. (2006a) employed Genetic Algorithms to optimize the controller parameter and Fuzzy membership functions for his research on Fuzzy-PID tilting control. Michail et al. (2008) proposed a systematic approach for selecting the minimum number of sensors for an electromagnetic suspension system that satisfies both optimized deterministic and stochastic performance objectives. The performance is also optimized by tuning the controllers (LQG and H_∞) with GA.

2.5 Embedded digital control

With the development of the computer technology, digital control becomes popular which uses digital computers to act as system controllers instead of using analog electronics. The normal digital control scheme is shown in Figure 2.3.

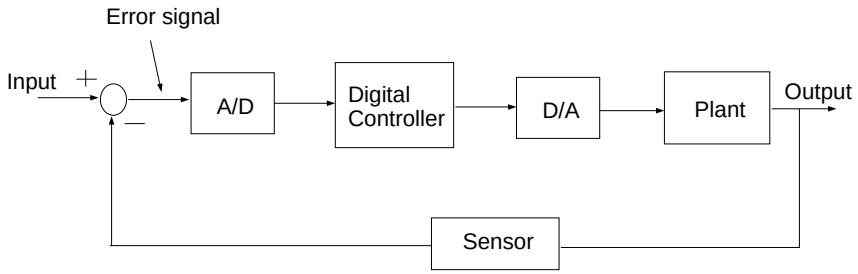

Figure 2.3: Digital control system

The interface at the input of the digital controller is an analog-to-digital (A/D) converter, and is required to convert the continuous error signal into a form that can be readily processed by the digital controller. At the controller output a digital-to-analog (D/A) converter is required to convert the binary signals of the computer into a analog form to drive the plant (Phillips and Nagle (1990)). The digital controller can take the form of a microcontroller, an ASIC or a standard desktop computer depending on the design requirements. Also, the Laplace transform is replaced with the z transform in the digital control, which converts a discrete time-domain signal into a complex frequency-domain representation. There are several ways to transfer the complex variable s to z:

Zero order hold transform:

$$s = \frac{1}{T} ln(z) \tag{2.8}$$

Bilinear (Tustin) transform:

$$s = \frac{2}{T} \frac{z-1}{z+1} \tag{2.9}$$

where T is the sampling interval. Bilinear transform is relatively accurate and commonly used by control engineers when sampling rate ares relatively high.

The sampling rate is defined as the rate at which analogue input values are sampled or processed, and determines the required speed of the controller implementation. In order to obtain a stable digital control system, the well known Nyquist sampling theorem requires that the minimum sampling frequency to be greater than twice the highest frequency of the signal bandwidth, but practically real-time control requires the sampling rate to be 100 times of the controller bandwidth to keep the phase lag introduced by the sampling within 5^0 (Goodall (2001)). Slow sampling frequency results in poor control performance, but when the sampling frequency is extremely high, significant numerical problems may be introduced, which results in the system being highly sensitive to coefficient variation. The δ transform is introduced to overcome this issue (Forsythe and Goodall (1991)). However, for a practical control system, the sampling rate is always limited by the computational processor, algorithm complexity as well as device inter-communication speeds.

Another issue for digital control systems implementation is the type of binary numeric representation. It can significantly affect the behavior and performance of the controller. Fixed-point arithmetic represents the number in a fixed range with a finite number of bits (word length = integral bits + fractional bits), which is used by the most microcontrollers and some DSPs, e.g. TMS320LF2407 for the motion control. To improve computational efficiency, state variables and coefficients must be scaled to fit the word length provided by the processor. There is always a trade-off between the word length arrangement and the computational precision. Also, internal variable overflow/underflow is also needed to be considered during the design process, particularly for the fully integral arithmetic. Floating point arithmetic provides wider dynamic range and usually gives higher precision than fixed-point arithmetic. Although the

floating-point arithmetic is generally slower, expensiver and more difficult to implement in hardware, it provides an easy solution for the implementation of control algorithms designed in floating-point data type. Texas Instruments (TI) company provides TMS320c6xxx floating point DSP. Also, many Float Point Units (FPU) for FPGAs are designed to perform the floating-point arithmetic, e.g. Xilinx Microblaze soft processor provides an optional IEEE-754 compatible single-precision Floating-Point Unit (FPU) (Xilinx).

2.6 Summary

In this chapter, the survey and study on local tilting control, lateral active secondary suspension control, MIMO system configuration, control and optimization as well as the embedded digital control are presented. It provides a basic foundation for the research in the following chapters. The integrated tilt and active lateral secondary suspension control, which is suggested to be a solution to further enhance the local tilting control performance has not been studied previously. The vehicle system integrated tilt and lateral actuators can be controlled either by the separated SISO controllers or the MIMO controller. Furthermore, RGA provides a method for the system control loops interaction analysis. Finally, the sampling rate and word length are the main issues encounted during the Hardware-In-the-Loop (HIL) design.

Chapter 3

Railway track geometry, active suspension design requirements and assessment approaches

In this chapter, active suspension design requirements and assessment approaches for the integrated tilt and active lateral secondary suspension are presented after a brief introduction of the railway track geometry. The controller design for the integrated tilt and active lateral secondary suspension needs to meet both tilting performance and active lateral suspension design requirements, which is a multi-objective optimisation process.

3.1 Railway track geometry

The railway track is subdivided into two types:
(1) Deterministic track (or design track), such as curves, gradients as well as steps, dips, short ramps, etc..
(2) Stochastic track (or track irregularities), i.e. random changes in the track vertical, lateral and cross-level position.

The lateral features of railway track are discussed in this section, which is used to assess

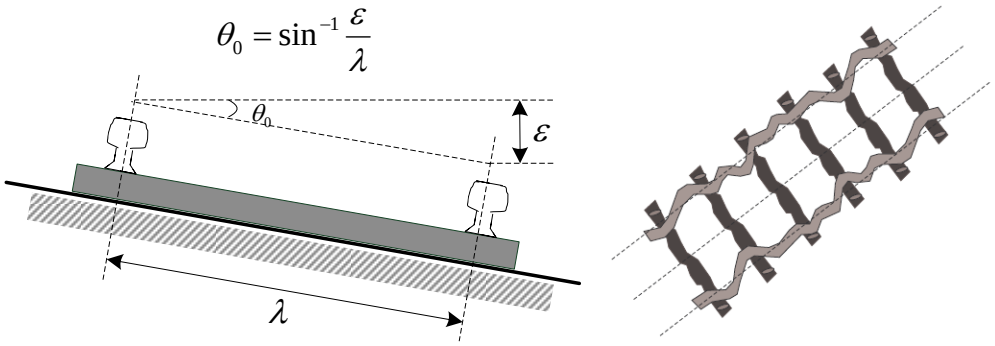

(a) Canted track (b) Track irregularity

Figure 3.1: Railway track

the performance of the integrated tilt and active lateral secondary suspension control in this research.

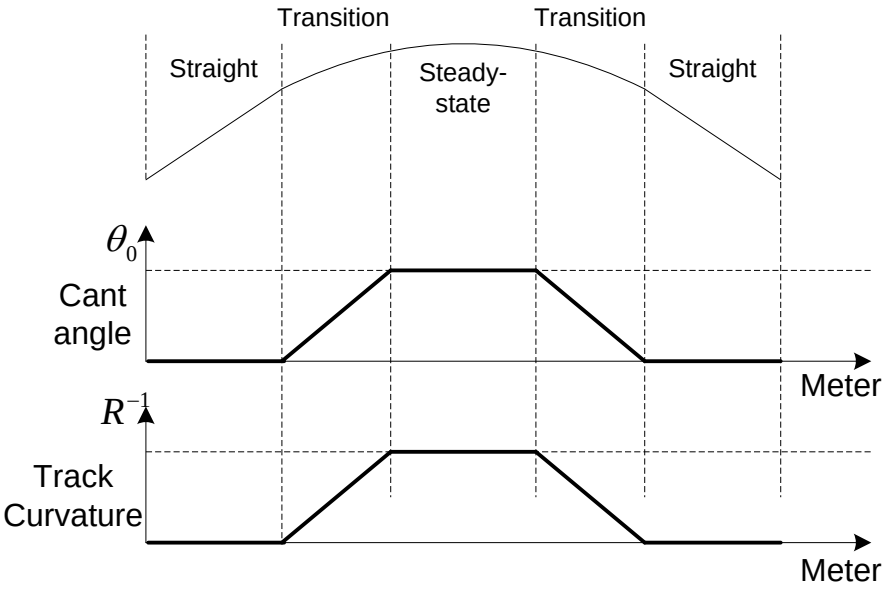

Figure 3.2: Curved track section

3.1.1 Deterministic curved track

The basic characteristics of the curved track are illustrated in Figure 3.1(a) (λ is the track gauge, 1435 mm for a standard gauge) and Figure 3.2. Curved track consists of two transitions and one steady-state section. The value of track curvature($\frac{1}{R}$) and cant angle (θ_0) are varied (increase/decrease) linearly during the transitions simultaneously, reach to the maximum at the steady-state section. This simultaneous variation produces a complex feature of the transition and introduces a complex dynamics response from railway vehicles, such as the coupled lateral and roll dynamics modes of the vehicle body.

3.1.2 Stochastic straight track

Straight track irregularities (shown in Figure 3.1(b)) are mainly caused by the track misalignment. For simulation purpose, the lateral track spatial spectra can be approximately expressed as:

$$S_s(f_s) = \frac{\Omega_l}{{f_s}^3} \quad m^2(cycle/m)^{-1} \tag{3.1}$$

in which, Ω_l is the track roughness, f_s is the spatial frequency (Pratt (1996)). It needs to be converted to temporal frequency for the dynamic analysis.

Due to

$$f_s(cycles/m) = \frac{f_t(cycles/s)}{v(m/s)} \tag{3.2}$$

That means a given wavelength would excite the vehicle with a different frequency at a different speed. Thus, the track wavelengths in terms of the temporal frequency f_t can be given by

$$S_s(f_t) = \frac{\Omega_l v^3}{{f_t}^3} \quad m^2(cycle/m)^{-1} \tag{3.3}$$

Also, $S_s(f_t)$ can be converted to a spectrum with a temporal base by performing the following division:

$$\begin{aligned} S_T(f_t) &= \frac{S_s(f_t)}{v} \\ &= \frac{\Omega_l v^2}{2\pi f_t^3} \quad m^2(rad/m)^{-1} \end{aligned} \tag{3.4}$$

Then the derivative of the above spectrum is derived by:

$$\begin{aligned} \dot{S}_T(f_t) &= S_T(f_t) \times (2\pi f_t)^2 \\ &= \frac{(2\pi)^2 \Omega_l v^2}{f_t} \quad (m/s)^2 (Hz)^{-1} \end{aligned} \tag{3.5}$$

This represents the velocity of the track spectrum and is used in this research. It can be easily seen that the lateral track velocity represents a colored noise and has a steady roll-off as frequency increases. An appropriately defined shaping filter was used to shape the noise spectrum. Further details about the modelling railway track can be found in Paddison (1995); Pratt (1996).

3.2 Design requirements and assessment approaches for the integrated tilt and active lateral secondary suspension control

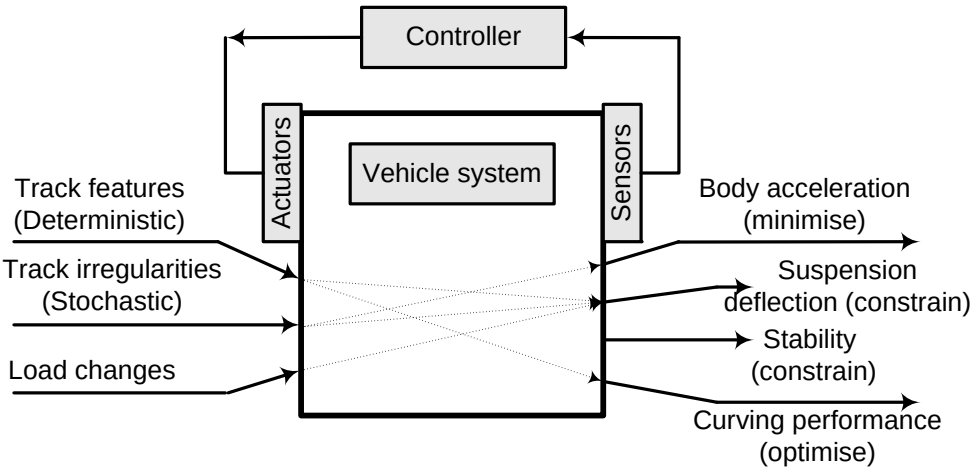

Figure 3.3: Active suspension design requirements

The overall railway vehicle active suspension control system is shown in Figure 3.3. Track features, track irregularities and load changes are the main inputs to the active suspensions. Then the design of the suspension controller needs to minimize the body acceleration on straight track, consider the constraints for suspension deflection (to avoid the bump stop) and system stability during curving (i.e. derailment), and

optimize the curving performance. Tilting is a special secondary railway suspension, main requirements are to reduce the lateral acceleration perceived by the passengers on curves and to provide a comfortable response during curve transitions, and maintain a good ride quality on straight track at the same time. System performance requirement and control assessment approaches for active railway suspensions as well as tilting design are detailed in Goodall and Mei (2006); Goodall et al. (2000).

Controller design for the integrated tilt and active lateral secondary suspension control needs to meet both the tilting performance requirements and the lateral suspension requirements, which is divided into two parts based on the track profile and summarized as follows:

Deterministic performance criterion:

• Maintain appropriate curve transition comfort levels for standing and seated passengers, it is qualified by P_{ct} value (Goodall et al. (2000)), which provides the percentage of (both standing and seated) passengers who feel uncomfortable during the curve transition, and can be calculated with the vehicle body lateral acceleration, lateral jerk and roll rate. More details can be found in Appendix A.

• Further, the tilt controller assessment also relies upon identifying what a tilting vehicle would ideally perform on the transition from straight to curved track and then quantifying the deviation of the actual response compared with this ideal.
(1) Minimize the R.M.S. value of the deviation between actual measured body lateral acceleration ($\ddot{y}_{bm}^{actual}$) from the dynamics simulation compared with the ideal tilting case ($\ddot{y}_{bm}^{ideal}$).

$$R.M.S._{Acceleration\ deviation} = \sqrt{\sum_{i=1}^{N}(\ddot{y}_{bm}^{actual} - \ddot{y}_{bm}^{ideal})^2} \tag{3.6}$$

(2) Minimize the R.M.S. value of the absolute body roll velocity deviation between measured ($\dot{\theta}_{bm}^{actual}$) and ideal ($\dot{\theta}_{bm}^{ideal}$) responses.

$$R.M.S._{Roll\ rate\ deviation} = \sqrt{\sum_{i=1}^{N}(\dot{\theta}_{bm}^{actual} - \dot{\theta}_{bm}^{ideal})^2} \tag{3.7}$$

• Associated with ride quality improvement is the constraint on lateral suspension deflection, which should not exceed the maximum available before bump stops are reached. A maximum of $\pm 60mm$ is used in this study.

Note that the calculation of the R.M.S. deviation error is based in the time interval between 1s before the start of the curve transition and 3.6s after the end of the transition, as shown in Figure 3.4.

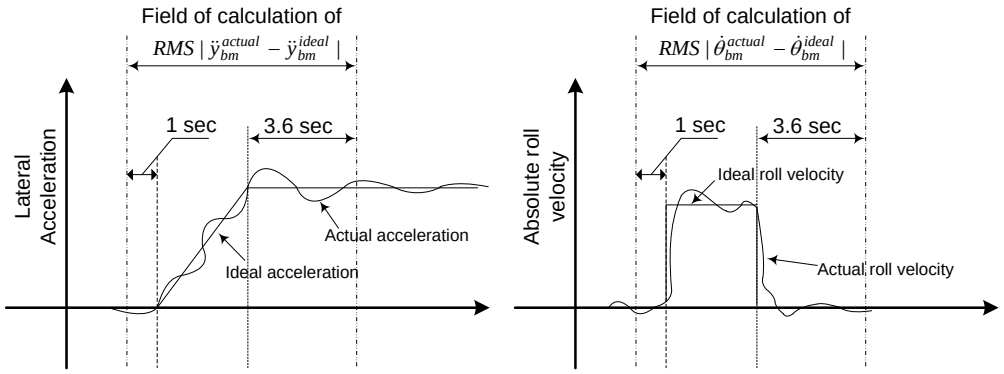

(a) Lateral acceleration (b) Body roll velocity

Figure 3.4: Calculation of dynamics effects on lateral acceleration and body roll velocity for curved track assessments

Stochastic performance criteria:

• Straight-track ride quality at no more than 7.5% worse compared to the non-tilting train equivalent at high speed; aim to provide the minimization of ride quality (in terms of passenger lateral acceleration measurement) by the lateral actuator. It is assessed by the R.M.S. value of the measured body lateral acceleration.

3.3 Design benchmark for this research

(1) The benchmark for the integrated tilt and active lateral secondary suspension control design in this research is the Precedence Tilting (tilt-only) control with passive secondary suspensions (PT control), which represents the current industry state-of-the-art, a non-local tilting control strategy, the performance of which is hoped to match or

exceed using a local control strategy. The integrated tilt and active lateral secondary suspension control aims to provide a better performance compared to PT control.

(2) Also, Nulling Tilting (tilt-only) with PI control (NT control) with passive secondary suspensions is used to provide the comparison with classical dual-actuator control for the integrated tilt and active lateral secondary suspension in following chapters. The design process and simulation results of the PT and NT control can be found in Zolotas (2002a); Zolotas and Goodall (2007a); Zolotas et al. (2007b).

Chapter 4

Active Anti-Roll Bar (ARB) with integrated active lateral secondary suspension control

In this chapter, modelling and control for the integrated active ARB with active lateral secondary suspensions are presented. The simplified mechanical configuration is illustrated in Figure 4.1.

The active ARB is configured by a transversely-mounted torsion tube on the bogie with vertical links to the vehicle body, except that one of the links is replaced by a tilt actuator, and thereby applies tilt via the torsion tube. In this research, a lateral actuator is installed between the vehicle body and bogie in parallel with the original secondary damper. The original secondary damper also can be replaced by the lateral actuator, but keeping the original damper reduces the maximum force required for the lateral actuator. In this configuration, the actuators for the tilt suspension and lateral suspension can be easily fitted as an optional extra during manufacture. If actuators lose control, the system can roll back to the non-tilting train with passive suspension system.

The control system design for this dual-actuator system is carried out in both decentralised and centralised way. In this chapter, Classical Decentralised control, H_∞-based

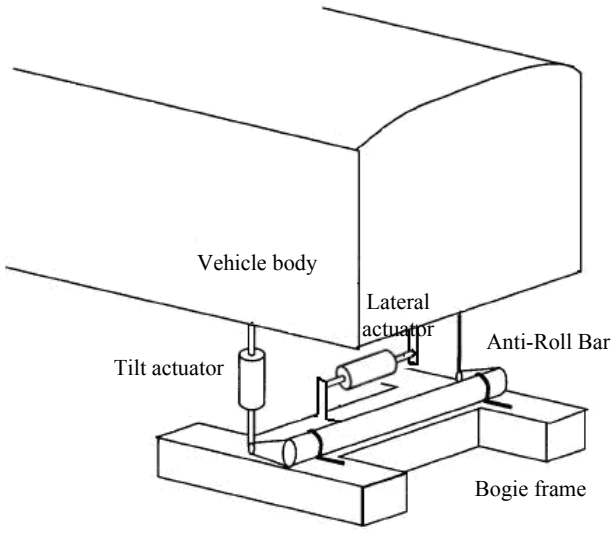

Figure 4.1: The integration of roll and lateral actuators

Decentralised control and LQG centralised control are designed. Genetic Algorithm is employed to optimize the controller parameters due to the multiple design requirements. The design process is based on a 4 DOF end-view linear model, but the controllers can be directly applied to a 9 DOF full vehicle model, which is discussed in Chapter 7.

4.1 End-view modelling and validation

4.1.1 Vehicle modelling

The model is originally designed by Dr. Zolotas in his Ph.D thesis for the study on advanced control strategies for high speed tilting trains (Zolotas (2002a)). This has been extended by adding a lateral actuator into the system and its dynamic effects on the model are mainly addressed in this section.

Figure 4.2 shows the end-view scheme of a railway vehicle. The lateral and roll degrees of freedom for both the body and the bogie systems are included in this model while the vertical degrees of freedom are ignored, although the effects of the roll stiffness and damping introduced by the vertical suspension are included. A rotational displacement actuator shown by δ_a is included in series with the roll stiffness. Moreover, a lateral

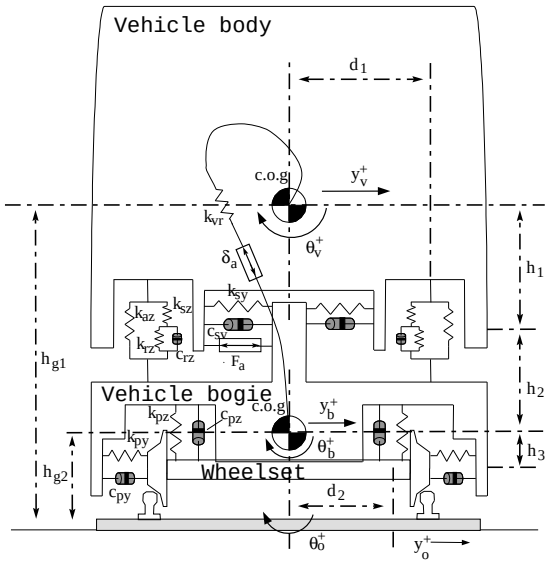

(a) Vehicle end-view model

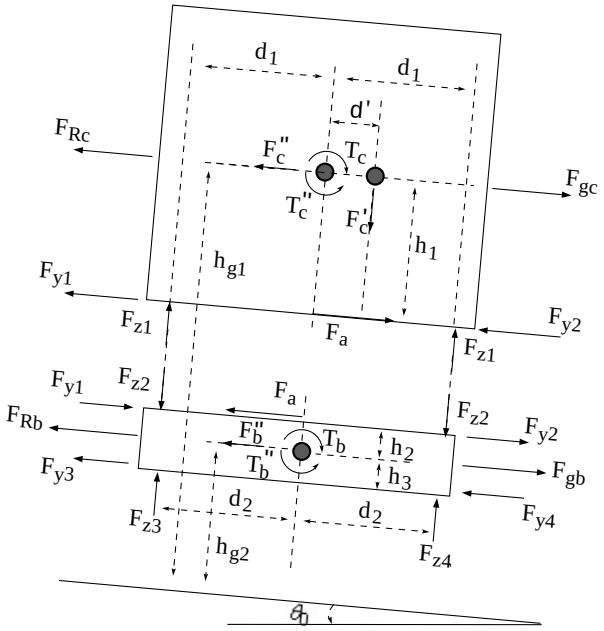

(b) Force analysis

Figure 4.2: End-view modelling

actuator shown by F_a is installed in parallel with the original lateral damper between the bogie and the body. Both actuators are assumed to be ideal. Since in this study the focus is on the behavior of the roll and lateral motion of the vehicle, the effect of the wheelset dynamics is incorporated simply by using a 2rd order low pass filter with $20Hz$ cut-off frequency and 20% damping.

The primary (bogie-wheelsets) lateral, primary vertical and secondary (body-bogie) lateral suspensions are modeled by pairs of parallel spring/damper combinations. A representation of a pair of air-springs is used to model the roll effect of the secondary vertical suspension. Via the Newtonian approach, the 4 DOF end-view model is illustrated below.
Body lateral dynamics:

$$\begin{aligned} m_v\ddot{y}_v &= -2k_{sy}(y_v - h_1\theta_v - y_b - h_2\theta_b) - 2c_{sy}(\dot{y}_v - h_1\dot{\theta}_v - \dot{y}_b - h_2\dot{\theta}_b) \\ &\quad -\frac{m_v v^2}{R} + m_v g\theta_0 - h_{g1}m_v\ddot{\theta}_0 + F_a \end{aligned} \tag{4.1}$$

Body roll dynamics:

$$\begin{aligned} i_{vr}\ddot{\theta}_v &= 2h_1k_{sy}(y_v - h_1\theta_v - y_b - h_2\theta_b) + 2h_1c_{sy}(\dot{y}_v - h_1\dot{\theta}_v - \dot{y}_b - h_2\dot{\theta}_b) \\ &\quad -k_{vr}(\theta_v - \theta_b - \delta_a) - F_a h_1 + m_v g(y_v - y_b) - 2{d_1}^2 k_{az}(\theta_v - \theta_b) \\ &\quad -2{d_1}^2 k_{sz}(\theta_v - \theta_r) - i_v r\ddot{\theta}_0 \end{aligned} \tag{4.2}$$

Bogie lateral dynamics:

$$\begin{aligned} m_v\ddot{y}_b &= 2k_{sy}(y_v - h_1\theta_v - y_b - h_2\theta_b) + 2c_{sy}(\dot{y}_v - h_1\dot{\theta}_v - \dot{y}_b - h_2\dot{\theta}_b) \\ &\quad +2k_{py}(y_b - h_3\theta_b - y_0) - 2c_{py}(\dot{y}_b - h_3\dot{\theta}_b\dot{y}_0) \\ &\quad -\frac{m_v v^2}{R} + m_v g\theta_0 - h_{g1}m_v\ddot{\theta}_0 - F_a \end{aligned} \tag{4.3}$$

Bogie roll dynamics:

$$\begin{aligned} i_{br}\ddot{\theta}_b &= 2h_2k_{sy}(y_v - h_1\theta_v - y_b - h_2\theta_b) + 2h_2c_{sy}(\dot{y}_v - h_1\dot{\theta}_v - \dot{y}_b - h_2\dot{\theta}_b) \\ &\quad -2h_3k_{py}(y_b - h_3\theta_b - y_0) + c_{py}(\dot{y}_b - h_3\dot{\theta}_b - \dot{y}_0) + k_{vr}(\theta_v - \theta_b - \delta_a) \\ &\quad +2{d_1}^2 k_{az}(\theta_v - \theta_b) + k_{sz}(\theta_v - \theta_r) \\ &\quad -2{d_2}^2(k_{pz}\theta_b + c_{pz}\dot{\theta}_b) - i_{br}\ddot{\theta}_0 - F_a h_2 \end{aligned} \tag{4.4}$$

For the additional air-spring state (more details can be found in Appendix B):

$$\dot{\theta}_r = -\frac{k_{sz} + k_{rz}}{c_{rz}}\theta_r + \frac{k_{sz}}{c_{rz}}\theta_v + \frac{k_{rz}}{c_{rz}}\theta_b + \dot{\theta}_b \tag{4.5}$$

An 'end-moment' effect: $m_v g(y_v - y_b)$ is included in (4.2) which models the roll effect of the body weight due to the lateral displacement of its centre of gravity (c.o.g.). Both the translation and rotation of the reference axis associated with curves are considered in the equations. The dynamic interactions between the lateral and roll motions are obvious from this model. The equations of motion described above can be arranged into a state space model:

$$\begin{aligned} \dot{x} &= Ax + Bu + \Gamma w \\ y &= Cx + Du + Hv \end{aligned} \tag{4.6}$$

System states:

$x = [y_v \;\; \theta_v \;\; y_b \;\; \theta_b \;\; \dot{y}_v \;\; \dot{\theta}_v \;\; \dot{y}_b \;\; \dot{\theta}_b \;\; \theta_r]'$

Control inputs:

$u = [\delta_a \;\; F_a]'$ δ_a: Tilt angle command; F_a: Actuator force command;

Track disturbance:

$w = [R^{-1} \;\; \dot{R^{-1}} \;\; \theta_0 \;\; \dot{\theta_0} \;\; \ddot{\theta}_0 \;\; y_0 \;\; \dot{y_0}]'$

For the purpose of the simulation, the disturbance parameters (θ_0, $\dot{\theta_0}$, y_0) are included in matrix A and the rest of disturbance signals w are included in B matrix. The state space matrices form can be seen in Appendix C. The parameters for the vehicle and suspension components are based upon a typical high speed passenger vehicle and are listed in Appendix D.

The vehicle model and control system are tested with specific track inputs including both deterministic (low frequency signals) and stochastic (high frequency signals) features. The deterministic track input was a curved track with a radius of $1000m$ and a maximum track cant angle (θ_{0max}) of 6^0, with a transition ($150m$) at the start and end of the steady curve. The stochastic track inputs represent the irregularities in the

track alignment on both straight track and curves, and these were characterised by an approximate spatial spectrum equal to $(2\pi)^2\Omega_l v^2/f_t(m^2/(cycle/m))$ with a lateral track roughness (Ω_l) of $0.33 \times 10^{-8}m$.

4.1.2 Model validation and analysis

4.1.2.1 Mode validation

The system is dynamically complex with strong coupling between the lateral and roll modes of the vehicle body which results in two sway modes combining both lateral and roll movement. An 'upper sway' mode, its node appears above the body c.o.g., characterised predominately by a roll movement; and a 'lower sway' mode, its node located below the body c.o.g., characterised predominantly by a lateral motion.

Table 4.1: Vehicle dynamics modes (Active ARB tilting)

Mode	Damping(%)	Frequency(Hz)
Body lower sway	10.49	0.65
Body upper sway	17.22	1.52
Bogie roll	20.66	11.13
Bogie lateral	9.06	26.88
Airspring	100	3.69

The mode analysis is shown in Table 4.1, with the frequency of modes being close to the industrial-norm, damping is changed due to the damper coefficients of the lateral secondary suspension being reduced. Active lateral secondary suspension control can provide more damping for these modes. Figure 4.3 shows the pole-zero map for the vehicle dynamics model, the RHP (Right-Half Plane) zeros illustrate the non-minimum phase feature of the system. It is caused by the roll dynamics and is evident particularly when the train starts to negotiate the transition (vehicle body rolls out of the curve with a small angle at the start of the transited curve).

4.1.2.2 State analysis

The eigenstructure of the model is analysed via straightforward modal analysis starting from the non-diagonal state matrix and, using similarity transformations, getting a

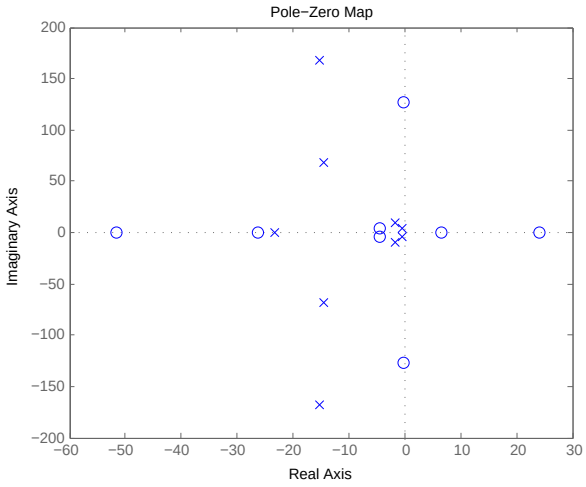

Figure 4.3: Pole-zero map for the vehicle model

diagonal form in which the diagonal elements are the eigenvalues of the system. The transformations can be done by

$$z = T^{-1}x \tag{4.7}$$

T is the modal matrix with each column representing the motion along the coordinate axes of the state vector for a particular mode, thus providing useful information on the participation of states for each of the system modes. Figure 4.4 shows the state participation for the body upper and lower sway, also the bogie modes. The main points to note are the roll contributions for the body upper and bogie roll modes, and the lateral contributions for the body lower and bogie lateral modes.

4.2 Classical Decentralised control

In this section, the Classical Decentralised (CD) control is studied with two separated control loops for the tilt and lateral actuators. Skyhook damping control is employed for the lateral actuator and Approximate PID controller is designed for the tilting control. It is an intuitive control configuration for this integrated suspension system and is also the easiest strategy for the real train implementation. A sequential design process is used because the lateral actuator control loop is a high bandwidth strategy

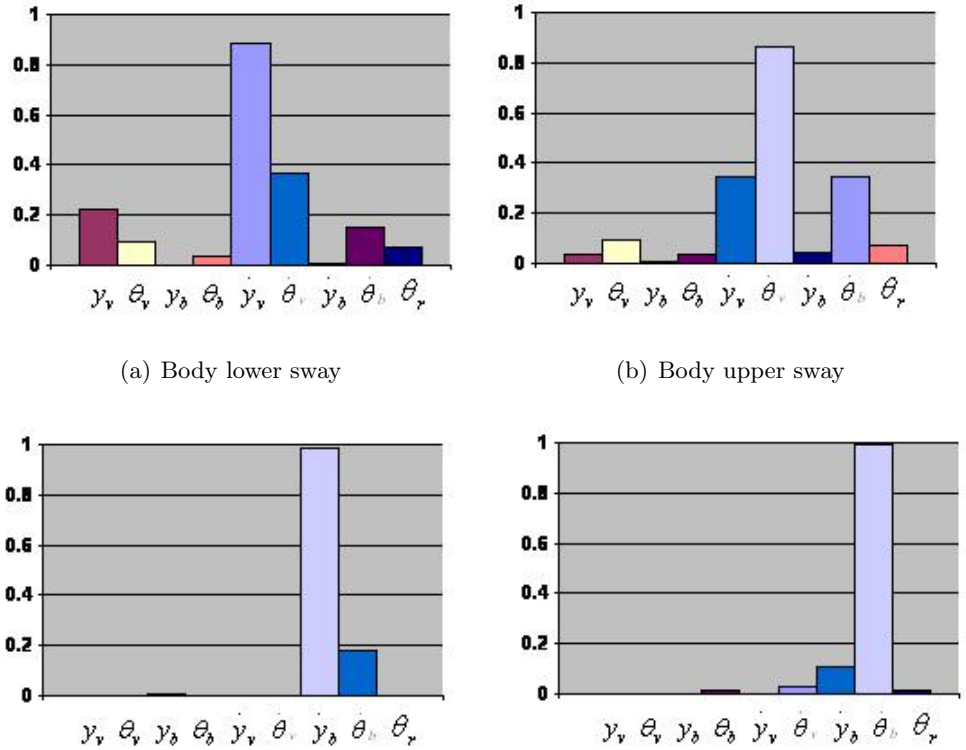

(a) Body lower sway

(b) Body upper sway

(c) Bogie lateral

(d) Bogie roll

Figure 4.4: State participation for the main vehicle modes

that mainly responds to the high frequency track irregularity (2-10Hz), which is faster than the tilting action (responding to the low frequency curved track (below 1Hz)). Controller parameters are tuned by Genetic Algorithm to obtain the best simulation performance.

4.2.1 Active lateral secondary suspension control

The complementary filter skyhook damping control combined with the integral of the lateral secondary suspension deflection is designed for the lateral actuator control in this study, which has the function to improve the lateral ride quality whilst keeping the deflection within the required limit to avoid the lateral bump stop. It is a better solution compared with the semi-active damper combined with a hold-off device (Streiter et al. (2001)). Figure 4.5 shows the overall configuration. A pair of complementary second

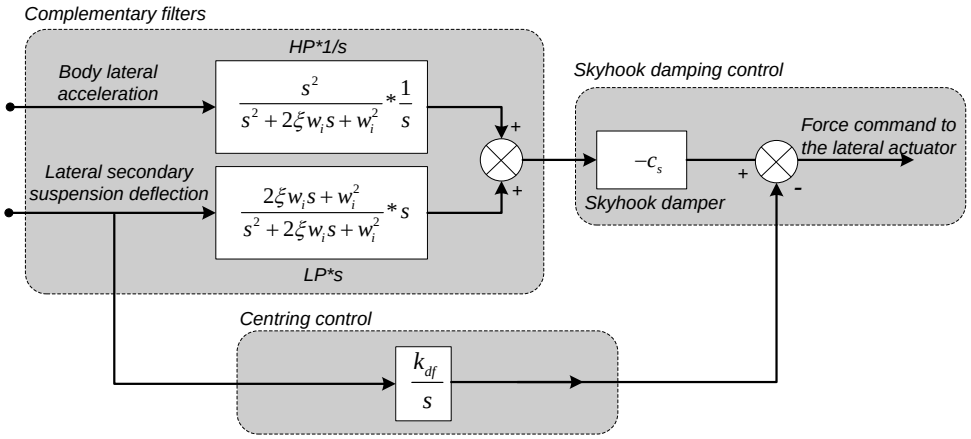

Figure 4.5: Complementary filter skyhook damping control

order filters (High Pass + Low pass = 1) with flat "Butterworth response" are utilised. The Low Pass filter (LP) combined with a derivative of suspension deflection, plus the High Pass filter (HP) combined with an integrator processing the measured lateral acceleration together generate a composite lateral damping command and feed into the skyhook damper coefficient, which in turn feeds into the lateral actuator as the force command. The LP acts to minimise suspension excursion which is predominantly low frequency effect, the HP provides the ride improvement function. Furthermore, the integral of the lateral secondary suspension deflection is added to the lateral actuator control loop to provide centring actions and keep the lateral suspension deflection within the limit ($60mm$).

4.2.2 Integrated tilt and active lateral secondary suspension control

Figure 4.6 is the system configuration for the integrated tilt and active lateral secondary suspension control. The effective cant deficiency (e.c.d.) is used to drive the tilting controller (See Section 2.1). Approximate PID controller (N=1000) is used for the tilting control. The vehicle forward speed used in the simulation is $58m/s$.

$$f_{A.PID} = (k_p + \frac{k_i}{s} + \frac{k_d s}{s/N+1}) \tag{4.8}$$

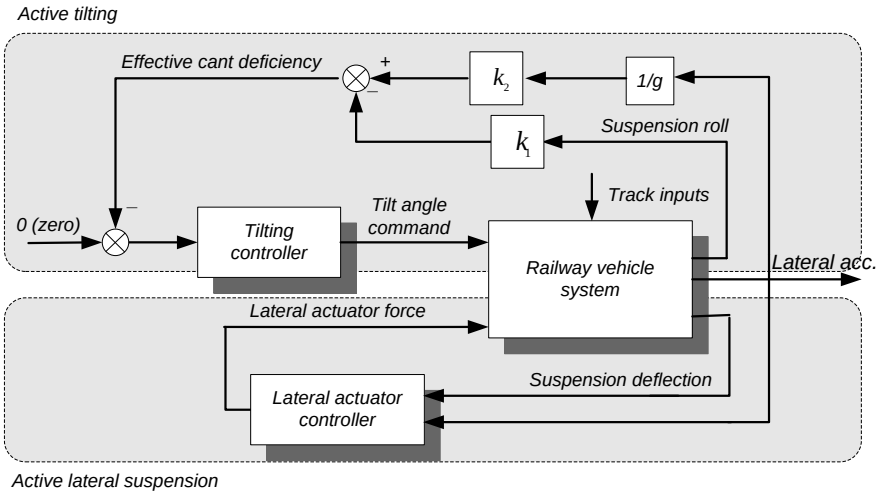

Figure 4.6: The integration of roll and lateral actuators

4.2.3 Control parameter tuning

Parameter tuning for the control system is a difficult task, which has to meet all the requirements presented in Chapter 3. There are four trade-offs between these criteria that need to be optimized:

(1) The trade-off for the tilting controller between the curving performance (P_{ct} value) and the suspension deflection. If the loop bandwidth is low enough not to interfere with the lateral suspension, it is then too slow acting on the curve transition. It is a critical problem for the local tilting control system design (the signals for the controller are just from the local vehicle).

(2) The trade-off for tilting controller performance between the curved track (P_{ct} value) and the straight track responses (R.M.S. value). The tilting train runs at higher speed on the same rail infrastructure compared with non-tilting train which deteriorates the ride-quality on the straight line and introduces a trade-off for tilting controller performance between the curved track and the straight track responses.

(3) The trade-off for the lateral actuator controller between the ride quality on the straight track (R.M.S. value) and the curving suspension deflection.

(4) The trade-off for the lateral actuator control between the actuator power consumption and overall system performance. Large lateral actuator force improves the curving performance at the expense of higher power consumption.

The integration of active 'anti-roll bar' system and active lateral secondary suspension system can help to optimize the first two trade-offs. With appropriate system configuration, the third trade-off can be optimized. The last trade-off is optimized by installing the lateral actuator in parallel with the original damper rather than replacing it. However, to achieve the performance of the local control system better than commercial precedence control is still a complicated multi-objective design process.

4.2.3.1 Manual tuning

The parameters for the lateral actuator control (cut-off frequency (w_c), skyhook damping coefficient (c_s), and coefficient for the centring control (k_{df})) can be tuned first to improve the straight track ride-quality without interfering with the suspension curving deflection. Then, the tilting controller is designed to minimize the P_{ct} value and R.M.S. value of the measured body lateral acceleration, but retuning the lateral actuator control parameters is needed because there is interaction existing between these two control loops.

4.2.3.2 Genetic Algorithm optimization

To obtain the best simulation result, the Genetic Algorithm approach, in particular the Non-dominated Sort Genetic algorithm ($NSGA\_II$, Srinivas and Deb (1994)), is used to tune the controller parameters, which are cut-off frequency (w_c), skyhook damping coefficient (c_s), coefficient for the centring control k_{df} and PID controller parameters. Objective functions designed for $NSGA\_II$ are based on the performance requirements presented in Chapter 3 and listed as follows:
(1) f_1 = the P_{ct} value for seated/standing passengers

(2) $f_2 = \sqrt{\frac{1}{n}\sum_{i=1}^{n} y_{vm}^2}$ (R.M.S. value of the measured body lateral acceleration)

(3) $f_3 = \sqrt{\frac{1}{n}\sum_{i=1}^{n}(\ddot{y}_{vm}^{actual} - \ddot{y}_{vm}^{ideal})^2}$ (R.M.S. value of the deviation between actual measured body lateral acceleration with respect to ideal cases)

(4) $f_4 = \sqrt{\frac{1}{n}\sum_{i=1}^{n}(\dot{\theta}_{vm}^{actual} - \dot{\theta}_{vm}^{ideal})^2}$ (R.M.S. value of absolute body roll velocity deviation between measured and ideal responses)

The calculation of f_3 and f_4 is based in the time interval between 1s before the start of the curve transition and 3.6s after the end of the transition, as shown in Chapter 3.

Constraint functions for $NSGA\_II$:
(1) $w_1 = f_2 \ \ when f_2 < 3.78\% g$ (the value in the passive situation: non-tilt with passive suspension system), otherwise, $w_1 = 1000$;

(2) $w_2 < 60$mm (the lateral secondary suspension deflection)

(3) $w_3 > 0$ dB (Tilting controller Gain Margin (with closed lateral actuator control loop)

(4) $w_4 > 30$ deg. (Tilting controller Phase Margin (with closed lateral actuator control loop)

(5) Constraints on the internal stability of the overall system. It is guaranteed by checking the poles for a set of internal transfer functions. More details can be found in Appendix E.

Death penalty function is used for the constraints. The initial boundaries for $NSGA\_II$ are set around the value based on the results of manual tuning. The Genetic Algorithm procedure is simulated for 300 generations with 50 populations.

Figure 4.7 illustrates the trade-off plot for the tilting control between the curving performance and straight track ride quality, '+' curve is the plot for the tilt-only Nulling Tilting (NT) control (Zolotas (2002a)), and 'o' curve is for the integrated tilt and active lateral secondary suspension control (Classical Decentralised control). It is obvious that the trade off for the local tilting control design is significantly improved by the

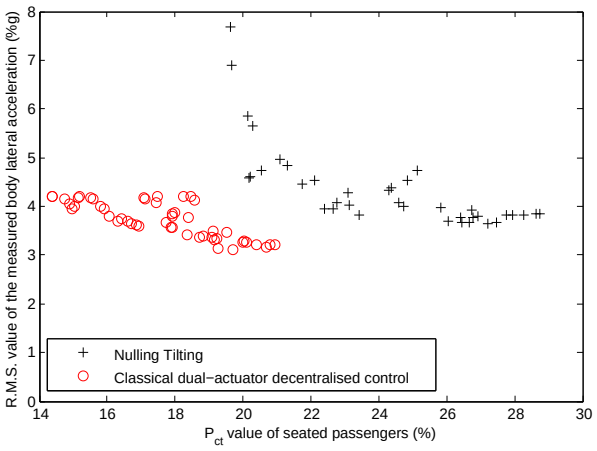

Figure 4.7: Trade-off plot for the tilting control between the curving performance and straight track ride quality

integration strategy. Compared with NT, most of the solutions from 'o' curve can meet performance requirements in Chapter 3. In actuality, it was found very difficult to satisfy both deterministic and stochastic criteria for the local tilting control with the passive lateral secondary suspension, but the introduction of the active secondary suspension solves this difficulty even with classical controller. The final controller parameters are selected to be:

---

k_p: 1.95; k_i: 1.61; k_d: 0.012;

c_s: $20058N{\cdot}s/m$; w_i: $2.04rad/s$; k_{df}: $50145N/m$;

4.2.4 Simulation results

The simulation results are illustrated in Figure 4.8 and the assessment values are presented in Table 4.2. The P_{ct} value for seated passengers is reduced to 15.7%g (close to the value of PT control (13%g)) while keeping the straight track ride quality below 3.778%g (the R.M.S. value (body lateral acceleration) in the passive situation) which is found impossible to be achieved in the situation of NT control. The transition performance is also improved and closer to the ideal situation, with the peak value of the lateral acceleration is 13.7%g (Figure 4.8(a)). Figure 4.9 gives the P.S.D.

analysis of the measured body lateral acceleration, which shows that the integration strategy helps to attenuate the body lateral vibration. However, further improvement of the controller performance is limited by the lateral secondary suspension deflection constraint (60mm), as shown in Figure 4.8(d). Also, the Gain Margin for the tilting control system is $4.18dB$, Phase Margin is $41.9deg$ (within the closed lateral actuator control loop), as shown in Figure 4.10. Details about the system internal stability are presented in Appendix E. To further improve the robustness and performance of the decentralised control strategy, Mixed-sensitivy H_∞ control is considered to replace the Approximate PID tilting control.

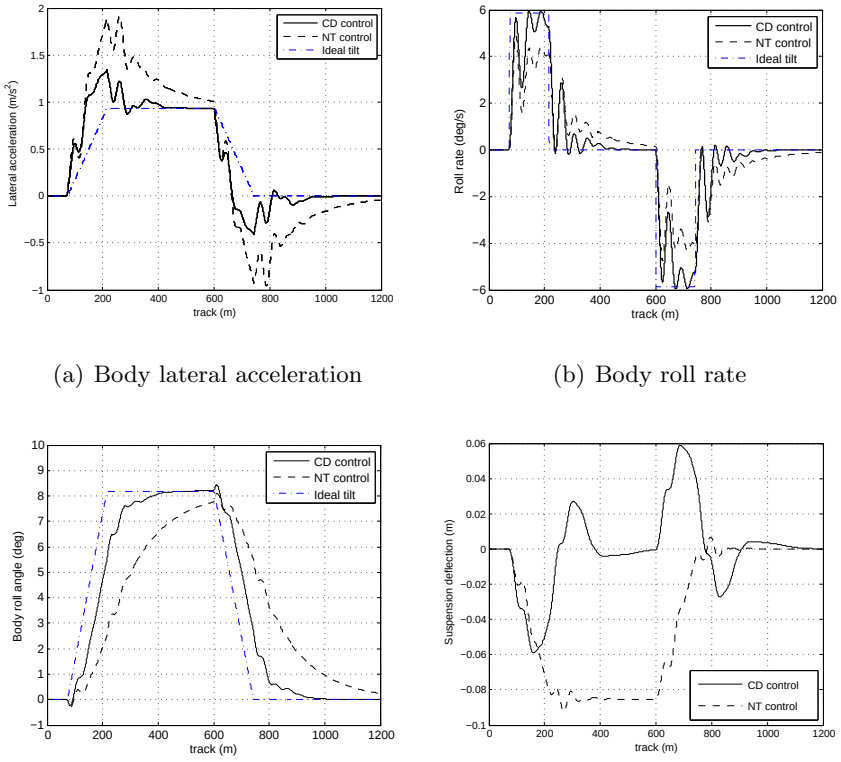

(a) Body lateral acceleration

(b) Body roll rate

(c) Tilt angle

(d) Suspension deflection

Figure 4.8: Simulation results for CD control

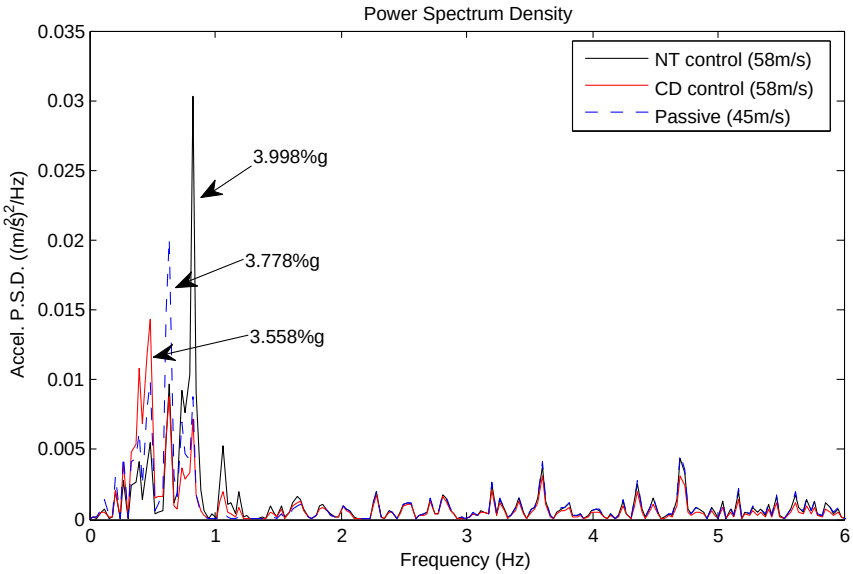

Figure 4.9: P.S.D. analysis for the measured body lateral acceleration (on straight track)

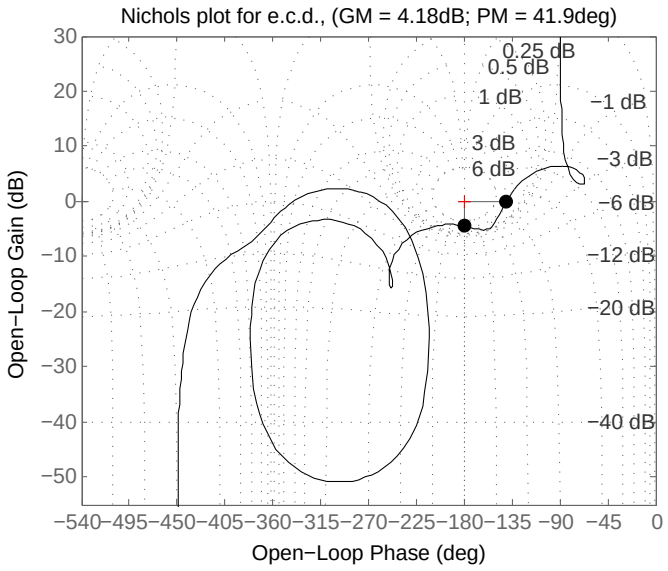

Figure 4.10: Nichols plot for e.c.d.

Table 4.2: Control system assessment for CD control @ 58(m/s)

Deterministic(CURVED TRACK)				
		CD	NT	PT
Lateral acceleration.	-Steady-state(%g)	9.530	n/a	9.530
	-R.M.S deviation error(%g)	4.576	5.555	1.54
	-Peak value(%g)	13.714	19.510	12.18
Roll gyroscope	- R.M.S. deviation(rad/s)	0.021	0.032	0.018
	-Peak value(rad/s)	0.104	0.086	0.104
	-Peak jerk level(%g/s)	7.687	10.286	6.80
P_{ct}(P-factor)	-standing(% of pasengers)	53.846	71.411	47.62
	-seated(% of pasengers)	15.674	22.640	13.455
Stochastic(STRAIGHT TRACK)				
passenger comfort	- R.M.S. passive(%g)	3.778	3.778	3.778
	- R.M.S. active(%g)	3.568	3.998	3.31
	- degradation (%g)	-5.558	5.802	-12.12

4.3 H_∞-based Decentralised control

H_∞ based Decentralised (HD) control is introduced in this section. It was found that the H_∞ tilting control combined with the intuitive skyhook damping control can meet all the design requirements, which simplifies the controller design. It becauses the H_∞ tilting provides a faster response compared to PID tilting when the train starts to negotiate the curve transition, hence reducing the interaction between the tilting response and lateral suspension. Centring control loop is still used.

4.3.1 Intuitive skyhook damping lateral actuator control

The configuration of intuitive skyhook damping control with centering loop is illustrated in Figure 4.11. The actuation force is proportional to the absolute body velocity. A High Pass filter (HP) is used to eliminate the integrator drifting due to zero-offset and also to reduce the low frequency velocity signal, which in turn reduces the suspension

deflection for the deterministic inputs.

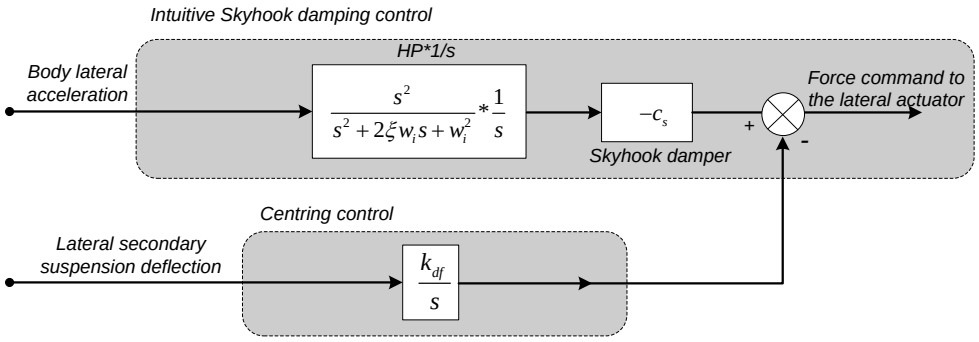

Figure 4.11: Intuitive skyhook damping control with centring loop

The parameters for the lateral actuator control in this design are listed as follows:

c_s: $59000N{\cdot}s/m$; w_i: $0.7rad/s$; k_{df}: $590000N/m$;

4.3.2 Mixed-sensitivity H_∞ tilting control

Mixed-sensitivity is the name given to transfer function shaping problems in which the sensitivity function $S = (I + GK)^{-1}$ is shaped along with one or more other closed-loop transfer functions such as $R = KS$ or the complementary sensitivity function $T = I - S$. The objective of Mixed-sensitivity design is to minimize the H_∞ norm of the closed-loop transfer function GAM (γ):

$$\left\| \begin{bmatrix} W_1 S \\ W_2 R \\ W_3 T \end{bmatrix} \right\|_\infty$$

Where W_1, W_2 and W_3 are the weighting filters for sensitivity transfer function (S), complementary sensitivity transfer function (T) and control inputs sensitivity (R) respectively. The returned values of S, R and T should satisfy the following loop shaping inequalities:

$\overline{\sigma}(S(jw)) \leqslant \gamma \underline{\sigma}({W_1}^{-1}(jw))$; $\overline{\sigma}(R(jw)) \leqslant \gamma \underline{\sigma}({W_2}^{-1}(jw))$; $\overline{\sigma}(T(jw)) \leqslant \gamma \underline{\sigma}({W_3}^{-1}(jw))$

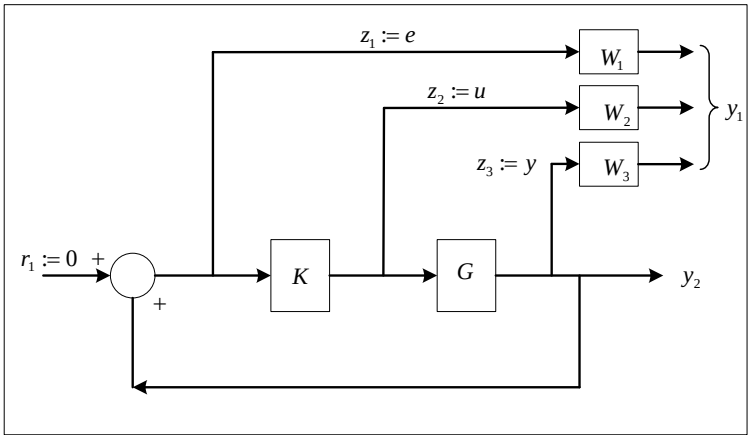

Figure 4.12: Mixed-Sensitivity control formulation for tilting control

Figure 4.12 illustrates the general control problem configuration for tilting control, r represents a set-point zero reference command, and the regulated outputs are z_1 (the weighted e.c.d. error signal), z_2 (the weighted control signal u) and z_3 (the weighted e.c.d. output signal). Note that regulating z_1 to zero will provide the required 60% tilt compensation, the regulation of z_2 will satisfy control limitation and noise attenuation at high frequencies, while regulation of z_3 is for system robustness and modelling uncertainty. The main issue of designing the H_∞ controller is the selection of the weighting filters which in most case is the rule of thumb. W_1 was chosen to be a low-pass filter with a very low cut-off frequency essentially to enforce integral action on z_1. In contrast, W_2 and W_3 were chosen as high-pass filters with pole and zero cut-off frequencies. The weighting filters for the tilting control are chosen as:

$$w_1 = 1100\frac{s/30+1}{s/0.001+1};\;\; w_2 = 0.0032\frac{s/0.1+1}{s/30+1};\;\; w_3 = 0.00032\frac{s/0.008+1}{s/300+1}$$

Figure 4.13 gives the information about the mixsyn(G,W1,W2,W3) shapes sigma plots of S and T to conform to GAM/W1 and GAM*G/W2 respectively.

The assessment values are presented in Table 4.3. The Nichols chart for e.c.d. is illustrated in Figure 4.14, time domain simulation results are illustrated in Figure 4.15.

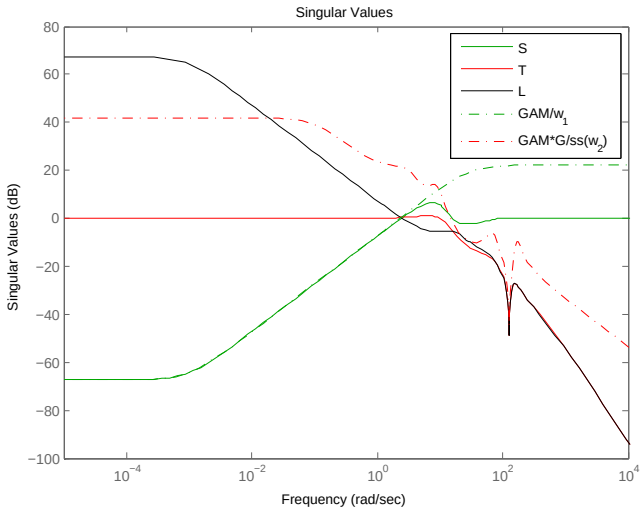

Figure 4.13: S and T to conform to GAM/W1 and GAM*G/W2, respectively

The simulation results of HD control show the improvement of the performance and system robustness compared to the CD control. The P_{ct} value for seated passengers is reduced to 14%, which is very close to the value of PT control (13.5%). The R.M.S. value of the lateral acceleration on straight track is less than 3.778%, which illustrates the good ride quality can be guranteed on the straight track. The Gain Margin for the tilting control system (with closed lateral actuator control loop) now is $5.6dB$ and Phase Margin is $58.9deg$.

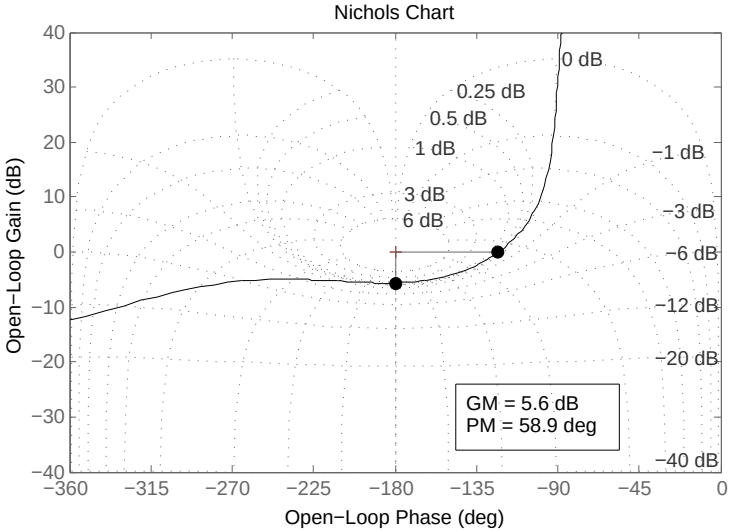

Figure 4.14: Nichols plot for e.c.d

Table 4.3: Control system assessment for HD control @ 58(m/s)

Deterministic(CURVED TRACK)					
		HD	CD	NT	PT
Lateral acceleration.	-Steady-state(%g)	9.530	9.530	n/a	9.530
	-R.M.S. deviation error(%g)	1.800	4.576	5.555	1.54
	-Peak value(%g)	12.144	13.714	19.510	12.18
Roll gyroscope	- R.M.S. deviation(rad/s)	0.020	0.021	0.032	0.018
	-Peak value(rad/s)	0.111	0.104	0.086	0.104
	-Peak jerk level(%g/s)	7.349	7.687	10.286	6.80
P_{ct}(P-factor)	-standing(% of pasengers)	50.548	53.846	71.411	47.62
	-seated(% of pasengers)	14.214	15.674	22.640	13.455
Stochastic(STRAIGHT TRACK)					
passenger comfort	- R.M.S. passive(%g)	3.778	3.778	3.778	3.778
	- R.M.S. active(%g)	3.569	3.568	3.998	3.31
	- degradation (%g)	-5.553	-5.558	5.802	-12.12

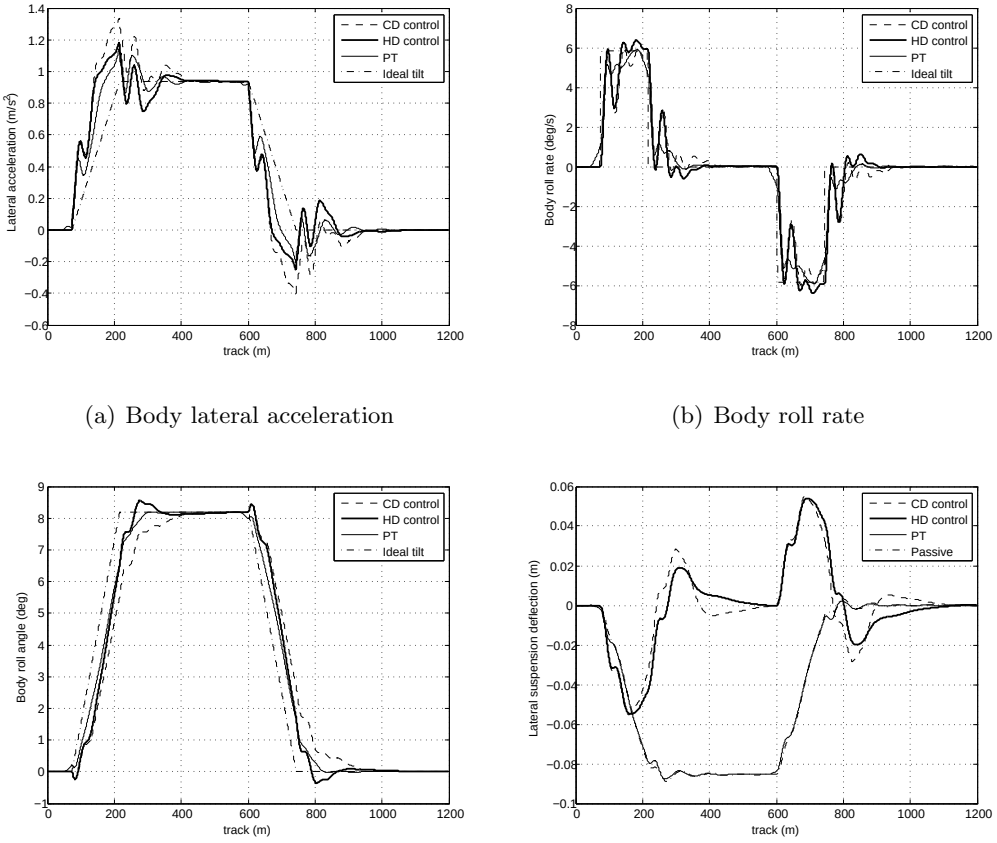

(a) Body lateral acceleration

(b) Body roll rate

(c) Body tilt angle

(d) Suspension deflection

Figure 4.15: Simulation results for HD control

4.4 LQG centralised control

Compared with the decentralized control, optimal control allows for direct use of the MIMO state space model thus allowing for any couplings in the states during the design process in a centralized solution.

The Linear Quadratic Regulator (LQR) is an optimal control design method that yields a full state feedback controller which minimizes the quadratic performance index (using

output regulation)

$$J = \int_0^\infty [z^T Q_0 z + u^T R_0 u] d\tau \tag{4.9}$$

The controller design process involves selecting the outputs to be weighted (z), and tuning the system output and control input weighting factors (Q_0, R_0). In the case where all required system states are not available for feedback, which may be difficult, impractical or sometimes not possible to measure, a Kalman filter can be combined with the optimal controller to provide the necessary state estimates for state feedback. This is the well known Linear Quadratic Gaussian (LQG) problem. The overall system structure is illustrated in Figure 4.16. The controller is designed via the separation principle.

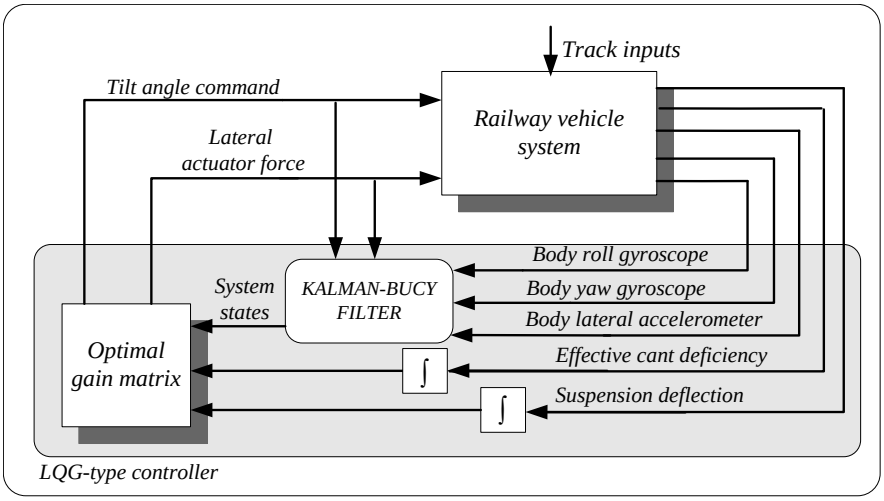

Figure 4.16: LQG control system

4.4.1 LQR design

The following states are selected: body lateral displacement, body roll angle, bogie lateral displacement, bogie roll angle, body lateral displacement velocity, body roll rate, bogie lateral displacement velocity, bogie roll rate and air spring roll angle. In addition, the integral of θ_{dm} (effective cant deficiency) is combined into the states for disturbance rejection and reference tracking. Also, the integral of x_{2dfl} (Lateral secondary suspension deflection) is required to minimise the lateral deflection and avoid

the lateral bump stop. Hence, the system is augmented to include ($\int \theta_{dm}$, $\int x_{2dfl}$) as extra states. The state vector is given by:

$$x = [y_v \;\; \theta_v \;\; y_b \;\; \theta_b \;\; \dot{y}_v \;\; \dot{\theta}_v \;\; \dot{y}_b \;\; \dot{\theta}_b \;\; \theta_r \;\; \int \theta_{dm} \;\; \int x_{2dfl}]$$

The weighted outputs selected are the body roll rate, $\int \theta_{dm}$, $\int x_{2dfl}$. The output weighting factor Q_0 and control weighting factor R_0 can be initially set to $1/(signal\ expected\ value)^2$ (using Bryson's rule) with further fine tuning required. In particular, GA techniques are utilized in this work for tuning the weighting matrices subject to satisfying given tilt performance metrics.

4.4.2 GA optimization

Non-dominated Sort Genetic Algorithm ($NSGA\_II$) is used to tune the weighting factor Q_0 and R_0. Setting objective functions and initial optimization boundary for the parameters are the main issues for the GAs. In this study, the optimization boundary set for the tilting control weighting is from $1/(0.1745)^2$ to $1/(0.05)^2$. The vehicle body tilt angle is expected in the range 2.8 degrees-10 degrees. $1/(20000)^2$ to $1/(8000)^2$ is set for the lateral actuator force command. The large lateral force is required particularly when the train negotiates the curve. The initial boundaries can be set in the similar way for the output weighting function,

$$Q_0 = diag([\tfrac{1}{0.15^2}\ to\ \tfrac{1}{0.05^2}],\ [\tfrac{1}{0.01^2}\ to\ \tfrac{1}{0.001^2}]),\ [\tfrac{1}{0.06^2}\ to\ \tfrac{1}{0.01^2}])$$

The objective functions and constraints are set the same as in Section 4.3.2, Figure 4.17 shows the trade-off for the controller design between curving performance and straight track ride quality. Also, the optimization process is illustrated. We give the results for 200 and 500 generations with 30 populations.

The final weightings for the best design are chosen to be:

$$Q_0 = diag(\tfrac{1}{0.0574^2},\ \tfrac{1}{0.0052^2},\ \tfrac{1}{0.01745^2})$$
$$R_0 = diag(\tfrac{1}{0.1655^2},\ \tfrac{1}{12958^2})$$

And the final optimal gain K:

$$\begin{bmatrix} 2.41 & 13.1 & 0.1 & 0.72 & 2.40 & 2.87 & -0.0071 & 0.00051 & 0.43 & 31.74 & 0.68; \\ 170297.2 & 263579.9 & -176571.8 & -36660 & 133736 & -2759.8 & 133.03 \\ 191.73 & -988.7 & -178523.6 & 740690.12 \end{bmatrix}$$

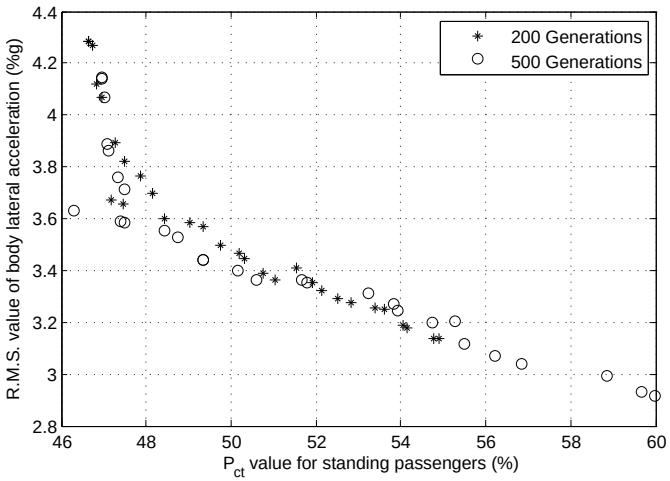

Figure 4.17: GA tuning results for LQG control

Note that large gains exist in the second row for the lateral actuator force command, due to the relatively large lateral actuator forces compared with the drive signal for the tilting action.

4.4.3 Kalman-Bucy Filter design

Kalman-Bucy filter (KBF) is used as the optimal state estimator. The inputs to the KBF are the two system inputs and three measurements: vehicle body roll velocity (cant information), body lateral acceleration (for cant deficiency information) and vehicle body yaw velocity (required only for extra information on the curvature R^{-1}). The body roll gyroscope measures absolute roll rate ($\dot{\theta_v} + \dot{\theta_0}$), thus $\dot{\theta_0}$ must also be included in the state estimates. The system state space can be reformulated for the design of the KBF in order to treat parts of disturbance ($\theta_0 \;\; \dot{\theta}_0 \;\; R^{-1}$) as states. The reformulated state vector for the estimation is:

$$x = [y_v \;\; \theta_v \;\; y_b \;\; \theta_b \;\; \dot{y}_v \;\; \dot{\theta}_v \;\; \dot{y}_b \;\; \dot{\theta}_b \;\; \theta_r \;\; \theta_0 \;\; \dot{\theta}_0 \;\; R^{-1}]'$$

And the process noise is characterized by $w = [\dot{R^{-1}} \;\; \dot{\theta}_0]'$, the two inputs are $[\delta_a \;\; F_a]'$. The KBF can be designed offline using (4.10) and (4.11).

$$\dot{x}_{kf} = A_{kf} x_{kf} + B_{kf} u + \Gamma_k w_k \tag{4.10}$$

$$y_{kf} = C_{kf}x_{kf} + D_{kf}u + v \tag{4.11}$$

while the state estimates will be calculated by solving the following differential equation:

$$\dot{\widehat{x}} = A_k\widehat{x} + B_k u + K_f(y_k - C_k\widehat{x} - D_k u) \tag{4.12}$$

where $\widehat{x}$ is the vector of the state estimates and K_f is the KBF gain matrix. The sensor noise levels are characterised by a covariance matrix with each diagonal value is set to 1% of the expected maximum value taken as, 3 times the true R.M.S. value of the sensor output signal on straight track with irregularities, plus the peak value on the pure curved track. Sensor noise covariance (R_k) and process noise covariance (Q_k) are to be as follows,

$$R_k = diag(1.62 \times 10^{-3},\ 1.88 \times 10^{-6},\ 1 \times 10^{-6})$$
$$Q_k = diag(\tfrac{1}{0.1655^2},\ \tfrac{1}{12958^2})$$

Final Kalman gain K_f is:

$$\begin{bmatrix} -0.2417 & -2.4557 & -0.2671; \\ -0.0900 & -2.6223 & 0.0160; \\ 0.0020 & 0.0994 & -0.1718; \\ -0.0379 & -1.0614 & 0.0221; \\ -1.0787 & 7.1346 & -57.5770; \\ -0.4257 & 0.7823 & -0.0504; \\ 0.0460 & -0.0593 & -31.4448; \\ -0.1723 & 0.2823 & 2.7934; \\ -0.0687 & -2.1104 & 0.0263; \\ 0.0631 & 4.2355 & -0.0101; \\ 0.4439 & 16.7855 & -0.0774; \\ 0.0004 & -0.0012 & 3.1622 \end{bmatrix}$$

The performance of the LQG control is very similar to the industrial-used Precedence Tilting (PT) control, which is of course closer to the ideal response, as shown in Figure 4.18. The R.M.S. deviation error of the lateral acceleration is 1.3%g, which is less than the value for PT control, as shown in Table 4.4.

The assessment is also performed by comparison of the P_{ct} values (for curving transition performance) and R.M.S. value of the body lateral acceleration (for straight track ride quality). The P_{ct} value of the LQG control for the seated passenger is 12.8%, which is slightly less than the value for the PT control. Also the improvement on straight track

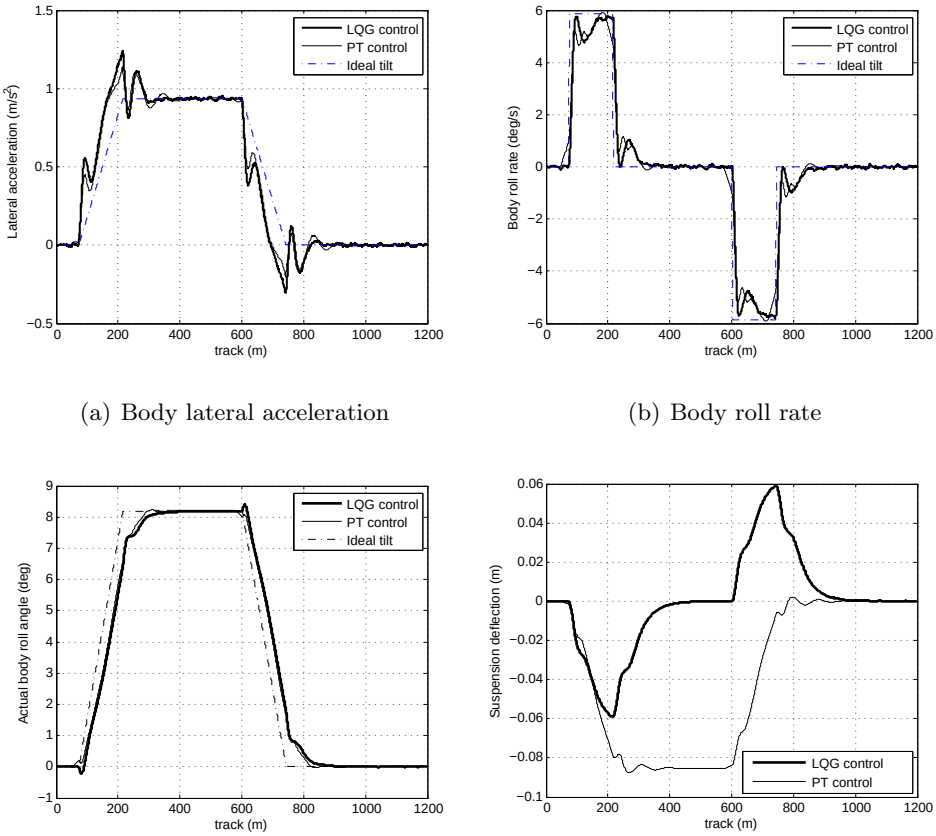

(a) Body lateral acceleration

(b) Body roll rate

(c) Body tilt angle

(d) Suspension deflection

Figure 4.18: Simulation results for LQG control

is illustrated by the R.M.S. value of 3.63%g which gives 4% improvement compared to the passive value. Note that the PT controller has an advantage due to the previous information. The actual body roll angle with the LQG control is also close to the ideal one, which is shown in Figure 4.18.

Table 4.4: Control system assessment for LQG control @ 58(m/s)

Deterministic(CURVED TRACK)						
		LQG	HD	CD	NT	PT
Lateral acceleration.	-Steady-state(%g)	9.530	9.530	9.530	n/a	9.530
	-R.M.S. deviation error(%g)	1.500	1.800	4.576	5.555	1.54
	-Peak value(%g)	12.600	12.144	13.714	19.510	12.18
Roll gyroscope	- R.M.S. deviation(rad/s)	0.016	0.020	0.021	0.032	0.018
	-Peak value(rad/s)	0.101	0.111	0.104	0.086	0.104
	-Peak jerk level(%g/s)	5.870	7.349	7.687	10.286	6.80
P_{ct}(P-factor)	-standing(% of pasengers)	46.300	50.548	53.846	71.411	47.62
	-seated(% of pasengers)	12.800	14.214	15.674	22.640	13.455
Stochastic(STRAIGHT TRACK)						
passenger comfort	- R.M.S. passive(%g)	3.778	3.778	3.778	3.778	3.778
	- R.M.S. active(%g)	3.630	3.569	3.568	3.998	3.31
	- degradation (%g)	-4.000	-5.553	-5.558	5.802	-12.12

4.5 Summary

In this chapter, the control system design for the integrated active anti-roll bar and active lateral secondary suspension is introduced. The trade-off for the tilting control between curving performance and straight track ride quality has been significantly optimised by this integration strategy even with Classical Decentralised (CD) control. Modern control: H_∞ Decentralized (HD) control and LQG centralized control give further improvement of this dual-actuator control system. The performance of LQG centralized control is very close to the performance of PT control. However, further improvement of the controller performance is limited by the suspension deflection constraint. Figure 4.19 gives the curving performance and straight track ride quality comparison between the 3 new controllers for the dual-actuator system, industrial tilt-only PT control and conventional tilt-only Nulling Tilting (NT) control. The LQG control provides the best performance on curved track ($P_{ct} = 12.8\%$), meanwhile improves the straight track ride qulity compared to the passive situation. Classical Decentralised (CD) control also provides the improvement of the local tilting control performance ($P_{ct} = 15.7\%$, R.M.S. value (lateral acceleration) = 3.57%g), which is a simple solution

for the real train implementation.

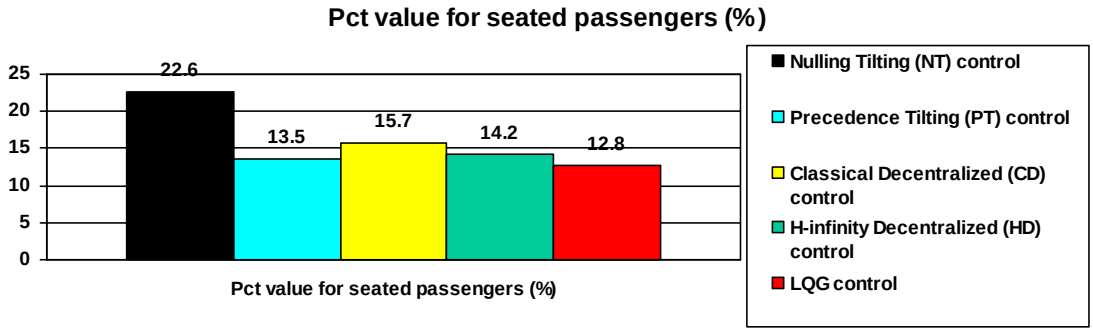

(a) Controller performance comparison on curved track

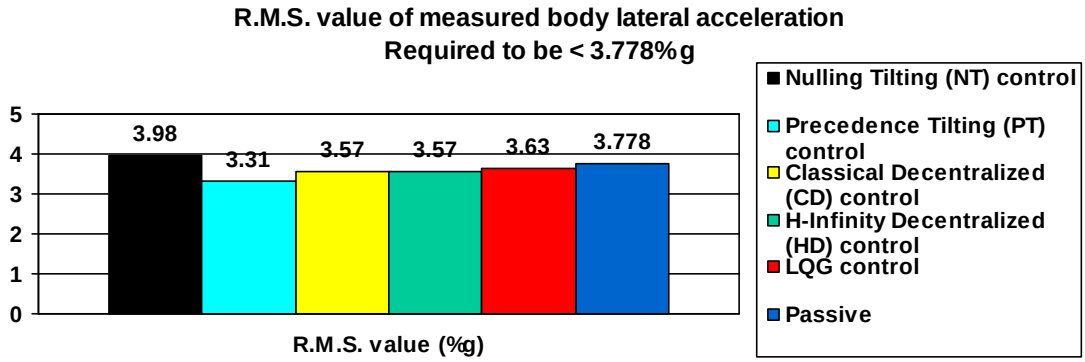

(b) Controller performance comparison on straight track

Figure 4.19: Controller performance comparison

Chapter 5

Tilting bolster with integrated active lateral secondary suspension control

A tilting bolster is widely utilised by tilting trains all over the world. Figure 5.1(a) shows the X2000 tilting train. In the mechanical system of this tilting train, inclined swing links are employed to connect vehicle body and bogie, to provide the tilting action below secondary suspension via controlling an actuator fitted between the bogie and the bolster. As a consequence the lateral suspension does not have to react to the increased curving forces and helps to avoid contact with the lateral bump stop, a benefit that does not apply to the tilting train with active ARB system. The tilting bolster is able to provide the maximum tilt up to 10 degrees, although the tilting action is below the vehicle body, the effective tilt centre is still above the vehicle body floor level. Bogie weight, the complexity of the configuration and cost are the issues for this mechanical system.

In this chapter, the work on the integrated tilting bolster with active lateral secondary suspension is summarized. As shown in Figure 5.1(b), a lateral actuator is installed between the vehicle body and tilting bolster replacing the original damper (the lateral actuator force is not a critical issue here). Controllers for this dual-actuator system can

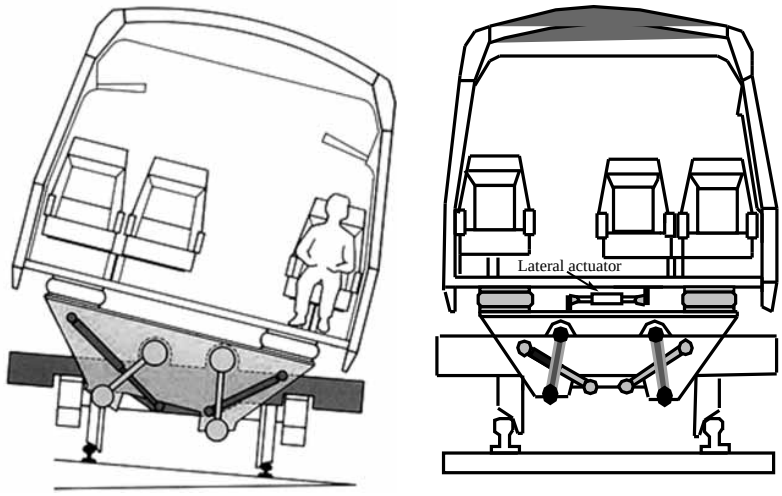

(a) X2000 End-view

(b) Integrated tilting bolster and lateral actuator

Figure 5.1: Tilting train with tilting bolster

be designed in the similar way as the design process in Chapter 4, but different control strategies are studied as follows:

- Classical Decentralised control
- Command Driven Decentralised control
- MIMO Optimal control
- Estimator-Based Decoupling control

5.1 System modelling

Figure 5.2 illustrates the end-view model and the force analysis diagram. The model is also originally designed as part of research on advanced local tilting control system (Zolotas (2002a)). In this model, the lateral dynamics and roll dynamics of the vehicle body and bogie are presented. The vertical dynamics are ignored but the vertical suspension is represented by a pair of airsprings which contributes to the roll dynamics. An anti-roll bar system, the end moment effect (due to the movement of the body center of gravity), the translation and rotation of these reference axis associated with curves are all depicted in the model. The tilt actuation system is modelled as a position servo

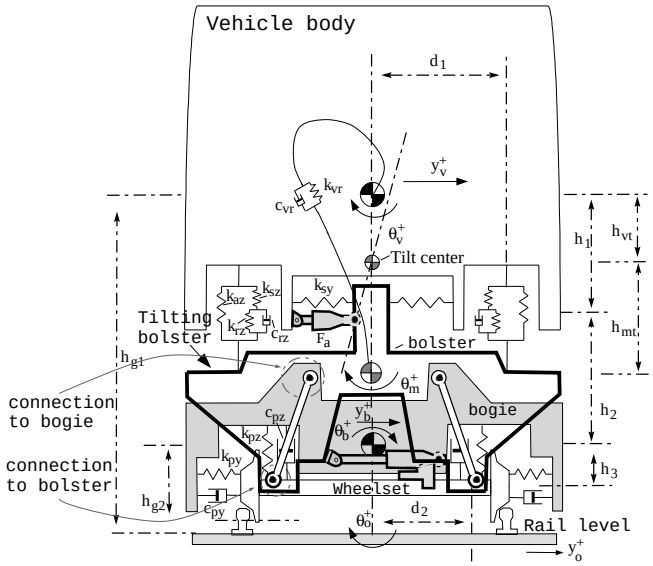

(a) End-View Model

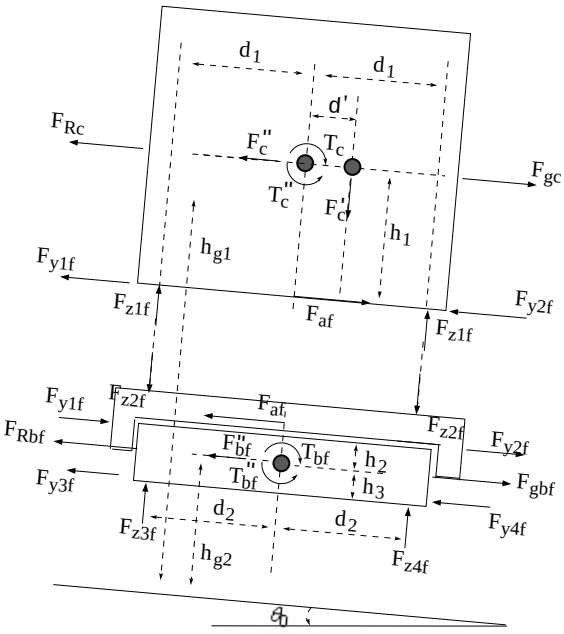

(b) Force analysis

Figure 5.2: End-view modelling

mechanism which gives $3.5Hz$ bandwidth (w_{cm}) and 50% damping (ζ_m), it is reasonable because tilting is a low bandwidth action. For simplicity, the wheelset dynamics effects are incorporated in the model by using an appropriate 2nd order low pass filter (Bogie lateral kinematics) which characterised by a $5Hz$ cut-off frequency and 20% damping. In this study, an actuator (F_a) is installed between the body and tilting bolster in the lateral direction. Ideal actuator is used for the controller design, but the lateral actuator dynamics will be addressed in Chapter 6, which should be properly modelled in terms of the movement across the actuator, otherwise important dynamic limitations are missed. The numerical equations for the integrated tilting bolster and active lateral secondary suspension are presented below, the parameters are listed in Appendix D.

Body lateral dynamics:

$$\begin{aligned} m_v\ddot{y}_v &= -2k_{sy}y_v + 2k_{sy}h_1\theta_v + 2k_{sy}y_b + 2k_{sy}h_2\theta_b - (2h_{mt}k_{sy} - m_vg)\theta_m \\ &\quad + m_vg\theta_0 - \frac{m_vv^2}{R} - m_vh_{g1}\ddot{\theta}_0 + F_a \end{aligned} \tag{5.1}$$

Body roll dynamics:

$$\begin{aligned} i_{vr}\ddot{\theta}_v &= (2h_1k_{sy} + m_vg)y_v - [k_{vr} + 2h_1{}^2k_{sy} + 2d_1{}^2(k_{az} + k_{sz})]\theta_v - 2h_1y_b(k_{sy} + m_vg) \\ &\quad + (k_{vr} + 2d_1{}^2k_{az} - 2h_1h_2k_{sy})\theta_b - c_{vr}\dot{\theta}_v + c_{vr}\dot{\theta}_b + 2k_{sz}d_1{}^2\theta_r \\ &\quad + (k_{vr} + 2d_1{}^2k_{az} + 2k_{sy}h_1h_{mt})\theta_m + c_{vr}\dot{\theta}_m - i_{vr}\ddot{\theta}_0 - F_ah_1 \end{aligned} \tag{5.2}$$

Bogie lateral dynamics:

$$\begin{aligned} m_b\ddot{y}_b &= 2k_{sy}y_v - 2h_1k_{sy}\theta_v - 2(k_{sy} + k_{py})y_b - 2(h_2k_{sy} - h_3k_{py})\theta_b \\ &\quad - 2c_{py}\dot{y}_b + 2h_3c_{py}\dot{\theta}_b + 2k_{py}y_w + 2c_{py}\dot{y}_w + 2h_{mt}k_{sy}\theta_m + m_bg\theta_0 \\ &\quad - \frac{m_bv^2}{R} - m_bh_{g2}\ddot{\theta}_0 - F_a \end{aligned} \tag{5.3}$$

Bogie roll dynamics:

$$\begin{aligned} i_{br}\ddot{\theta}_b &= 2h_2k_{sy}y_v + [k_{vr} - 2h_2h_1k_{sy} + 2d_1{}^2(k_{az} + k_{sz})]\theta_v - 2[h_2k_{sy} - h_3k_{py}]y_b \\ &\quad - (k_{vr} + 2h_2{}^2k_{sy} + 2h_3{}^2k_{py} + 2d_2{}^2k_{pz} + 2d_1{}^2k_{az})\theta_b + c_{vr}\dot{\theta}_v + 2h_3c_{py}\dot{y}_b \\ &\quad - (c_{vr} + 2d_2{}^2c_{pz} + 2h_3{}^2c_{py})\dot{\theta}_b - 2k_{sz}d_1{}^2\theta_r - 2h_3k_{py}y_w - 2h_3c_{py}\dot{y}_w \\ &\quad - (k_{vr} + 2d_1{}^2k_{az} - 2k_{sy}h_2h_{mt})\theta_m - c_{vr}\dot{\theta}_m - i_{br}\ddot{\theta}_0 - F_ah_2 \end{aligned} \tag{5.4}$$

Tilting actuation system:

$$\frac{\theta_m}{\theta_{m_i}}(s) = \frac{483.6}{s^2 + 22s + 483.6} \tag{5.5}$$

Wheelset dynamics:

$$\frac{y_w}{y_0}(s) = \frac{987}{s^2 + 12.57s + 987} \tag{5.6}$$

For the air spring state:

$$\dot{\theta}_r = {c_{rz}}^{-1}(\theta_r(k_{sz} + k_{rz}) + k_{sz}\theta_v + k_{rz}(\theta_b + \theta_m) + c_{rz}(\dot{\theta}_b + \dot{\theta}_m) \tag{5.7}$$

The system state space form is presented below, the system has two inputs which are the tilt angle command and lateral actuator force command, 13 states and 6 track disturbances.

$$\dot{x} = Ax + Bu + \Gamma\omega \tag{5.8}$$

$$y = Cx + Du + H\omega \tag{5.9}$$

where, $\dot{x} = [y_v \;\; \theta_v \;\; y_b \;\; \theta_b \;\; \dot{y}_v \;\; \dot{\theta_v} \;\; \dot{y}_b \;\; \dot{\theta_b} \;\; \theta_r \;\; y_w \;\; \dot{y}_w \;\; \theta_m \;\; \dot{\theta}_m]^T$
$u = [\theta_{m_i} \;\; F_a]^T \qquad \omega = [R^{-1} \;\; \dot{R^{-1}} \;\; \theta_0 \;\; \dot{\theta}_0 \;\; \ddot{\theta}_0 \;\; y_0]^T$

For the purpose of the simulation, the disturbance parameters (θ_0, $\dot{\theta}_0$, y_0) are included in matrix A and the rest of the disturbance signals w are included in B matrix. The details of Matrix A and B can be found in Appendix C. The system modes are listed in Table 5.1. Compared with system modes in Zolotas (2002a) (the active tilting with passive secondary suspensions), the frequencies are the same while the dampings are changed due to the damper coefficients of the lateral secondary suspension being set to zero (the lateral damper is replaced by the lateral actuator). Only 0.75% and 4.41% damping remain for the lateral body modes. Of course the active lateral secondary suspension control will provide more damping for these modes, which will be discussed in following sections.

The vehicle models and control systems are tested with specific track inputs including both deterministic (low frequency) and stochastic (high frequency) features. The deterministic track used was a curved track with a radius of 1200m and a maximum track cant angle (θ^0) of 5.84^o, with a 150m transition at the start and end of the steady

Table 5.1: Tilt mechanism vehicle dynamic modes

Original system model		
Mode	Damping(%)	Frequency(Hz)
Lower sway	21.8	0.48
Upper sway	20.9	1.35
Bogie lateral	9.95	16.7
Bogie roll	28.3	7.26
New system model		
Mode	Damping(%)	Frequency(Hz)
Lower sway	0.75	0.4714
Upper sway	4.41	1.3696
Bogie lateral	6.35	16.5482
Bogie roll	25.22	7.2675

curve. The stochastic track inputs represent the irregularities in the track alignment on both straight track and curves, and these were characterised by an approximate spatial spectrum equal to $((2\pi)^2\Omega_l v^2/f(m^2/(cycle/m))$ with a lateral track roughness (Ω_l) of 0.33×10^{-8}.

5.2 Classical Decentralised control

The system configuration for the Classical Decentralised (CD) control is illustrated in Figure 5.3, which is similar to the configuration for the tilting train with active ARB. Complementary filter skyhook damping control with centring loop is used for the lateral actuator control driven by the measured body lateral acceleration and lateral secondary suspension deflection. Effective cant deficiency (e.c.d.) (See Section 2.1) is used to drive the tilt actuator with approximate PID control.

The controller parameters are tuned via GA. The set up of the GA tuning process is the same as the one in Section 4.2, except that the first constraint is changed to $3.24\%g$, also $NSGA\_II$ is used. Figure 5.4 shows the trade off for the local tilting control between curving performance (P_{ct} value) and straight track ride quality (R.M.S. value). It is

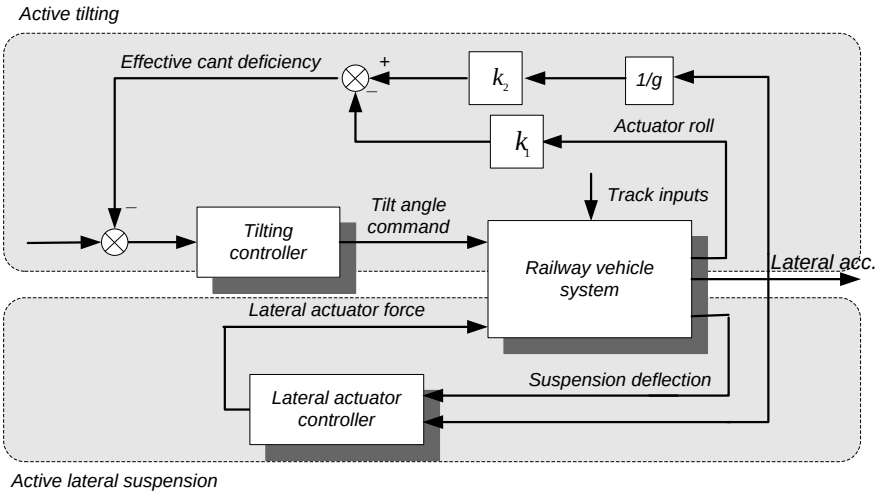

Figure 5.3: Classical Decentralised control

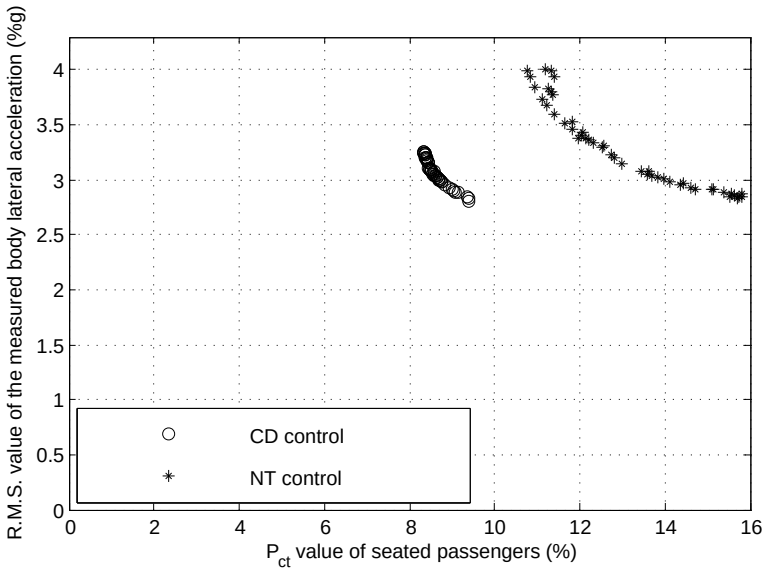

Figure 5.4: Trade off plot from GA tuning

obvious that the trade-off is significantly optimized by integrating the lateral actuator control with the tilting control compared with NT control. All solutions in 'o' curve can meet all requirements presented in Section 4.2.3. Final control parameters are listed below:

k_p: 0.15; k_i: 1.46; k_d: 0.018;
c_s: $35720N{\cdot}s/m$; w_i: $3.18rad/s$; k_{df}: $8930N/m$;

The simulation results are illustrated in Figure 5.5, Figure 5.6 and Table 5.2. The P_{ct} value for seated passengers is reduced to 8.63%g while keeping the straight track ride quality below 3.24%g (the R.M.S. value (body lateral acceleration) in the passive situation (Zolotas (2002a))). The transition performance is also improved and closer to the ideal situation with the peak value of the lateral acceleration is 8.5%g. Figure 5.6(a) shows the efficiency of the integration strategy on straight track, which gives a lower R.M.S. value compared with NT control at frequenies 0-6Hz. However, further improvement of the controller performance is limited by the lateral secondary suspension deflection constraint ($60mm$) (Figure 5.5(d)) as well as the system robustness (Figure 5.6(b)).

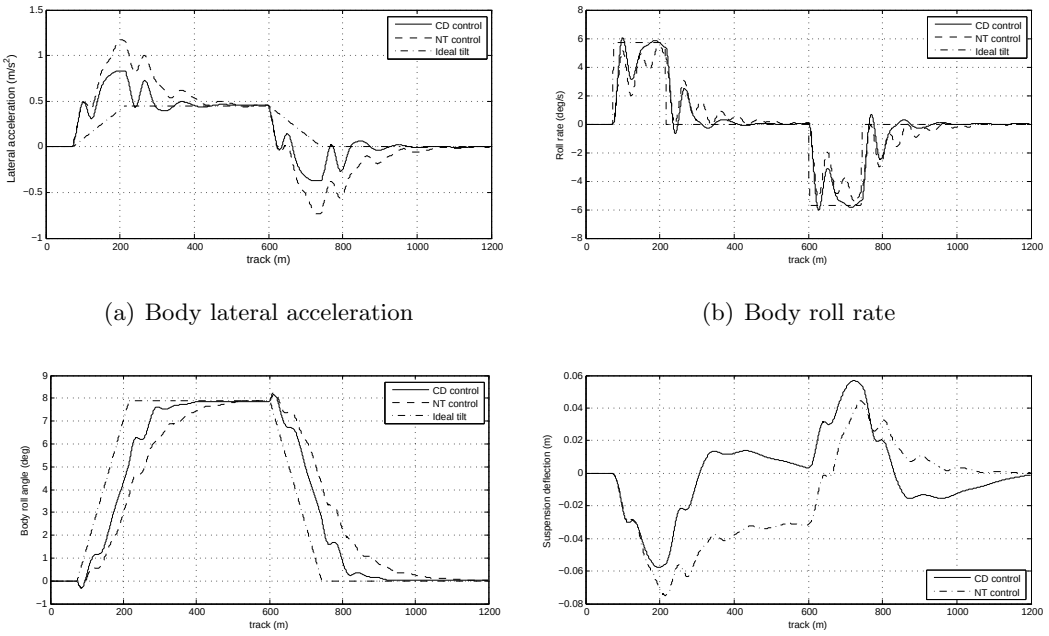

(a) Body lateral acceleration

(b) Body roll rate

(c) Tilt angle

(d) Suspension deflection

Figure 5.5: Simulation results for CD control

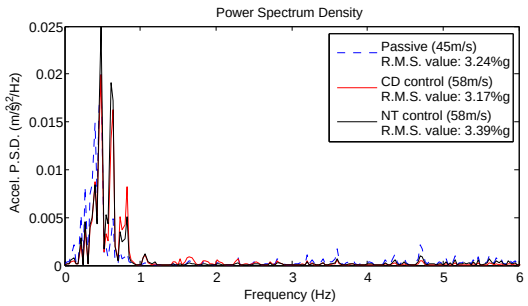

(a) P.S.D. analysis for the measured body lateral acceleration (on straight track)

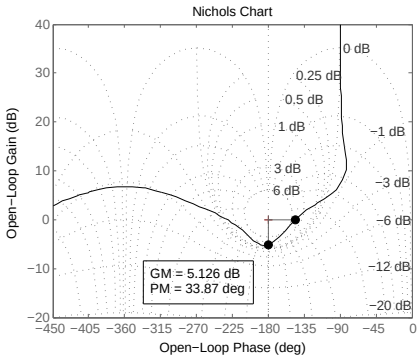

(b) Nichols plot for e.c.d.

Figure 5.6: P.S.D. analysis and Nichols plot

Table 5.2: Control system assessment for CD control@ 58(m/s)

Deterministic(CURVED TRACK)				
		CD	NT	PT
Lateral acceleration.	-Steady-state(%g)	4.6	n/a	4.6
	-R.M.S. deviation error(%g)	1.9	4.7	0.73
	-Peak value(%g)	8.5	13.0	5
Roll gyroscope	- R.M.S. deviation(rad/s)	0.021	0.03	0.015
	-Peak value(rad/s)	0.110	0.093	0.11
	-Peak jerk level(%g/s)	5.1	6.95	3.02
P_{ct}(P-factor)	-standing(% of pasengers)	34.2	47.9	20.6
	-seated(% of pasengers)	8.63	14	3.7
Stochastic(STRAIGHT TRACK)				
passenger comfort	- R.M.S. passive(%g)	3.24	3.24	3.24
	- R.M.S. active(%g)	3.17	3.39	2.29
	- degradation(%)	-1.85	5.94	-28.6

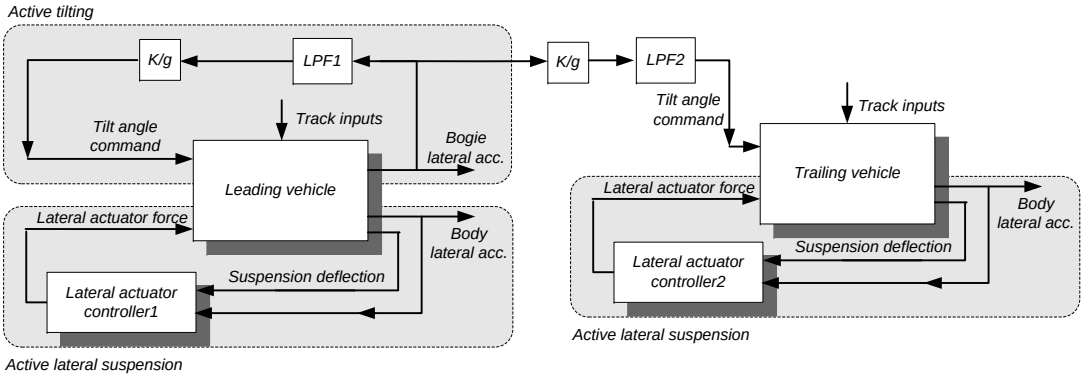

Figure 5.7: Precedence Command Driven Decentralised control

5.3 Command-Driven Decentralised control

In this section, the Command-Driven Decentralised (CDD) control is studied. Local CDD control is designed for the leading vehicle, while the precedence CDD control is employed for the trailing vehicle. The overall configuration is illustrated in Figure 5.7. Note that, the configuration duplicates the real configuration used in the operational tilting train nowadays. The tilt command is provided by an accelerometer mounted on the bogie of the local vehicle, with Low Pass Filter (LPF1 and LPF2 in Figure 5.7) used to remove unwanted high frequencies due to the bogie harsh environment, while K = 0.75 to achieve the 75% compensation of the body lateral acceleration. The parameters for the overall system design are listed below:

Control parameters for the leading vehicle:

$w_{lpf1} = 2\pi \times 0.7 rad/s$: Cut-off frequency for the LPF1;
$\xi = 0.707$: Damping ratio for the LPF1;
$w_i = 2\pi \times 0.3654 rad/s$: Cut-off frequency for the complementary filters;
$c_s = 112053 N \cdot s/m$: Skyhook damping coefficient;
$k_{df} = 268.9 N/m$: Centring control coefficient.

Control parameters for the trailing vehicle:

$w_{lpf2} = 2\pi \times 0.45 rad/s$: Cut-off frequency for the LPF2;
$\xi = 0.707$: Damping ratio for the LPF2;

$w_i = 2\pi \times 0.3 rad/s$: Cut-off frequency for the complementary filters;
$c_s = 140000 N \cdot s/m$: Skyhook damping coefficient.

Note that:
(1) A prefileter is used to guarantee a tilt command for 75% compensation.
(2) The cut-off frequency of the LPF2 is set to $0.45 Hz$, which introduces a 0.5s delay. The preview time is chosen to match the filter delay. It takes $\mathrm{l} = (58 m/s \times 0.5) = 29 m$ precedence, approximately 1.5 vehicle length.
(3) The precedence strategy helps to reduce the influence from tilting on the secondary suspension deflection. Thus, no centring control loop for the trailing vehicle is provided.

The simulation results for both trailing vehicle and leading vehicle are illustrated in Figure 5.8 and Figure 5.9, and the assessment is presented in Table 5.3. The performance of the trailing vehicle has been improved with the helps from the lateral actuator control, the P_{ct} value of seated passengers is 2.9% which is less than the value of NT control (3.7%). It also provides 55% ride quality improvement on straight track. P.S.D. analysis shows the lateral vibration of the vehicle body has been attenuated at all frequencies, as shown in Figure 5.8. However, the performance of the leading vehicle is similar to the performance of the CD control. To further improve the performance of the leading vehicle, two advanced control strategies are studied, which are MIMO optimal control and Estimator-Based Decoupling control.

Table 5.3: Control system assessment for CDD control @ 58(m/s)

Deterministic(CURVED TRACK)				
		Leading Dual-actuator	Trailing Dual-actuator	Trailing PT
Lateral acceleration.	-Steady-state(%g)	n/a	4.6	4.6
	-R.M.S. deviation error(%g)	4.65	0.4	0.73
	-Peak value(%g)	6.8	5.2	5
Roll gyroscope	- R.M.S. deviation(rad/s)	0.022	0.018	0.015
	-Peak value(rad/s)	0.110	0.106	0.11
	-Peak jerk level(%g/s)	5.384	2.42	3.02
P_{ct}(P-factor)	-standing(% of pasengers)	31.3	18.85	20.6
	-seated(% of pasengers)	7.6	2.94	3.7
Stochastic(STRAIGHT TRACK)				
passenger comfort	- R.M.S. passive(%g)	3.24	3.24	3.24
	- R.M.S. active(%g)	3.18	1.45	2.29
	- degradation(%)	-1.85	-55.45	-28.6

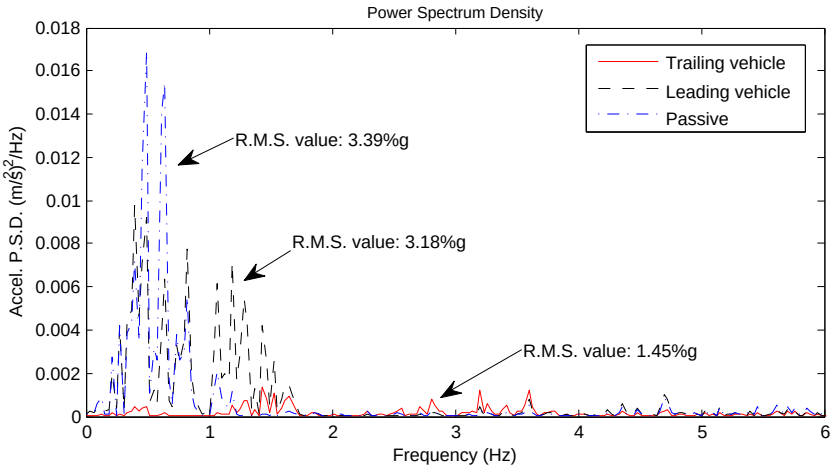

Figure 5.8: P.S.D. analysis for the measured body lateral acceleration (on straight track)

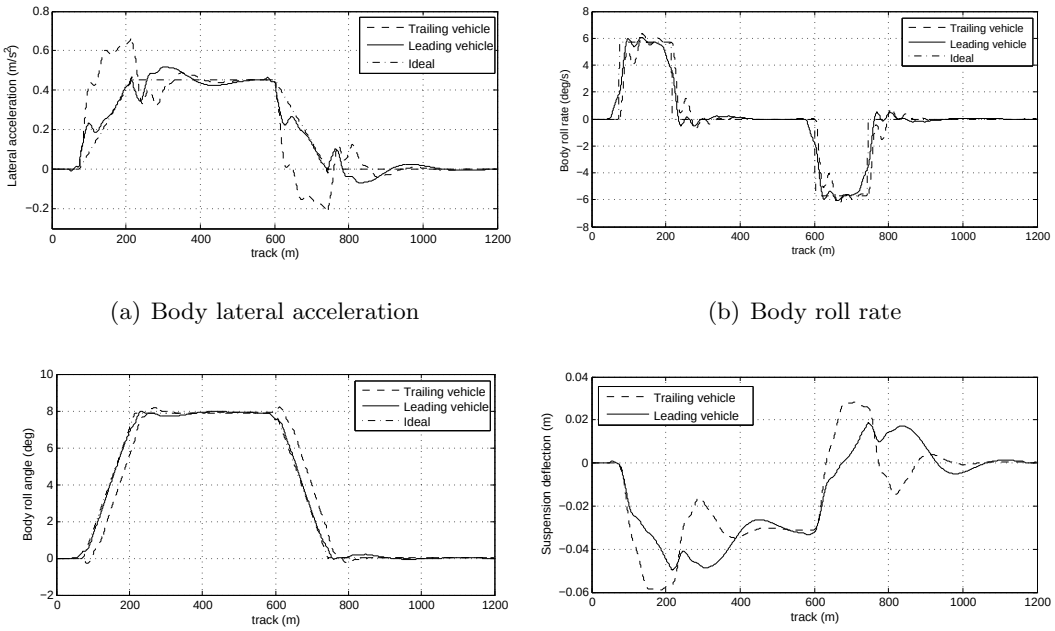

(a) Body lateral acceleration

(b) Body roll rate

(c) Tilt angle

(d) Suspension deflection

Figure 5.9: Simulation results for CDD control

5.4 MIMO Optimal control

The design process of MIMO Optimal control is well discussed in Section 2.3 and Section 4.4. In this design, two extra states are included to the system as the extra system states for disturbance rejection, reference tracking and decreasing the lateral suspension deflection, which are the integral of the effective cant deficiency and the integral of lateral secondary suspension deflection ($\int \theta_{dm}$, $\int x_{2dfl}$). Thus the augmented system is now of the form:

$$\begin{pmatrix} \dot{x} \\ \dot{x'} \end{pmatrix} = \begin{pmatrix} A & 0 \\ C' & 0 \end{pmatrix} \begin{pmatrix} x \\ x' \end{pmatrix} + \begin{pmatrix} B \\ 0 \end{pmatrix} u$$

where x'=($\int \theta_{dm}, \int x_{2dfl}$)', $u = [\delta_a \;\; F_a]$. Now the state space matrices for the vehicle model includes the following states:

$$\dot{x} = [y_v \;\; \theta_v \;\; y_b \;\; \theta_b \;\; \dot{y}_v \;\; \dot{\theta}_v \;\; \dot{y}_b \;\; \dot{\theta}_b \;\; \theta_r \;\; y_w \;\; \dot{y}_w \;\; \theta_m \;\; \dot{\theta}_m \;\; \int \theta_{dm} \;\; \int x_{2dfl}]^T$$

The weighted outputs selected are body roll rate $(\dot{\theta}_v - \dot{\theta}_m)$, body roll angle $(\theta_v - \theta_b - \theta_m)$, $\int \theta_{dm}$ and $\int x_{2dfl}$. Final value for the weights Q_0, R_0 are listed below.

$$Q_0 = diag(\frac{1}{0.1419^2},\ \frac{1}{0.6408^2},\ \frac{1}{0.0093^2},\ \frac{1}{0.0066^2}); \quad R_0 = diag(\frac{1}{4.2299^2},\ \frac{1}{13960^2})$$

The simulation results are presented in Figure 5.10, Figure 5.11 and Table 5.4. Optimal control has a similar curving performance to the local CDD control, but it provides a significant ride quality improvement on straight track, with R.M.S. value of the measured body lateral acceleration decreasing to 1.93%g, as shown in Figure 5.10.

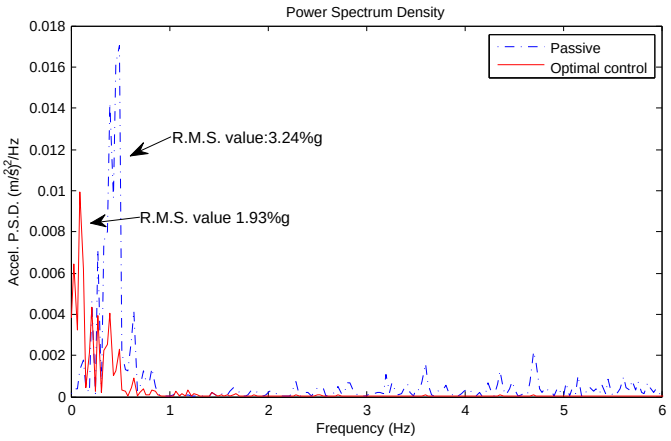

Figure 5.10: P.S.D. analysis for the measured body lateral acceleration (on straight track)

5.5 Estimator-Based Decoupling control

Traditionally, decoupling control can be performed in a classical way to separate the MIMO dynamic system into a series of independent SISO sub-systems. However, the RHP zeros limit the performance for the individual loops and also increase the complexity of the pre-compensator and controller design process, particularly for the integration system in this study since the RHP zeros exist in two loops. However, the decoupling process not only relies on the decoupling method but also upon the system configuration, i.e. which outputs are used to provide the feedback signal. The more effective feedback signal for the lateral actuator control is the body lateral acceleration $(\ddot{y}_v)$, which is unaffected by the curving response and relative to the track reference axles. It

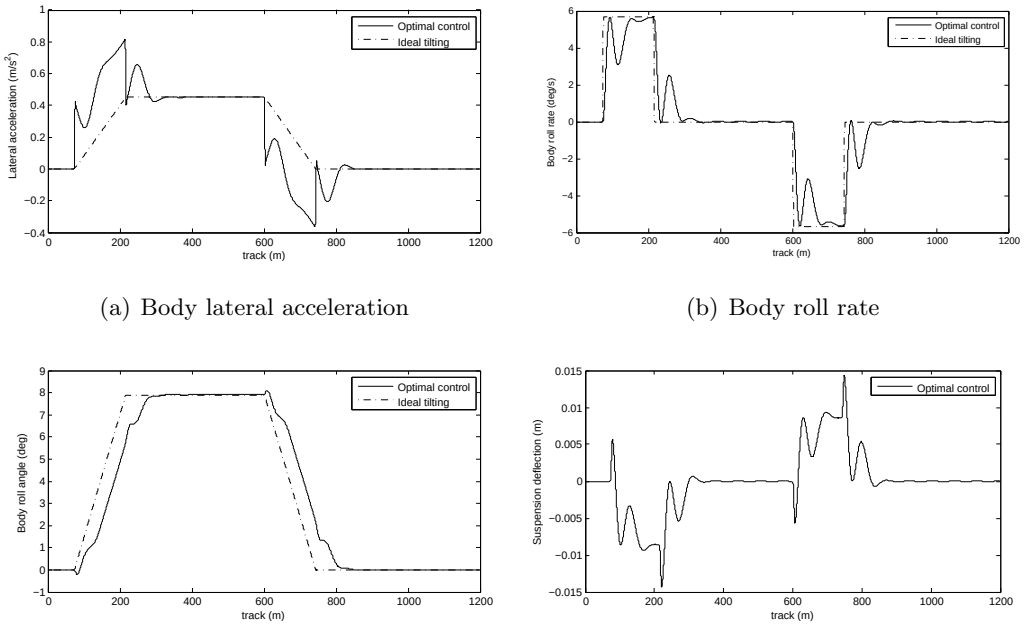

(a) Body lateral acceleration

(b) Body roll rate

(c) Tilt angle

(d) Suspension deflection

Figure 5.11: Simulation results for MIMO optimal control

Table 5.4: Control system assessment for Optimal control @ 58(m/s)

Deterministic(CURVED TRACK)		
		MIMO Optimal
Lateral acceleration.	-Steady-state(%g)	4.6
	-R.M.S. deviation error(%g)	1.7
	-Peak value(%g)	8.3
Roll gyroscope	-R.M.S. deviation(rad/s)	0.018
	-Peak value(rad/s)	0.099
	-Peak jerk level(%g/s)	4.92
P_{ct}(P-factor)	-standing(% of pasengers)	31.8
	-seated(% of pasengers)	8.1
Stochastic(STRAIGHT TRACK)		
passenger comfort	-R.M.S. passive(%g)	3.24
	-R.M.S. active(%g)	1.93
	-degradation(%)	-40.43

is not measured by the lateral accelerometer. Therefore, the lateral active suspension can purely deal with the lateral irregularity without increasing the lateral suspension curving deflection. While the different way to derive the curving acceleration experienced on the vehicle body, which is unaffected by the suspension dynamic interactions, is to use the true cant deficiency (t.c.d.) (See Section 2.1).

5.5.1 Control loop interaction analysis

The combination of body lateral acceleration ($\ddot{y}_v$) and t.c.d. as the control feedback can significantly attenuate the loop interaction and hence improve the controller performance. In this section, Relative Gain Array (RGA) is utilised to illustrate the efficiency of the I/O configuration on the control loop interaction attenuation.

The RGA of a non-singular square complex matrix G is a square complex matrix defined as

$$RGA(G) = \Lambda(G) = G \times (G^{-1})^T \tag{5.10}$$

where $\times$ denotes element by element multiplication. It is a very useful tool to measure control loop interactions and first introduced by Bristol (1966). Two rules which are useful for the design process are represented here:
(1) Large RGA elements at frequencies important for control indicate that the plant is fundamentally difficult to control due to strong interactions and sensitivity to uncertainty.
(2) Good system configuration with the selected pairings along the diagonal, has an RGA matrix close to identity at frequencies around the closed-loop bandwidth. If the RGA matrix equal to identity matrix, then the selected input-output pairing can completely decouple the interaction.

Figure 5.12 is the system input-output configuration for the conventional CD control design and the Estimator-Based Decoupling (EBD) control design. The conventional design has the measured body lateral acceleration and e.c.d. as the feedback whereas the estimated body lateral acceleration and t.c.d. are used for the EBD control.

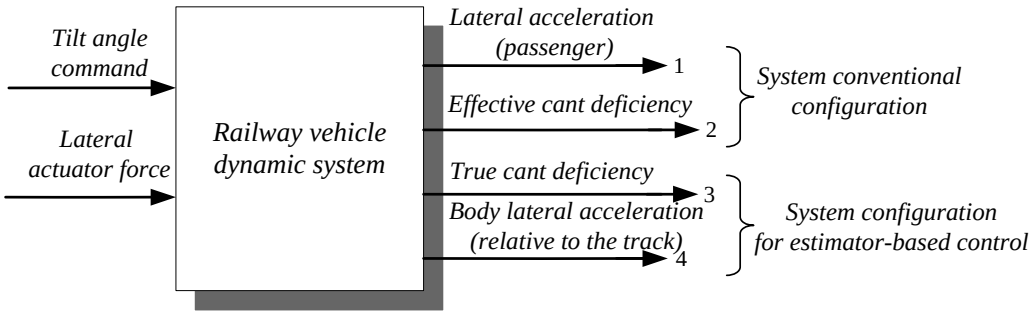

Figure 5.12: Control system configuration (conventional vs. new)

Figure 5.13(a, b) show the frequency dependent RGA element for these two 2×2 system configurations. The conventional control configuration has the larger RGA element (far more than 5) indicating the difficulty of decentralised controller design due to the strong interaction (shown in Figure 5.13(a)). Figure 5.13(b) shows the efficiency of the new configuration. RGA matrix approaches the identity matrix particularly at low frequencies (steady-state) and after $10rad/s$ with the steady-state value equal to 1.1, and the loops are fully decoupled at high frequencies. The cut-off frequency of tilting controller needs to be designed within $3rad/s$ to keep the diagonal RGA elements around 1. The RGA elements are less than 1.3 at frequencies below $3rad/s$ with the steady-state value equal to 1.1.

5.5.2 Preliminary of H_∞ filter

However, to measure t.c.d. and body lateral acceleration (relative to the track reference) is not a practical solution. Therefore, the estimator technology can be adopted. In this section, H_∞ filter (Simon (2006)) is employed to estimate these quantities.
The continuous-time system state space model is as follows:

$$\begin{aligned} \dot{x} &= Ax + Bu + \Gamma w \\ y &= Cx + Du + Hv \\ z &= Lx \end{aligned} \tag{5.11}$$

where L is a user-defined matrix and z is the vector that we want to estimate (the Identy matrix for full states estimation), but in general we may only be interested in certain linear combinations of the state. $\widehat{z}$ denotes the estimated z, and $\widehat{x}(0)$ denotes

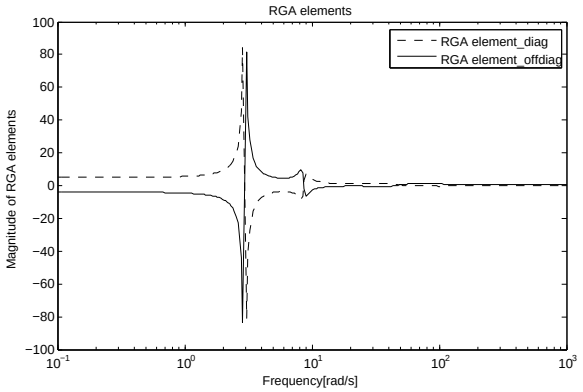

(a) Frequency dependent RGA for the conventional control configuration

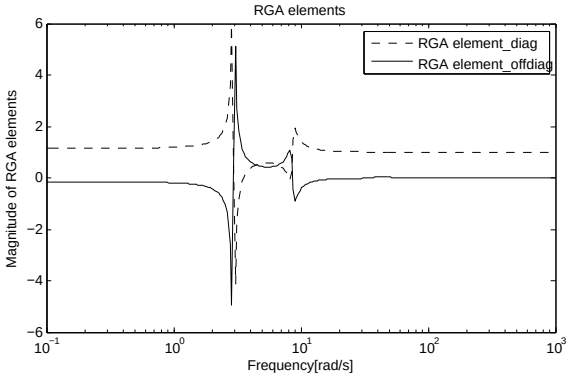

(b) Frequency dependent RGA for the estimator based control configuration

Figure 5.13: Frequency dependent RGA

the estimated state at time 0. w and v are disturbances with unknown statistics (no restriction on the zero-mean). The following cost function is defined:

$$J_1 = \frac{\int_0^T ||z - \widehat{z}||^2_S dt}{||x(0) - \widehat{x}(0)||^2_{P_0{}^{-1}} + \int_0^T (||w||^2_{Q^{-1}} + ||v||^2_{R^{-1}}) dt} \tag{5.12}$$

where $||A||^2_B \triangleq A^T B A$. J_1 is defined based on the game theory approach (Simon (2006)). The goal of H_∞ design is to find an estimate $\widehat{z}$ to minimize J_1. The direct minimization of J_1 is not tractable, so instead a performance bound is choose such that:

$$J_1 < \frac{1}{\theta} \tag{5.13}$$

P_0, Q, R, and S are positive definite matrices chosen by the engineer based on the specific problem. The estimator that solves this problem is given by

$$\begin{aligned} P(0) &= P_0 \\ \dot{P} &= AP + PA^T + Q - KCP + \theta PL^T SLP \\ K &= PC^T R^{-1} \\ \dot{\widehat{x}} &= A_k\widehat{x} + B_k u + K_f(y_k - C_k\widehat{x} - D_k u) \\ \widehat{z} &= L\widehat{x} \end{aligned} \tag{5.14}$$

These equations are similar to the continuous-time Kalman filter equations except for the θ term in the $\dot{P}$ equation. The increase of θ results in the increase of the gain K, which tends to make the estimator more responsive to measurements than the Kalman filter. This is a way of making the filter more robust to uncertainty in the system model. Let $\dot{P} = 0$ gains the steady-state continuous-time H_∞ filter. P can be obtained by solving the Riccati equation (Simon (2006)).

5.5.3 H_∞ filter design and Parametric uncertainty test

This section presents the design process of H_∞ filter for the integrated tilting bolster and active lateral secondary suspension control. The inputs to the H_∞ filter are three measurements and two system inputs. The system disturbances (θ_0 $\dot{\theta}_0$ R^{-1}) are included into the system state space model as the states. Now the system holds the following states:

$$\dot{x} = [y_v \;\; \theta_v \;\; y_b \;\; \theta_b \;\; \dot{y}_v \;\; \dot{\theta}_v \;\; \dot{y}_b \;\; \dot{\theta}_b \;\; \theta_r \;\; y_w \;\; \dot{y}_w \;\; \theta_m \;\; \dot{\theta}_m \;\; \theta_0 \;\; \dot{\theta}_0 \;\; R^{-1}]^T \tag{5.15}$$

System has two inputs

$$u = [\theta_{m_i} F_a]^T \tag{5.16}$$

And the process noise is characterised by

$$\omega = [\dot{R}^{-1} \;\; \ddot{\theta}_0]^T \tag{5.17}$$

The algebraic Riccati equation presented in (5.14) can be solved by the Matlab function 'care', and the estimation results are shown in Figure 5.14, which are the estimated t.c.d. and estimated relative lateral acceleration on curved track. The errors are small,

and mainly due to the noise in the measurements, however the estimator successfully estimates all necessary quantities even if the state vector included disturbance input components.

The parameters chosen for the H_∞ filter are:

$R = diag(1.1 \times 10^{-3},\ 1.4 \times 10^{-6},\ 1 \times 10^{-6})$
$Q = diag(8.33 \times 10^{-6},\ 2.32 \times 10^{-3})$
$L = diag(1, 1, 1, 1, 1, 1, 1, 1, 1, 1, 1, 1, 1, 1, 1, 1)$
$S = 9000 * diag(1, 1, 1, 1, 1, 1, 1, 1, 1, 1, 1, 1, 1, 1, 1, 1)$
$\theta = 0.2$

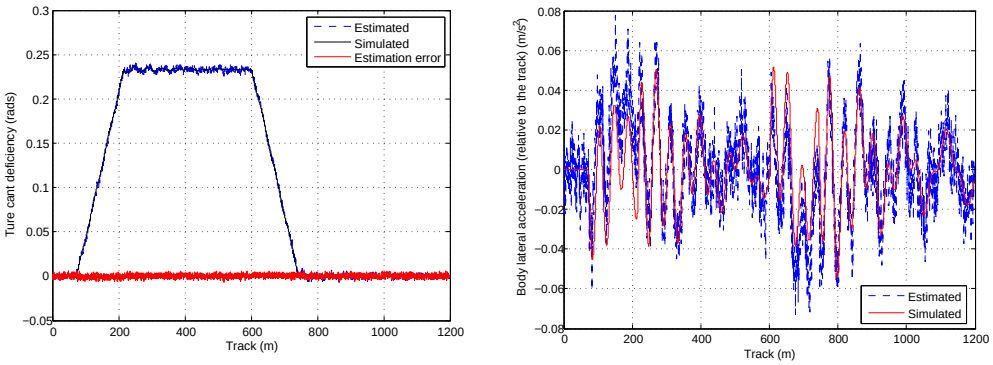

(a) Curved track estimation

(b) Straight track estimation

Figure 5.14: H_∞ filter estimation results

5.5.3.1 Parametric uncertainty test

The robustness test of H_∞ filter respect to parametric uncertainty is performed in this section with the comparison with Kalman-Bucy filter. The parameters chosen for the Kalman filter are:

$R = diag(1.1 \times 10^{-3},\ 1.4 \times 10^{-6},\ 1 \times 10^{-6})$
$Q = diag(8.33 \times 10^{-6},\ 2.32 \times 10^{-3})$

•Test case 1: The mass of vehicle body varies from $16000kg$ to $24000kg$ due to the variation of the vehicle load, but it is extended to $40000kg$ for the further worst case test. It is combined with the body roll inertia increasing from $20000kgm^2$ to $27000kgm^2$:

$$m = m_v(1 + p_m\delta_m); \quad i_{vr} = i_{vr}(1 + p_{i_{vr}}\delta_{i_{vr}}) \tag{5.18}$$

where $\delta_m = 0.125,\ p_m = [1\ to\ 12];\ p_{i_{vr}} = 0.04,\ \delta_{i_{vr}} = [1\ to\ 12]$, Figure 5.15 and Figure 5.16 show the R.M.S. value of the estimation error and maximum estimation error in the various mass and roll inertia for the true cant deficiency estimation and body lateral acceleration estimation. The test results show both Kalman filter and H_∞ filter can work well when the mass is less than $24000Kg$, but H_∞ filter has the robustness when further increase of the vehicle body mass as illustrated in Figure 5.16.
• Test case 2: The parameter for the lateral secondary spring decreases from $100000N/m$ to $5000N/m$:

$$k_{sy} = k_{sy}(1 - p_{k_{sy}}\delta_{k_{sy}}); \tag{5.19}$$

where $\delta_m = 0.05,\ p_m = [1\ to\ 16]$. The test results (shown in Figure 5.17 and Figure 5.18) illustrate the robustness of H_∞ filter when the spring coefficient is less than $45000N/m$, but the estimation for t.c.d. shows no difference for both methods.

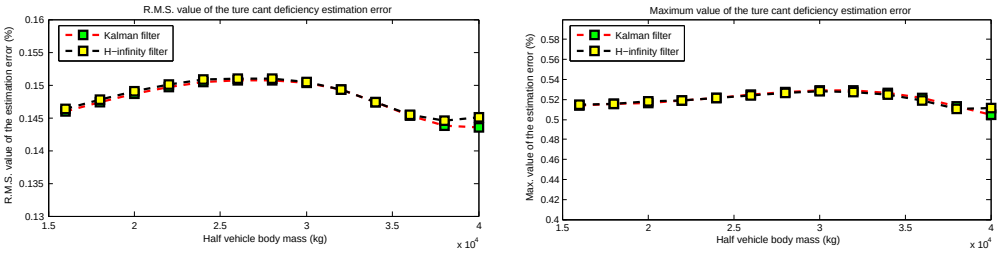

(a) R.M.S. value of the estimation error (b) Maximum value of the estimation error

Figure 5.15: t.c.d. estimation error with respect to parametric uncertainties

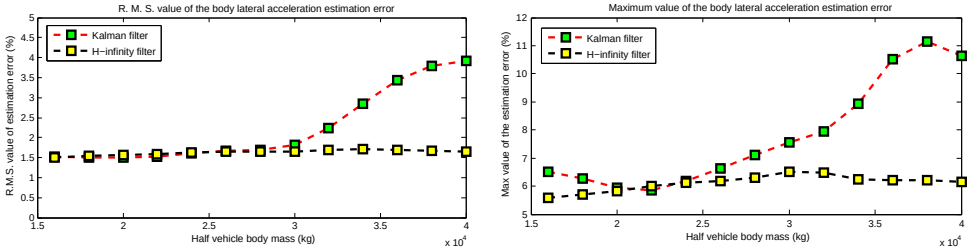

(a) R.M.S. value of the estimation error (b) Maximum value of the estimation error

Figure 5.16: Body lateral acceleration estimation error with respect to parametric uncertainties

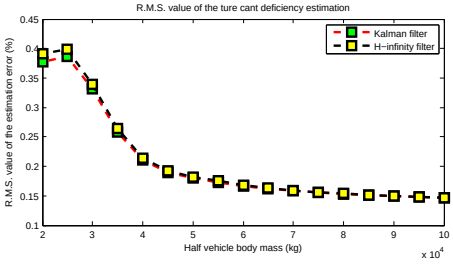

(a) R.M.S. value of the estimation error

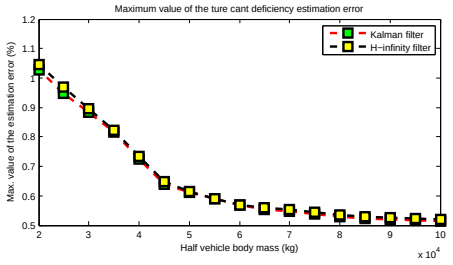

(b) Maximum value of the estimation error

Figure 5.17: t.c.d. estimation error with respect to parametric uncertainties

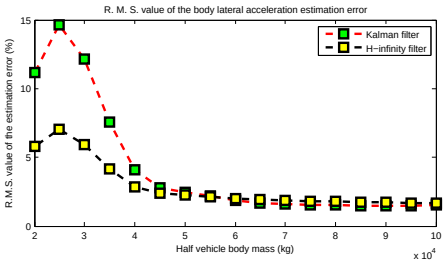

(a) R.M.S. value of the estimation error

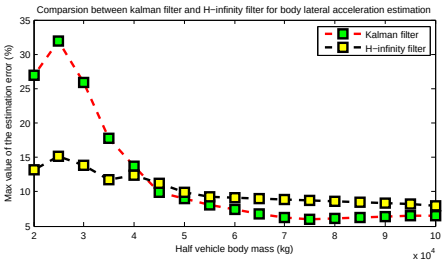

(b) Maximum value of the estimation error

Figure 5.18: Body lateral acceleration estimation error with respect to parametric uncertainties

5.5.4 Controller design

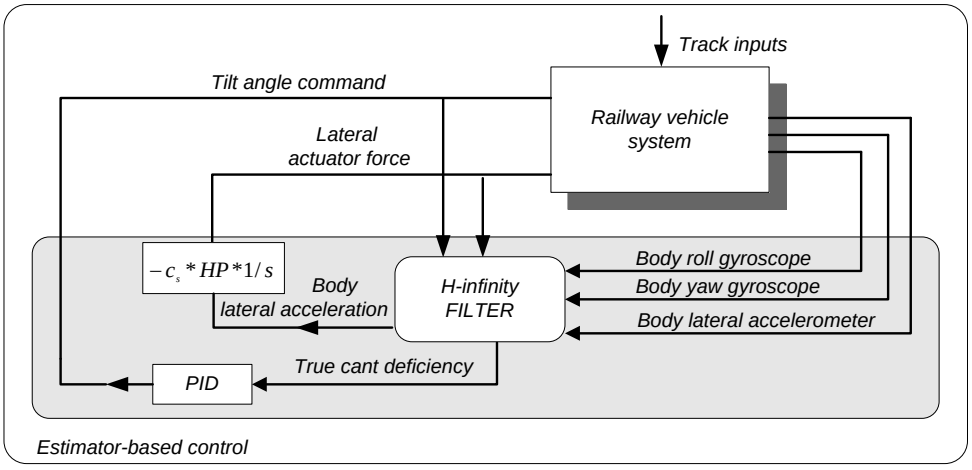

Figure 5.19: Control system configuration for EBD control

The skyhook damping control is adopted for the lateral actuator with the estimated body lateral acceleration.

$$-c_s * HP * 1/s = -58000 \times \frac{s^2}{s^2 + 2 \times w_i \times \xi s + {w_i}^2} \times \frac{1}{s} \tag{5.20}$$

where c_s is the skyhook damping coiffecient, w_i is the cut-off frequency with the value 2*pi*0.13rad/s, damping ratio $\xi = 0.707$.

An approximate PID controller ($k_p = 0.001, k_i = 4.8, k_d = 0.07, N = 1000$) is designed for tilting control with the t.c.d., the overall configuration is shown in Figure 5.19.

$$f_{A.PID} = (0.001 + \frac{4.8}{s} + \frac{0.07s}{s/1000 + 1}) \tag{5.21}$$

Note that, the t.c.d. is configured as (5.22) for providing 75% lateral acceleration compensation.

$$\theta_{tdm} = 0.78\frac{v^2}{g\widehat{R}} - (0.78\widehat{\theta_0} + \widehat{\theta_t}) \tag{5.22}$$

The simulation results are illustrated in Figure 5.20, Figure 5.21(a) and Table 5.5. The performance of the EBD control is close to PT control as well as the ideal situation. The R.M.S. deviation error of EBD control for the lateral acceleration is 0.9%g, which is close to the value of the PT control (0.73%g). Also, the P_{ct} value for seated passengers

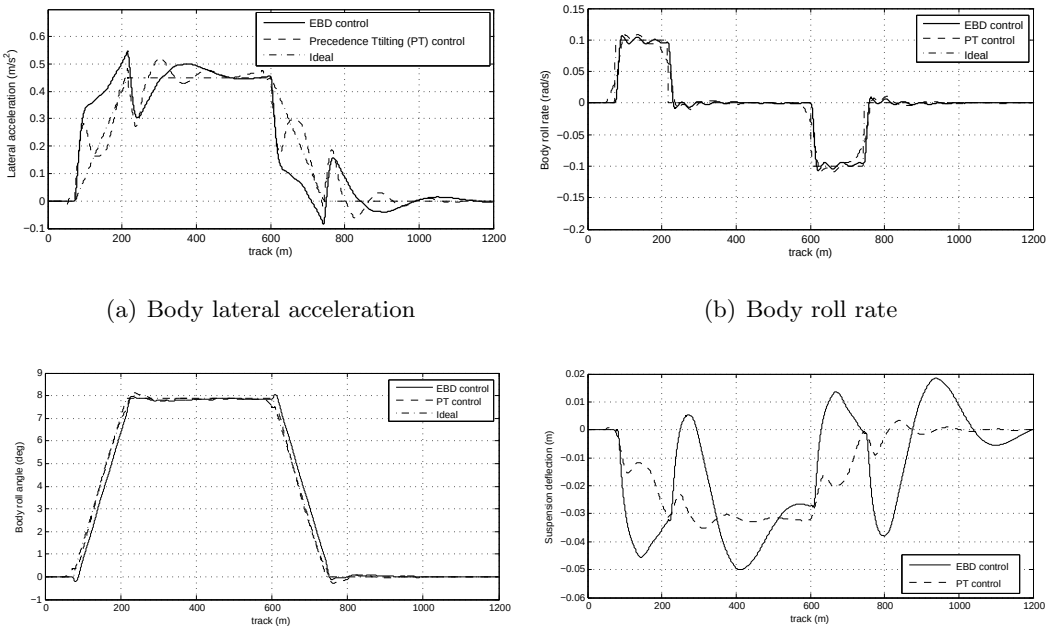

(a) Body lateral acceleration

(b) Body roll rate

(c) Tilt angle

(d) Suspension deflection

Figure 5.20: Simulation results for EBD control

(4.91%g) of the EBD control is close to the value for the PT control (3.7%g), and 50% ride quality improvement is provided (R.M.S. value is 1.64%g). Figure 5.21(b) also shows the robustness comparison between CD control and EBD control.

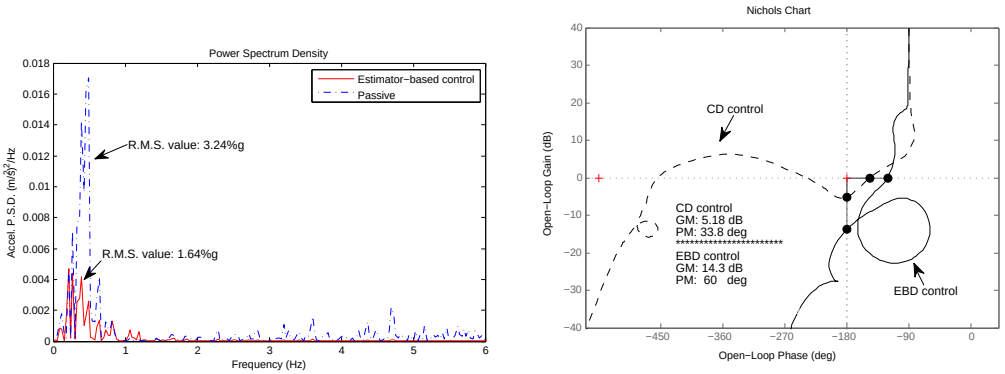

(a) P.S.D. analysis for the measured body lateral acceleration (on straight track)

(b) Nichols plot for the tilting control

Figure 5.21: P.S.D. analysis and Nichols plot

Table 5.5: Control system assessment for EBD control@ 58(m/s)

Deterministic(CURVED TRACK)			
		EBD	PT
Lateral acceleration.	-Steady-state(%g)	4.6	4.6
	-R.M.S. deviation error(%g)	0.9	0.73
	-Peak value(%g)	5.6	5
Roll gyroscope	-R.M.S. deviation(rad/s)	0.014	0.015
	-Peak value(rad/s)	0.107	0.11
	-Peak jerk level(%g/s)	3.79	3.02
P_{ct}(P-factor)	-standing(% of pasengers)	23.8	20.6
	-seated(% of pasengers)	4.91	3.7
Stochastic(STRAIGHT TRACK)			
passenger comfort	-R.M.S. passive(%g)	3.24	3.24
	-R.M.S. active(%g)	1.64	2.29
	-degradation(%)	-49.38	-28.6

5.6 Summary

5.6.1 Controller performance comparison

Figure 5.22 gives the curving performance and straight track ride quality comparison between 4 proposed controllers for the dual-actuator system, also for the comparison with the tilt-only Precedence Tilting (PT) and Nulling Tilting (NT) approaches. The Command-Driven Decentralised (CDD) control provides the best performance in trailing vehicles both on curved and straight track. It shows the potential benefit to use the active lateral secondary suspension in improving the commercial precedence tilting control system performance. Estimator-Based Decentralised (EBD) control gives a significant improvement of the ride quality on straight track and has a closer P_{ct} value for the seated passengers to the PT control. Hence, the estimator-based approach is a candidate strategy to be used in the case of leading vehicle performance improvement. Classical Decentralised (CD) control also provides the improvement to the problem of local tilt control performance, this is a simple solution for the implementation on the real train however the improvement is constrained.

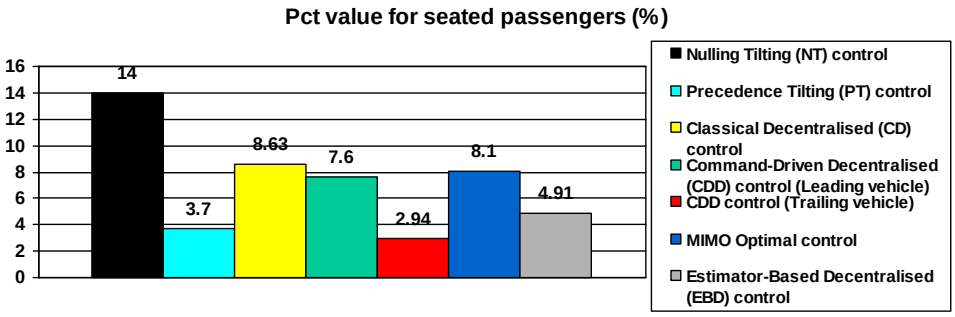

(a) Controller performance comparison on curved track

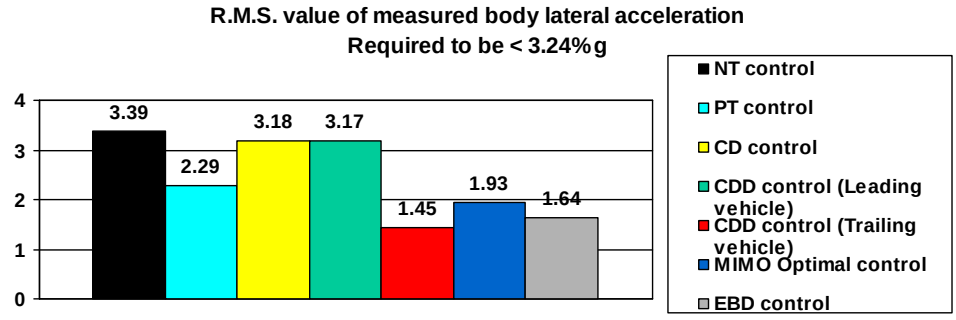

(b) Controller performance comparison on straight track

Figure 5.22: Controller performance comparison

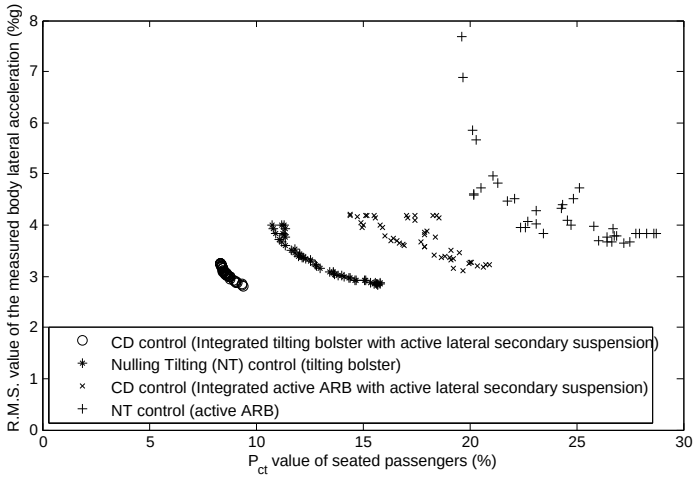

Figure 5.23: Trade-off plot for the tilting control between curving performance and straight track ride quality

5.6.2 Comparison between ARB tilting and Tilting bolster

Figure 5.23 shows the trade-off plot for the tilting control between curving performance and straight track ride quality. '+' and 'x' curve lines are for the tilting train with active ARB. '*' and 'o' curve lines are for the tilting train with tilting bolster. With the help from lateral actuator, the trade-off is optimised in both cases even with classical control, as indicated in 'x' and 'o' curve lines. The integrated tilting bolster and active lateral secondary suspension control gives the best result (as shown in 'o' curve line), because the tilting action is below secondary suspension which provides the capability to compensate 75% lateral acceleration. Chapter 6 will focus on the 9 DOF modelling and control for the integration of tilting bolster and active lateral secondary suspensions.

Chapter 6

Full vehicle modelling and control

The work summarized in previous chapters is based on the 4 DOF end-view model which only includes lateral and roll dynamics of railway vehicle body and bogie. The simulation results show the benefits we can obtain from the integration of tilt and active lateral secondary suspension control. In this chapter, a 9 DOF full vehicle modelling is presented including the dynamics of two bogies and one vehicle body, the yaw dynamic is taken into account. The control strategies designed based on the end-view model can be directly implemented into this full vehicle model. Furthermore, modal control approach is employed to control the lateral and yaw dynamics to enhance the ride quality on straight track. Also, the actuator dynamics are discussed.

6.1 Linear 9 DOF vehicle modelling for integrated tilting bolster and active lateral secondary suspension

The full vehicle model consists of a vehicle body, two bogie frames and four wheelsets. Each wheelset is constrained to run along the centerline of the track, and connected to the associated bogie through a primary suspension consisting of linear springs and dampers in the lateral, vertical, and longitudinal directions. Each bogie frame is assumed to be rigid and assigned lateral, yaw, and roll DOF. The carbody is attached to two bogies via tilting bolster and has lateral, yaw, and roll DOF. The modelling process is based on Newton laws and track references (Garg and Dukkipati (1984)), also includes the translation and rotation of these reference axis associated with curves. The

9 DOF vehicle model for the integrated tilting bolster and active lateral secondary suspension is detailed in this section. The end-view and plan-view model are illustrated in Figure 6.1, the dynamics force analysis and numerical equations are presented in Figure 6.2 and following subsections respectively.

Note that: The model for the integrated active ARB and active lateral secondary suspension can be developed in the similar way. The final numerical equations and parameters are detailed in Appendix F. Further details about full vehicle modelling for tilting trains with active ARB can be found in Zamzuri (2008).

6.1.1 Body dynamics

Body lateral dynamics:

$$m_v\ddot{y}_v = -\sum_{i=1}^{2} F_{yvfi} - \sum_{i=1}^{2} F_{yvri} + F_{gc} - F_{Rc} - F_c^{''} + F_{ar} + F_{af} \tag{6.1}$$

Body roll dynamics:

$$\begin{aligned} i_{vr}\ddot{\theta}_v &= h_1\sum_{i=1}^{2} F_{yvfi} + h_1\sum_{i=1}^{2} F_{yvri} + T_c + d^{'}F_c^{'} + d_1(F_{z1f} - F_{z2f}) \\ &\quad + d_1(F_{z1r} - F_{z2r}) - T_c^{''} - F_{ar}h_1 - F_{af}h_1 \end{aligned} \tag{6.2}$$

Body yaw dynamics:

$$i_{vy}\ddot{\psi}_v = L_v\sum_{i=1}^{2} F_{yvfi} - L_v\sum_{i=1}^{2} F_{yvri} - T_x - T_{\gamma c} + F_{af}L_v - F_{ar}L_v \tag{6.3}$$

F_{af} and F_{ar} are the front lateral actuator force and the rear lateral actuator force respectively.

$$F_{Rc} = m_v\frac{v^2}{R_c}; \quad F_{gc} = m_v g\theta_{oc}; \quad F_c^{''} = m_v h_{g1}\ddot{\theta}_{oc} \tag{6.4}$$

where F_{Rc} is the centrifugal force, F_{gc} is the force produced by the gravity of vehicle body and $F_c^{''}$ allows for the translation and rotation of the moving track reference at centre of the vehicle body.

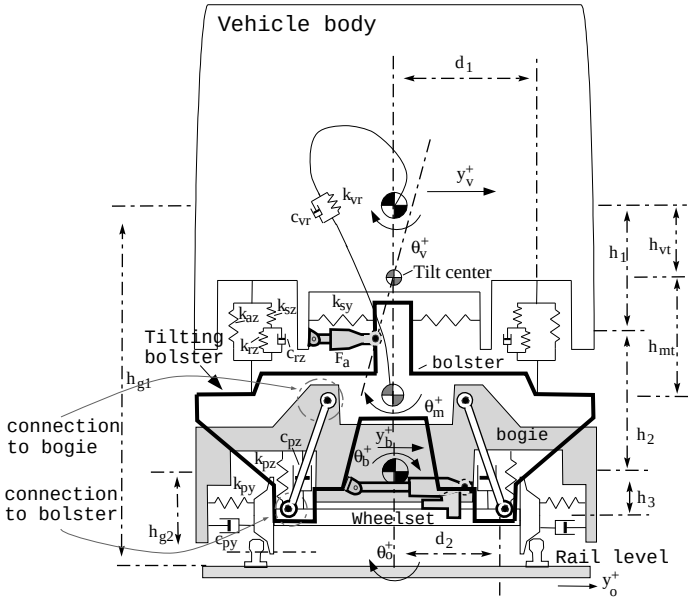

(a) End-view

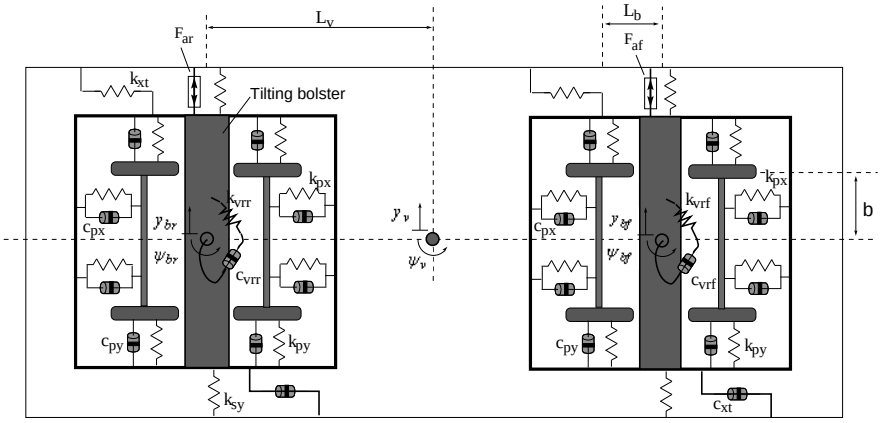

(b) Plan-view

Figure 6.1: End-view and Plan-view model

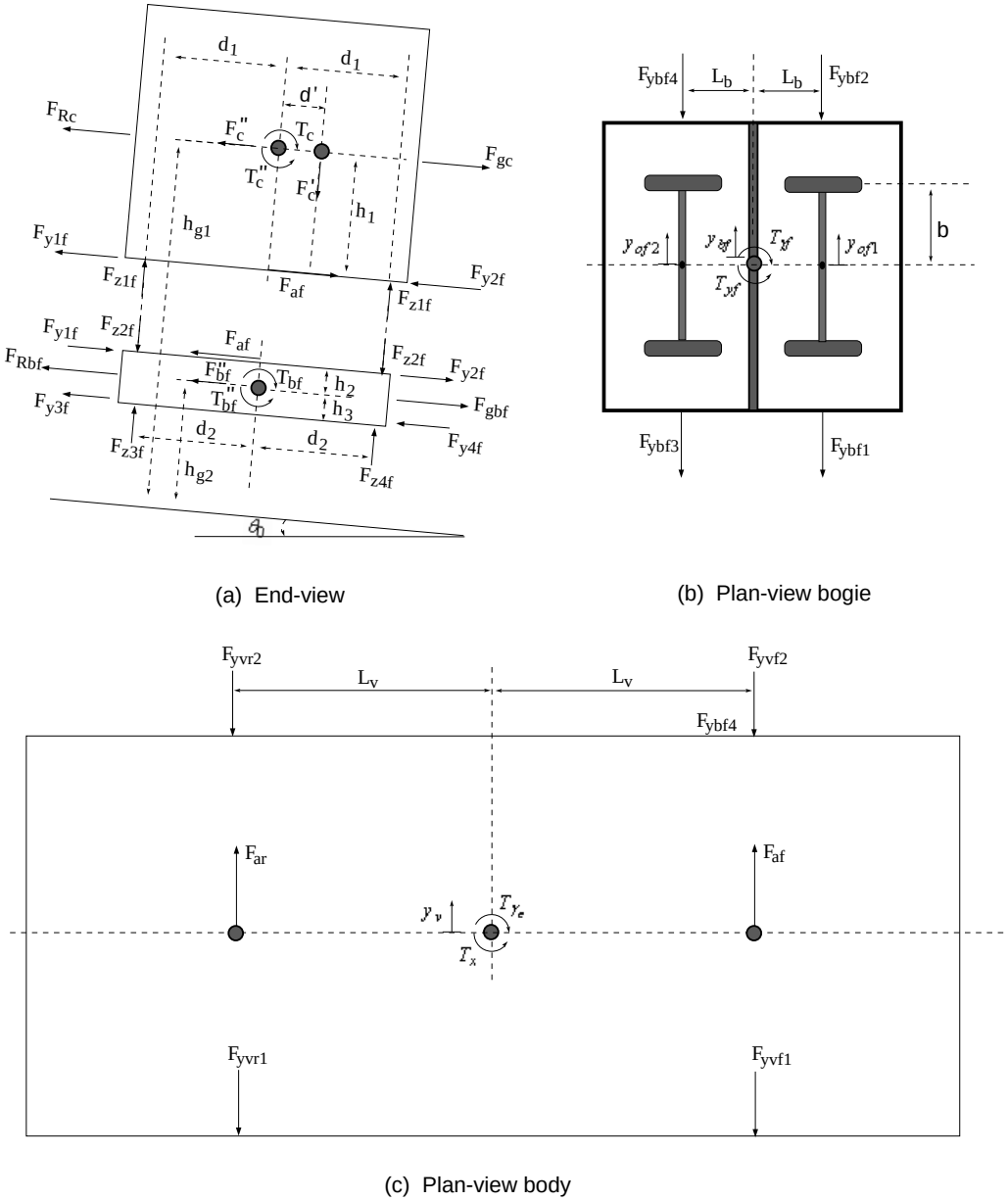

(a) End-view

(b) Plan-view bogie

(c) Plan-view body

Figure 6.2: Force analysis

The front lateral secondary suspension deflection and force are:

$$\begin{aligned} x_{deflf} &= y_v - h_1\theta_v + h_{mt}\theta_{mf} - y_{bf} - h_2\theta_{bf} - L_v\psi_v \\ F_{yvfi} &= k_{sy}(y_v - h_1\theta_v + h_{mt}\theta_{mf} - y_{bf} - h_2\theta_{bf} - L_v\psi_v) \end{aligned} \tag{6.5}$$

Note that: the lateral movement effect of the tilt bolster ($h_{mt}\theta_{mf}$) is included in the secondary suspension deflection.

The rear lateral secondary suspension deflection and force are:

$$\begin{aligned} x_{deflr} &= y_v - h_1\theta_v + h_{mt}\theta_{mr} - y_{br} - h_2\theta_{br} + L_v\psi_v \\ F_{yvri} &= k_{sy}(y_v - h_1\theta_v + h_{mt}\theta_{mr} - y_{br} - h_2\theta_{br} + L_v\psi_v) \end{aligned} \tag{6.6}$$

The torque produced by the front and rear anti-roll bar is:

$$\begin{aligned} T_f &= k_{vr}(\theta_v - \theta_{bf} - \theta_{mf}) + c_{vr}(\dot{\theta}_v - \dot{\theta}_{bf} - \dot{\theta}_{mf}) \\ T_r &= k_{vr}(\theta_v - \theta_{br} - \theta_{mr}) + c_{vr}(\dot{\theta}_v - \dot{\theta}_{br} - \dot{\theta}_{mr}) \end{aligned} \tag{6.7}$$

$$\begin{aligned} T_c &= -T_f - T_r \\ &= -k_{vr}(2\theta_v - (\theta_{bf} + \theta_{br}) - (\theta_{mf} + \theta_{mr})) \\ &\quad -c_{vr}(2\dot{\theta}_v - (\dot{\theta}_{bf} + \dot{\theta}_{br}) - (\dot{\theta}_{mf} + \dot{\theta}_{mr})) \end{aligned} \tag{6.8}$$

$F_c^{'}$ in (6.2) is the end moment effect defined as the body weight effect for both ends of the body roll due to the lateral displacement at the body centre of gravity, given by

$$\begin{aligned} F_c^{'} &= m_v g d^{'} \\ &= m_v g(y_v - (\frac{y_{bf} + y_{br}}{2})) \end{aligned} \tag{6.9}$$

The force produced by vertical suspension system:

$$F_{z1f} = -k_{az}d_1(\theta_v - \theta_{bf} - \theta_{mf}) - k_{sz}d_1(\theta_v - \theta_{rf}) \tag{6.10}$$

$$F_{z1r} = -k_{az}d_1(\theta_v - \theta_{br} - \theta_{mr}) - k_{sz}d_1(\theta_v - \theta_{rr}) \tag{6.11}$$

$$F_{z2f} = -F_{z1f}, F_{z2r} = -F_{z1r}, T_c^{''} = i_{vr}\ddot{\theta}_{oc} \tag{6.12}$$

The airspring reservoir roll states for both the front and the rear bogies are characterised by the following equations.

$$\dot{\theta}_{rf} = -\frac{k_{sz} + k_{rz}}{c_{rz}}\theta_{rf} + \frac{k_{sz}}{c_{rz}}\theta_v + \frac{k_{rz}}{c_{rz}}\theta_{bf} + \dot{\theta}_{bf} \tag{6.13}$$

$$\dot{\theta}_{rr} = -\frac{k_{sz} + k_{rz}}{c_{rz}}\theta_{rr} + \frac{k_{sz}}{c_{rz}}\theta_v + \frac{k_{rz}}{c_{rz}}\theta_{br} + \dot{\theta}_{br} \tag{6.14}$$

The yaw torque produced by the secondary yaw suspension is given by:

$$T_x = k_{xt}(\psi_{bf} + \psi_{br} - 2\psi_v) + c_{xt}(\dot{\psi}_{bf} + \dot{\psi}_{br} - 2\dot{\psi}_v) \tag{6.15}$$

6.1.2 Bogie dynamics

Based on the force analysis in Figure 6.2, the equations of motion for the front and rear bogie lateral, roll and yaw motions are as follows:
Front-bogie lateral:

$$m_b\ddot{y}_{bf} - \sum_{i=1}^{2} F_{yvfi} + \sum_{i=1}^{2} F_{ybfi} + \sum_{i=3}^{4} F_{ybfi} = -F_{Rbf} + F_{gbf} - F_f{}'' - F_{af} \tag{6.16}$$

Front-bogie roll:

$$\begin{aligned} & i_{br}\ddot{\theta}_{bf} - h_2\sum_{i=1}^{2} F_{yvfi} - h_3\sum_{i=1}^{2} F_{ybfi} - h_3\sum_{i=3}^{4} F_{ybfi} \\ = \;& -T_f - d_1(F_{z1f} - F_{z2f}) + d_2(F_{z3f} - F_{z4f}) - T_{bf}{}'' - F_{af}h_2 \end{aligned} \tag{6.17}$$

Front-bogie yaw:

$$i_{by}\ddot{\psi}_{bf} - b\sum_{i=1}^{2} F_{ybfi} + b\sum_{i=3}^{4} F_{ybfi} - T_{yf} = -T_{\gamma f} \tag{6.18}$$

where:

$$F_{Rbf} = m_v\frac{v^2}{R_f}; \quad F_{gbf} = m_v g\theta_{of}; \quad F_f{}'' = m_b h_{g2}\ddot{\theta}_{of} \tag{6.19}$$

are the centrifugal force on the front bogie, the force produced by the gravity of front vehicle bogie and the effect for the translation and rotation of the moving track reference at centre of the front vehicle bogie.

The lateral primary suspension forces are:

$$\begin{aligned} F_{ybf1} &= k_{py}(y_{bf} - h_3\theta_{bf} - y_{of1} - b\psi_{bf}) + c_{py}(\dot{y}_{bf} - h_3\dot{\theta}_{bf} - \dot{y}_{of1} - b\dot{\psi}_{bf}) \\ F_{ybf3} &= k_{py}(y_{bf} - h_3\theta_{bf} - y_{of2} + b\psi_{bf}) + c_{py}(\dot{y}_{bf} - h_3\dot{\theta}_{bf} - \dot{y}_{of2} + b\dot{\psi}_{bf}) \\ F_{ybf2} &= F_{ybf1}; \quad F_{ybf4} = F_{ybf3} \end{aligned} \tag{6.20}$$

The veritcal primary suspension force is:

$$F_{z1f} = -k_{pz}d_2\theta_{bf} - c_{pz}d_2\dot{\theta}_{bf} \tag{6.21}$$

The torque produced by the front tilt actuator is:

$$T_f = k_{vr}(\theta_v - \theta_{bf} - \theta_{mf}) \tag{6.22}$$

The rotation torque from the yaw secondary suspension is:

$$T_{yf} = k_{xt}(\psi_{bf} - \theta_v) + c_{xt}(\dot{\psi}_{bf} - \dot{\theta}_v) \tag{6.23}$$

Rear-bogie lateral:

$$m_b\ddot{y_{br}} - \sum_{i=1}^{2} F_{yvri} + \sum_{i=1}^{2} F_{ybri} + \sum_{i=3}^{4} F_{ybri} = -F_{Rbf} + F_{gbf} - F_f{}'' - F_{ar} \tag{6.24}$$

Rear-bogie roll:

$$\begin{aligned} & i_{br}\ddot{\theta_{br}} - h_2\sum_{i=1}^{2} F_{yvri} - h_3\sum_{i=1}^{2} F_{ybri} - h_3\sum_{i=3}^{4} F_{ybri} \\ = \; & -T_r - d_1(F_{z1r} - F_{z2r}) + d_2(F_{z3r} - F_{z4r}) - T_{br}{}'' - F_{ar}h_2 \end{aligned} \tag{6.25}$$

Rear-bogie yaw:

$$i_{br}\ddot{\psi_{br}} - b\sum_{i=1}^{2} F_{ybfi} + b\sum_{i=3}^{4} F_{ybri} - T_{yr} = -T_{\gamma r} \tag{6.26}$$

6.1.3 Numerical equations for the full railway vehicle

The full numerical equations for the body and bogies dynamics are as follows:
Body lateral:

$$\begin{aligned} m_v\ddot{y}_v = \; & -4k_{sy}y_v + 4k_{sy}h_1\theta_v + 2k_{sy}y_{bf} + 2k_{sy}h_2\theta_{bf} - 2k_{sy}h_{mt}\theta_{mf} \\ & +2k_{sy}y_{br} + 2k_{sy}h_2\theta_{br} - 2k_{sy}h_{mt}\theta_{mr} \\ & -\frac{m_v v^2}{R_c} + m_v g\theta_0 - h_{g1}m_v\ddot{\theta}_{0c} + F_{ar} + F_{af} \end{aligned} \tag{6.27}$$

Body roll:

$$\begin{aligned} i_{vr}\ddot{\theta}_v = \; & (4h_1k_{sy} + m_v g)y_v - (4h_1k_{sy} + 4{d_1}^2k_{az} + 4{d_1}^2k_{sz} + 2k_{vr})\theta_v \\ & -2c_{vr}\dot{\theta}_v - (2h_1k_{sy} + \frac{m_v g}{2})y_{bf} - (2h_1h_2k_{sy} - 2{d_1}^2k_{az} - k_{vr})\theta_{bf} \\ & +c_{vr}\dot{\theta}_{bf} - (2h_1k_{sy} + \frac{m_v g}{2})y_{br} - (2h_1h_2k_{sy} - 2{d_1}^2k_{az} \\ & +k_{vr})\theta_{br} + c_{vr}\dot{\theta}_{br} - i_{vr}\ddot{\theta}_{0c} + (k_{vr} + 2d_1d_1k_{sz} + 2k_{sz}h_1h_{mt})\theta_{mf} \\ & +(k_{vr} + 2d_1d_1k_{sz} + 2k_{sz}h_1h_{mt})\theta_{mr} + c_{vr}\dot{\theta}_{mf} + c_{vr}\dot{\theta}_{mr} \\ & -F_{af}h_1 - F_{ar}h_1 \end{aligned} \tag{6.28}$$

Body yaw:

$$\begin{aligned} i_{vy}\ddot{\psi}_v &= -2L_v k_{sy} y_{bf} - 2L_v h_2 k_{sy}\theta_{bf} \\ &\quad +2L_v y_{br} + 2L_v h_2 k_{sy}\theta_{br} + 2L_v c_{sy} h_2 \dot{\theta}_{br} + k_{xt}\psi_{bf} \\ &\quad +k_{xt}\psi_{br} - 2k_{xt}\psi_v + c_{xt}\dot{\psi}_{bf} + c_{xt}\dot{\psi}_{br} - 2c_{xt}\dot{\psi}_v + i_{vy}\dot{\gamma}_c \\ &\quad -2L_v k_{sy} h_{mt}\theta_{mf} + 2L_v k_{sy} h_{mt}\theta_{mr} + F_{af}L_v - F_{ar}L_v \end{aligned} \tag{6.29}$$

Front bogie lateral:

$$\begin{aligned} m_b\ddot{y}_{bf} &= 2k_{sy}y_v - 2k_{sy}h_1\theta_v - 2k_{sy}L_v\psi_v - (2k_{sy}+4k_{py})y_{bf} + 4c_{py}\dot{y}_{bf} \\ &\quad +2k_{sy}h_{mt}\theta_{mf} - (2k_{sy}h_2 - 4k_{py}h_3)\theta_{bf} \\ &\quad +4c_{py}h_3\dot{\theta}_{bf} + 2k_{py}y_{wf1} + 2k_{py}y_{wf2} + 2c_{py}\dot{y}_{wf1} + 2c_{py}\dot{y}_{wf2} \\ &\quad -\frac{m_b v^2}{R_f} + m_b g\theta_{of} + m_b h_{g2}\ddot{\theta}_{of} + F_{af} \end{aligned} \tag{6.30}$$

Front bogie roll:

$$\begin{aligned} i_{vr}\ddot{\theta}_{bf} &= 2h_2k_{sy}y_v - (2h_1h_2k_{sy} - k_{vr} - 2k_{az}{d_1}^2 - 2k_{sz}{d_1}^2)\theta_v \\ &\quad -2h_2k_{sy}L_v\psi_v - (2h_2k_{sy} + 4h_3k_{py})y_{bf} - 4h_3c_{py}\dot{y}_{bf} - (2{h_2}^2k_{sy} \\ &\quad +4{h_3}^2k_{py} + 2{d_2}^2k_{pz} + 2{d_1}^2k_{az} + k_{vr})\theta_{bf} + (4{h_3}^2c_{py} + 2{d_2}^2c_{pz})\dot{\theta}_{bf} \\ &\quad +(2k_{sy}h_{mt}h_2 + k_{vr} - 2d_1d_1k_{az})\theta_{mf} + 2k_{sz}{d_1}^2\theta_{rf} - i_{bf}\ddot{\theta}_{of} \\ &\quad -2h_3k_{py}y_{wf1} - 2h_3k_{py}y_{wf2} - 2h_3c_{py}\dot{y}_{wf1} - 2h_3k_{py}\dot{y}_{wf2} - F_{af}h_2 \end{aligned} \tag{6.31}$$

Front bogie yaw:

$$\begin{aligned} i_{by}\ddot{\psi}_{bf} &= -(4b^2k_{py} + k_{xt})\psi_{bf} - (4b^2c_{py} + c_{xt})\dot{\psi}_{bf} - 2bk_{py}y_{wf1} - 2bc_{py}\dot{y}_{wf1} \\ &\quad +2bk_{py}y_{wf2} - 2bc_{py}\dot{y}_{wf2} - i_{by}\dot{\gamma}_f \end{aligned} \tag{6.32}$$

Rear bogie lateral:

$$\begin{aligned} m_b\ddot{y}_{br} &= 2k_{sy}y_v - 2k_{sy}h_1\theta_v + 2k_{sy}L_v\psi_v - (2k_{sy}+4k_{py})y_{br} + 2c_{py}\dot{y}_{br} \\ &\quad -(2k_{sy}h_2 - 4k_{py}h_3)\theta_{br} + 4c_{py}h_3\dot{\theta}_{br} + 2k_{py}y_{wr1} + 2k_{py}y_{wr2} \\ &\quad +2c_{py}\dot{y}_{wr1} + 2c_{py}\dot{y}_{wr2} - \frac{m_b v^2}{R_f} + m_b g\theta_{or} + m_b h_{g2}\ddot{\theta}_{or} + F_{ar} \end{aligned} \tag{6.33}$$

Rear bogie roll:

$$\begin{aligned} i_{vr}\ddot{\theta}_{br} &= 2h_2k_{sy}y_v - (2h_1h_2k_{sy} - k_{vr} - 2k_{az}{d_1}^2 - 2k_{sz}{d_1}^2)\theta_v \\ &\quad -2h_2k_{sy}L_v\psi_v - (2h_2k_{sy} + 4h_3k_{py})y_{br} - 4h_3c_{py}\dot{y}_{br} - (2{h_2}^2k_{sy} \\ &\quad +4{h_3}^2k_{py} + 2{d_2}^2k_{pz} + 2{d_1}^2k_{az} + k_{vr})\theta_{bf} + (4{h_3}^2c_{py} + 2{d_2}^2c_{pz})\dot{\theta}_{br} \\ &\quad +(2k_{sy}h_{mt}h_2 + k_{vr} - 2d_1d_1k_{az})\theta_{mr} + 2k_{sz}{d_1}^2\theta_{rr} - i_{br}\ddot{\theta}_{or} \\ &\quad -2h_3k_{py}y_{wr1} - 2h_3k_{py}y_{wr2} - 2h_3c_{py}\dot{y}_{wr1} - 2h_3k_{py}\dot{y}_{wr2} - F_{ar}h_2 \end{aligned} \quad (6.34)$$

Rear bogie yaw:

$$\begin{aligned} i_{by}\ddot{\psi}_{br} &= -(4b^2k_{py} + k_{xt})\psi_{br} - (4b^2c_{py} + c_{xt})\dot{\psi}_{br} - 2bk_{py}y_{wf1} - 2bc_{py}\dot{y}_{wr1} \\ &\quad +2bk_{py}y_{wr2} - 2bc_{py}\dot{y}_{wf2} - i_{by}\dot{\gamma}_r \end{aligned} \quad (6.35)$$

Wheelset dynamics are modelled as (Zolotas (2002a)):

$$\frac{y_w}{y_0}(s) = \frac{987}{s^2 + 12.57s + 987} \quad (6.36)$$

The roll effect of the tilting bolster is represented by a position servo. The parameters were chosen such that it gave $3.5Hz$ bandwidth and 50% damping closed-loop position servo mechanism (Zolotas (2002a)).

$$\frac{\delta}{\theta_{m_i}}(s) = \frac{483.6}{s^2 + 22s + 483.6} \quad (6.37)$$

Different from the end-view model, four wheelsets ($y_{wf1}, y_{wf2}, y_{wr1}, y_{wr2}$) and two tilting actuation systems (θ_{mr}, θ_{mf}) are considered in the full vehicle model. The tilting bolster is able to provide the maximum tilt up to 10 degrees, as shown in Figure 6.3.

6.1.4 System analysis and mode validation

The system dynamics equations can be arranged in a state-space form for the system analysis and controller design:

$$\begin{aligned} \dot{x} &= Ax + Bu + \Gamma\omega \\ y &= Cx + Du + H\omega \end{aligned} \quad (6.38)$$

where:

$x = [y_v \;\; \theta_v \;\; \psi_v \;\; y_{bf} \;\; \theta_{bf} \;\; \psi_{bf} \;\; y_{br} \;\; \theta_{br} \;\; \psi_{br} \;\; \dot{y}_v \;\; \dot{\theta}_v \;\; \dot{\psi}_v \;\; \dot{y}_{bf} \;\; \dot{\theta}_{bf} \;\; \dot{\psi}_{bf} \;\; \dot{y}_{br} \;\; \dot{\theta}_{br} \;\; \dot{\psi}_{br} \;\; \dot{\theta}_{rr} \;\; \theta_{rf}$

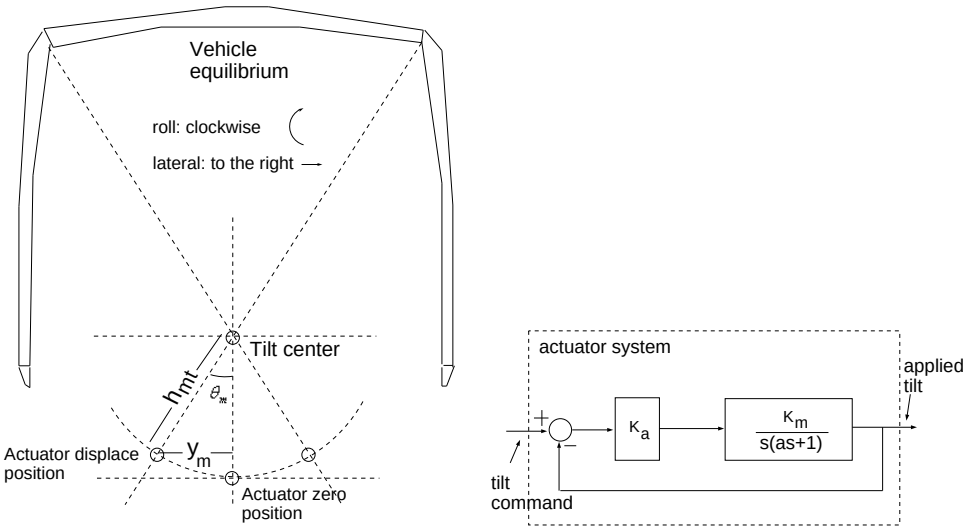

(a) Tilt Motion

(b) Tilt actuation system

Figure 6.3: Tilt actuation configuration (Zolotas (2002a))

$y_{wf1}\ \ y_{wf2}\ \ y_{wr1}\ \ y_{wr2}\ \ \dot{y}_{wf1}\ \ \dot{y}_{wf2}\ \ \dot{y}_{wr1}\ \ \dot{y}_{wr2}]^T$

$\omega = [{R_f}^{-1}\ \ {R_c}^{-1}\ \ {R_r}^{-1}\ \ \theta_{of}\ \ \theta_{or}\ \ \theta_{oc}\ \ \dot{\theta}_{of}\ \ \dot{\theta}_{or}\ \ \dot{\theta}_{oc}\ \ \ddot{\theta}_{of}\ \ \ddot{\theta}_{or}\ \ \ddot{\theta}_{oc}\ \ y_{of1}\ \ y_{of2}\ \ y_{or1}\ \ y_{or2}\ \ y_{oc}$
$\dot{y}_{of1}\ \ \dot{y}_{of2}\ \ \dot{y}_{or1}\ \ \dot{y}_{or2}\ \ \dot{y}_{oc}\ \ \gamma_f\ \ \gamma_c\ \ \gamma_r\ \ \dot{\gamma}_f\ \ \dot{\gamma}_c\ \ \dot{\gamma}_r]^T$

$u = [\delta_f\ \ \delta_r\ \ F_{af}\ \ F_{ar}]^T$

Vehicle dynamics modes (vehicle forward speed: $58m/s$) are presented in Table 6.1. Model 1 is the model for the tilting train with passive lateral dampers [1], while data of Model 2 present modes for the tilting train with uncontrolled lateral actuators. The modes of the tilting train with passive lateral dampers are close to the industry norms, but dampings in Model 2 are changed because the lateral passive dampers are replaced with uncontrolled lateral actuators. Also, the frequencies of tilt and lateral modes of 9 DOF model are similar to the modes of 4 DOF end-view model.

The vehicle model and control system are tested with the same track inputs used in

[1] Passive model can be obtained by replacing F_{af} and F_{ar} with
$-2c_{sy}(\dot{y}_v - h_1\dot{\theta}_v + h_{mt}\dot{\theta}_{mf} - \dot{y}_{bf} - h_2\dot{\theta}_{bf} - L_v\dot{\psi}_v)$ and
$-2c_{sy}(\dot{y}_v - h_1\dot{\theta}_v + h_{mt}\dot{\theta}_{mr} - \dot{y}_{br} - h_2\dot{\theta}_{br} + L_v\dot{\psi}_v)$
respectively

Table 6.1: Full vehicle dynamic modes

	Model 1		Model 2	
Mode	Damp. (%)	Freq. (Hz)	Damp. (%)	Freq. (Hz)
Body lower sway	25.79	0.49	0.98	0.47
Body upper sway	15.89	1.31	5.54	1.37
Body yaw	47.27	0.69	0.02	0.69
Front bogie roll	22.09	7.15	17.57	7.17
Front bogie lateral	10.55	16.54	6.09	16.56
Front bogie yaw	6.93	20.51	7.36	20.51
Rear bogie roll	21.31	7.22	17.52	7.25
Rear bogie lateral	10.51	16.54	6.10	16.56
Rear bogie yaw	6.93	20.51	7.36	20.51
Front airspring	100	3.78	100	3.78
Rear airspring	100	3.81	100	3.82

Chapter 5. In the vehicle model with passive suspensions, lateral secondary dampers are still used (without lateral actuator). The value of the lateral secondary damper is set as $22 \times 10^3 Ns/m$. Figure 6.4 illustrates the simulation results in the passive situation with the vehicle forward speed $45m/s$ and $58m/s$. For the simulation with $45m/s$, the measured vehicle body lateral acceleration is $0.85m/s^2$ in the steady-state curve, where the vehicle body rolls out of the curve with $1.2deg$. The steady-state yaw rate is $0.038rad/s$. However, the lateral acceleration increases to $2.4m/s^2$ when the forward speed is changed to $58m/s$, roll angle and yaw rate also increase. Table 6.2 and Table 6.3 present the assessment for the passive 9 DOF model. Only 3% of seated passengers may feel uncomfortable when the speed is $45m/s$. The P_{ct} value however becomes unacceptable with the vehicle forward speed of $58m/s$.

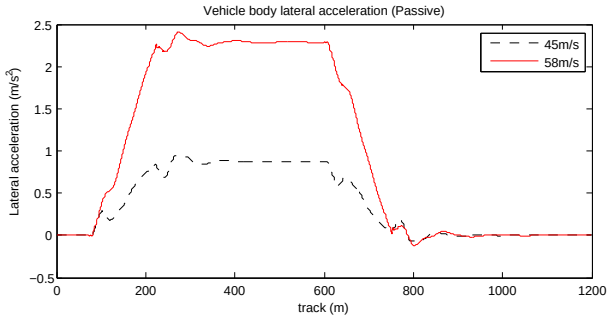

(a) Body lateral acceleration

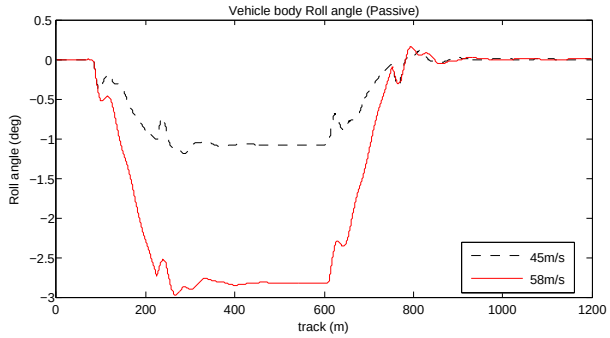

(b) Body roll angle

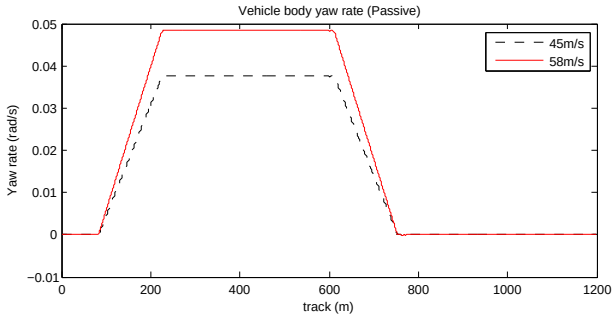

(c) Body yaw rate

Figure 6.4: Passive simulation

Table 6.2: Assessment for 9 DOF model in the passive simulation @ 45(m/s)

Deterministic(CURVED TRACK)			
P_{ct}(P-factor)	Centre	Front	Rear
-standing(% of pasengers)	15.242	15.397	15.315
-seated(% of pasengers)	3.325	3.397	3.359
Stochastic(STRAIGHT TRACK)			
Ride quality - R.M.S. value(%g)	1.58	2.12	2.23

Table 6.3: Assessment for 9 DOF model in the passive simulation @ 58(m/s)

Deterministic(CURVED TRACK)			
P_{ct}(P-factor)	Centre	Front	Rear
-standing(% of pasengers)	82.631	82.648	82.614
-seated(% of pasengers)	27.115	27.121	27.108
Stochastic(STRAIGHT TRACK)			
Ride quality - R.M.S. value(%g)	2.47	3.12	3.36

6.2 Control system design

6.2.1 Sensor placement

The controller design for end-view model is based on the signal from the vehicle body center of gravity (c.o.g.), but placing sensors in c.o.g. of the vehicle body is not a practical solution. Moreover, the centre of gravity will vary slightly when passengers enter and leave the vehicle.

Streiter et al. (2001) provided the details on calculating the lateral acceleration at automotive c.o.g. based on sensors placed in carbody, and Kalman filter is used to help estimating some non-measurable vehicle states. The method in Wenzel et al. (2007) determined the lateral and yawing acceleration of the railway car body at c.o.g. via the lateral acceleration sensors mounted in the rear and front vehicle body floor, and lateral displacement of the car body via relative stroke measurements at the airspring positions.

In this study, two lateral acceleramentors are placed in the front and rear of vehicle body face to measure the lateral acceleration and the displacement sensor is placed around airspring to detect the secondary suspension deflection. The roll angle of the vehicle body (assumed to be rigid) can be easily measured by the gyroscope which can be put in the same level as the body c.o.g..

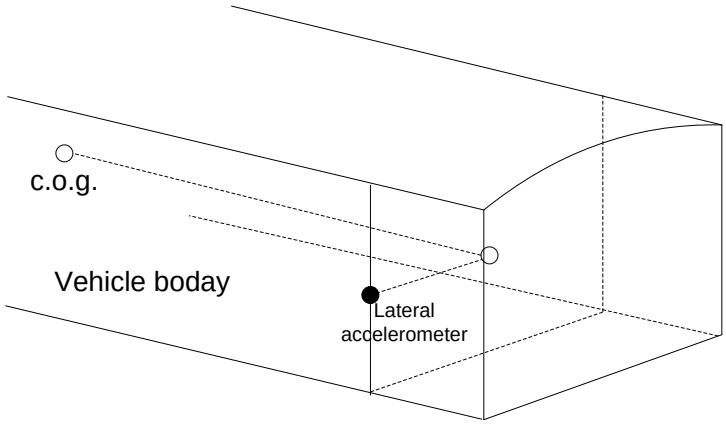

Figure 6.5: Lateral accelerometer placement

The method in Wenzel et al. (2007) is adopted here to calculate the lateral acceleration at body c.o.g., denoted by $a_{y_{cog}}$. The acceleration measured from front lateral accelerometer (as shown in Figure 6.5) is denoted by a_{meaf} (the measurement of rear lateral accelerometer is denoted by a_{mear}). The additional acceleration generated by the yaw motion in the horizontal plane can be resolved into a centrifugal component and a tangential component, denoted by a_{rxy} and $a_{\psi xy}$:

$$a_{\psi} = a_{rxy} + a_{\psi xy} = -\dot{\psi}^2 L_v \psi + \ddot{\psi} L_v \tag{6.39}$$

Therefore:

$$a_{cog} = a_{meaf} - \ddot{\psi} L_v + \dot{\psi}^2 L_v \psi \tag{6.40}$$

The yawing angle of the vehicle body in relation to the bogie is calculated with the aid of two displacement sensors (which measure the lateral secondary suspension deflections: x_{deflf} and x_{deflr}):

$$\psi = \frac{x_{deflf} - x_{deflr}}{2L_v} \tag{6.41}$$

The yawing acceleration can be determined in the similar way:

$$\ddot{\psi} = \frac{a_{meaf} - a_{mear}}{2L_v} \tag{6.42}$$

The yawing rate can be calculated by derivating the yaw angle.

6.2.2 Symmetric tilting controller design

For the tilting control, Pearson et al. (1998) presented 3 kinds of control configuration for the full vehicle with active ARB tilting:

(1) A symmetric control system. This system averages the signals from each end of the vehicle (tilt and acceleration) and drives each actuator with the same signal.

(2) Independent control systems for each of the active anti-roll bars. This strategy can avoid the delay introduced by the symmetric control. But the independent control system has the potential for the two active anti-roll bars to apply opposing torques on cant gradients. This would twist the body and could result in wheel off-loading and even derailment.

(3) A master/slave control system. This system uses the signals from one end of the vehicle to calculate drive signals for both actuators. This arrangement is directionally sensitive, but has the advantage that the slave actuator essentially has half vehicle preview.

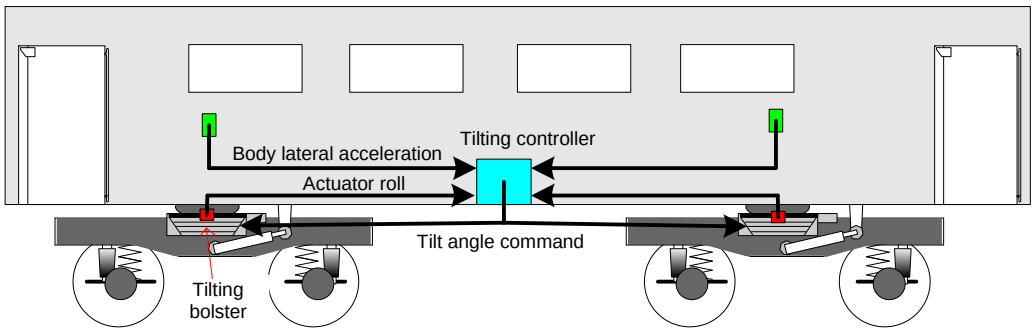

Figure 6.6: Symmetric tilt control system

The symmetric strategy controlling the actuators to the same length is used to implement the tilting control laws in this study, as shown in Figure 6.6. The average of two accelerations measured by the front and rear body lateral accelerometers is utilised and combined with the actuator roll angle forming the effective cant deficiency to drive the tilting controller.

6.2.3 Direct implementation of the lateral actuator controller

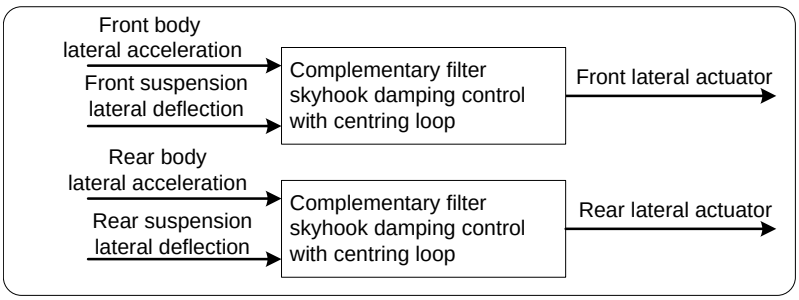

Figure 6.7: Direct implementation of the lateral actuator control

The lateral actuator controllers designed with end-view model can be directly implemented into the full vehicle control with the same controller parameters. Separated rear and front sensors are used. Figure 6.7 shows the overall control system configuration for the direct implementation of the lateral actuator control while symmetric tilting control is used.

6.2.4 Modal control

The modal control can be configured for the lateral actuator control implementation. In principle, modal control (Goodall and Mei (2006)) attempts to manage individual modes of the system by breaking down measurements into modal components. These are processed individually and then recombined to drive the actuators. As shown in Figure 6.8, the measured signals are split into modal components of lateral and yaw using the modal controller and these signals are processed before passing through the inverse modal controller to derive the force demanded by the front and rear lateral actuators. Parameters of the High Pass filter (HP) for yaw control are set to be $w = 0.1rad/s$, $\xi = 0.707$, and yaw damper coefficient $c_{sp} = 20000Ns/m$.

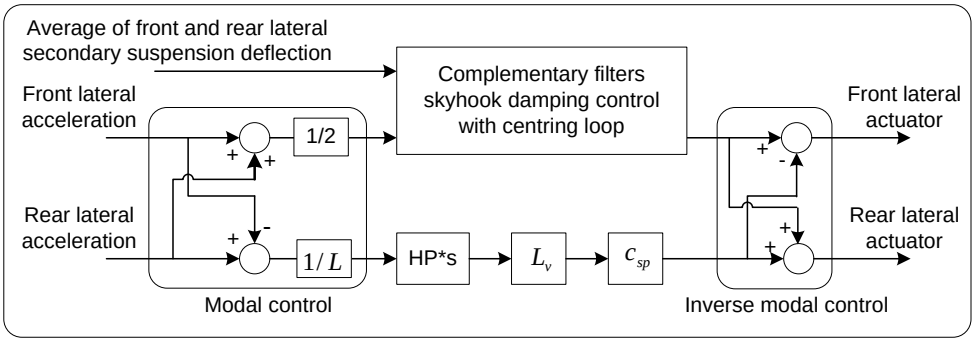

Figure 6.8: Modal control for integrated tilt and active lateral secondary suspension

6.2.5 Simulation results

The overall system is simulated with specified track inputs as presented in Chapter 5. Figure 6.9 and Figure 6.10 present the measured vehicle body lateral acceleration and suspension deflection on curved track. Both figures illustrate the similar performance for end-view and full vehicle model. In the case of direct implementation of lateral actuator control, the coupling between lateral and yaw dynamics introduces the oscillation. However, the modal control can attenuate this oscillation as shown in Figure 6.10.

Table 6.4 presents the R.M.S. value of measured body lateral acceleration of the front body, centre body and rear body. Modal control offers the ride quality improvement compared with the direct implementation. Table 6.4 also gives the information of the deterministic track simulation results. The results of the full vehicle control are slightly different compared with the results based on the end-view model.

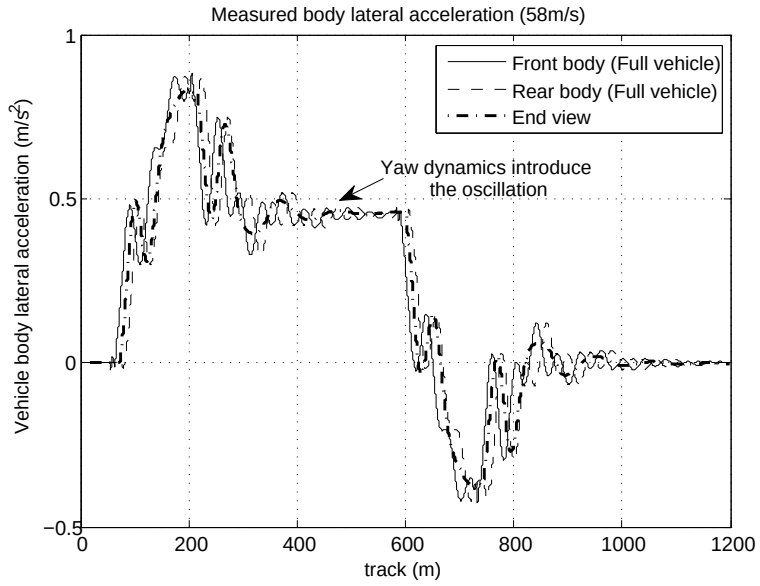

(a) Body lateral acceleration

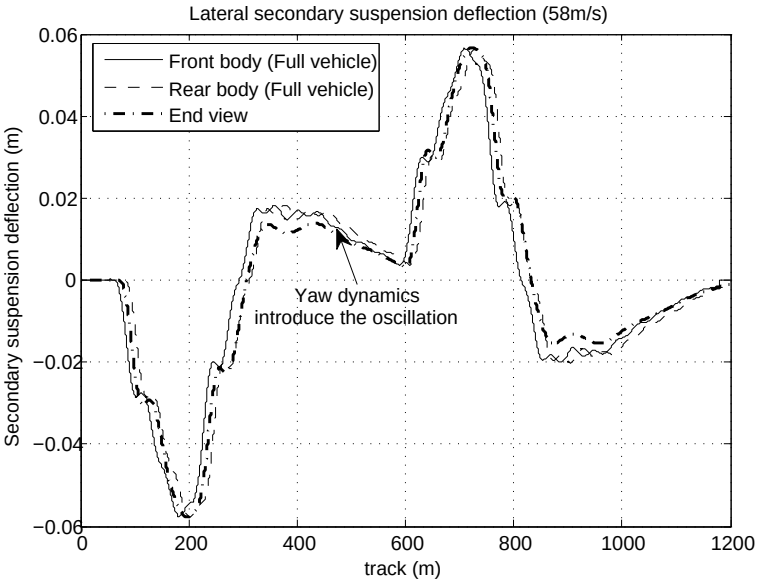

(b) Suspension deflection

Figure 6.9: Simulation results of direct implementation

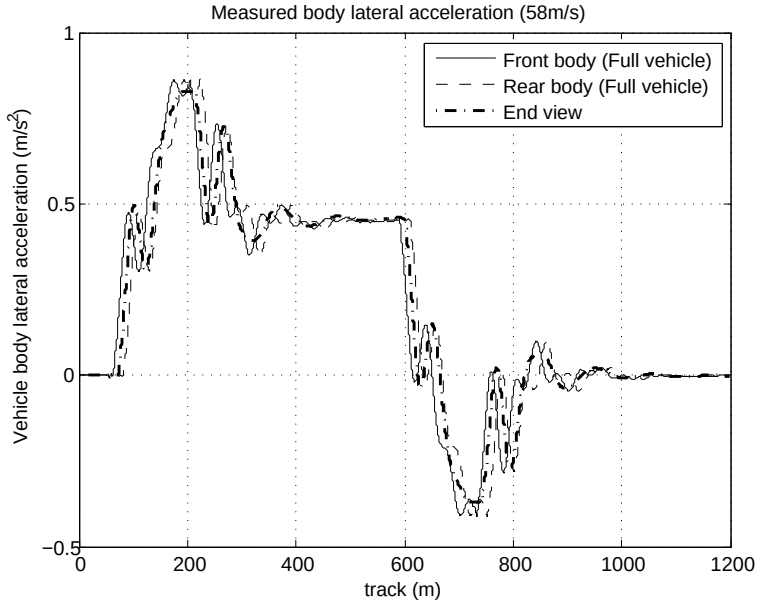

(a) Body lateral acceleration

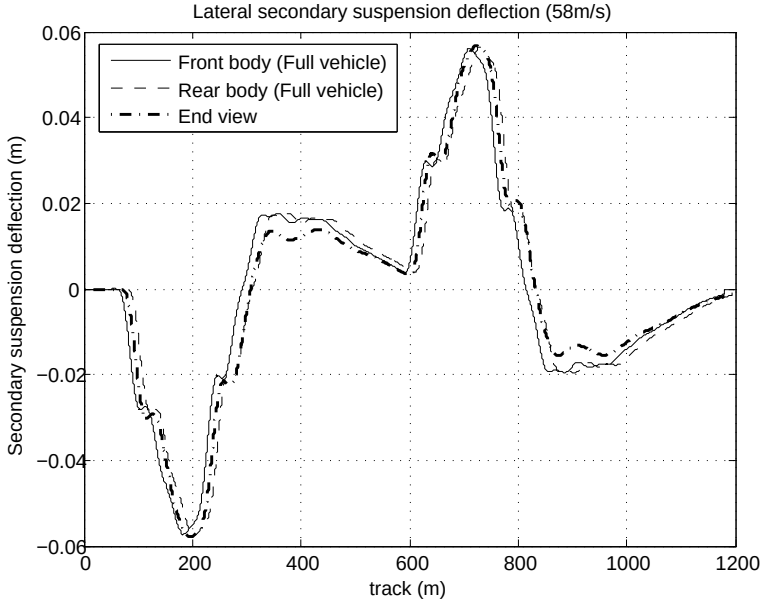

(b) Suspension deflection

Figure 6.10: Simulation results of modal control

Table 6.4: Control system assessment (9 DOF vehicle with tilting bolster)@ 58(m/s)

Deterministic(CURVED TRACK) end view		Full vehicle Directly implement		Full vehicle Modal control	
P_{ct}(P-factor):		Front	Rear	Front	Rear
-standing (% of pasengers)	34.2	38.05	37.81	36.49	36.45
-seated (% of pasengers)	8.63	9.83	9.75	9.40	9.38
Stochastic(STRAIGHT TRACK)					
passenger comfort:		Front	Rear	Front	Rear
-R.M.S. passive (%g)	3.24	3.12	3.36	3.12	3.36
-R.M.S. active (%g)	3.17	3.17	2.75	3.05	2.64
-degradation (%)	-1.85	1.6	-18.15	-2.24	-29.2

6.3 Lateral actuator dynamics

In this section, the actuator dynamics are discussed but only electromechanical actuator for the lateral direction is addressed. Tilting actuation system is modelled as a sevo-mechanism because tilting action is a low frequency action. The modelling process for the electro-mechanical actuator has been well presented in Pratt (1996). The mathmetical equations of the electro-mechanical actuator are summaried below:

The torque generated by the electric motor is given by:

$$\dot{t}_m = -\frac{r_{arm}}{l_{arm}} t_m + \frac{k_t}{l_{arm}} v_{act} - \frac{k_t k_e}{l_{arm}} \dot{\theta}_m \tag{6.43}$$

The mechanical inertia 'j_m' and inherent damping 'c_m' of the motor are accounted for in the dynamic equation:

$$\ddot{\theta}_m = \frac{t_m}{j_m} - \frac{c_m}{j_m} \dot{\theta}_m + \frac{k_m(\theta_m n^2 - x_m n)}{j_m} \tag{6.44}$$

The interconnected system of masses, dampers and springs shown in Figure 6.11 can be represented by (6.45) ,

$$\ddot{x} = -\frac{k_s + k_m}{m_s} x_m - \frac{c_s}{m_s} \dot{x}_m + \frac{c_s}{m_s} \dot{x}_{act} + \frac{k_s}{m_s} x_{act} + \frac{k_m n}{m_s} \theta_m \tag{6.45}$$

The force developed by this system is due to compression of the lead screw and is given by:

$$f_{act} = k_s x_m + c_s \dot{x}_m - k_s x_{act} - c_s \dot{x}_{act} \tag{6.46}$$

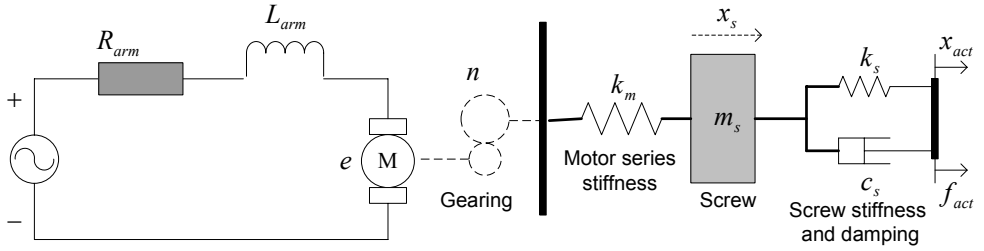

Figure 6.11: Equivalent electro-mechanical actuator model

The state space model is illustrated below, system has two inputs: the motor voltage and the actuator extension velocity. The output is the actuator force.

$$\begin{bmatrix} \dot{t}_m \\ \dot{\theta}_m \\ \ddot{\theta}_m \\ \dot{x}_m \\ \ddot{x}_m \\ \dot{x}_{act} \end{bmatrix} = \begin{bmatrix} -\frac{r_{arm}}{l_{arm}} & 0 & -\frac{k_t k_e}{l_{arm}} & 0 & 0 & 0 \\ 0 & 0 & 1 & 0 & 0 & 0 \\ \frac{1}{j_m} & \frac{D_w}{j_m} & \frac{c_m}{j_m} & -\frac{k_m l}{j_m} & 0 & 0 \\ 0 & 0 & 0 & 0 & 1 & 0 \\ 0 & \frac{k_m l}{m_s l^2} & 0 & -\frac{k_s + k_m/l^2}{m_s} & -\frac{c_s}{m_s} & \frac{k_m}{m_s} \\ 0 & 0 & 0 & 0 & 0 & 0 \end{bmatrix} . \begin{bmatrix} t_m \\ \theta_m \\ \dot{\theta}_m \\ x_m \\ \dot{x}_m \\ x_{act} \end{bmatrix}$$

$$+ \begin{bmatrix} 0 & \frac{k_t}{l_{arm}} \\ 0 & 0 \\ 0 & 0 \\ 0 & 0 \\ \frac{c_s}{m_s} & 0 \\ 1 & 0 \end{bmatrix} . \begin{bmatrix} \dot{x}_{act} \\ v_{act} \end{bmatrix}$$

$$f_{act} = \begin{bmatrix} 0 & 0 & 0 & k_s & c_s & -k_s \end{bmatrix} . \begin{bmatrix} t_m \\ \theta_m \\ \dot{\theta}_m \\ x_m \\ \dot{x}_m \\ x_{act} \end{bmatrix} + [-c_s \;\; 0] . \begin{bmatrix} \dot{x}_{act} \\ v_{act} \end{bmatrix}$$

The parameters for the actuator are chosen to accommodate maximum $10kN$ actuator force, maximum $270m/s$ actuator external velocity and maximum $0.25m$ displacement (Ltd (2010)), which are listed below:

---

k_t: Motor torque constant, $0.76Nm/A$; k_e: Motor back-emf gain, $0.4393V/rads^{-1}$;
l_{arm}: Winding inductance, $4.2mH$; r_{arm}: Winding resistance, 1.31Ω;
j_m: Motor inertia, $2.9 \times 10^{-3} kgm^2$; D_w: Motor friction, $795.8 \times 10^{-6} Nmrad/s$;

k_m: Motor series stiffness, $1 \times 10^7 N/m$; l: Screw pitch, 0.91×10^{-3};
m_s: Screw mass, 2kg; k_s: Screw stiffness, $2 \times 10^6 N/m$;
c_{sa}: Screw damping, $4 \times 10^3 Ns/m$;

A force control loop is designed to improve the actuator performance which is shown in Figure 6.12(a) and gives the $15Hz$ bandwidth (shown in Figure 6.12(b)). Parameters for the approximate PID actuator force control are listed below:
k_p: 0.04; k_i: 0.5; k_d: 0.0000008; N: 1000

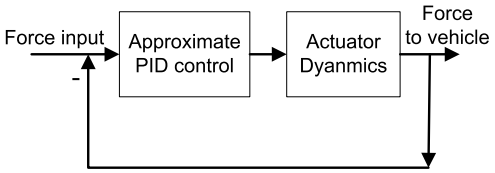

(a) Actuator force control

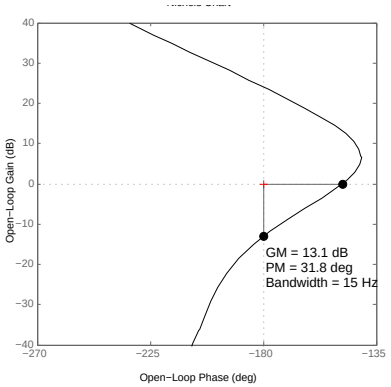

(b) Nichlos plot for the force control

Figure 6.12: Actuator force control

Requirements for the lateral actuator in the 9 DOF vehicle with symmetric tilting control and lateral actuator modal control are listed below, which are obtained from the simulation with ideal lateral actuator:
Maximum lateral actuator force: $9681N$
Maximum displacement velocity: $0.2584m/s$
Maximum deflection: $0.0561m$

The selected actuator can meet all these requirements. Figure 6.13 shows the control configuration for the 9 DOF vehicle model with actuator dynamics, note that the deflection rate is feedback to the lateral actuator to give the information of the external actuator displacement velocity. The same controller parameters are used as the

parameters in Section 5.2. Figure 6.14 and Table 6.5 shows the slight performance degradation for the controller with real lateral actuators (particularly after $5Hz$).

Table 6.5: Control system assessment for tilting train with tilting bolster (ideal vs. real actuator) @ 58(m/s)

Deterministic(CURVED TRACK)	centre		Front		Rear	
P_{ct}(P-factor):	Ideal	Real	Ideal	Real	Ideal	Real
-standing (% of pasengers)	36.47	36.33	36.49	36.24	36.45	36.40
-seated (% of pasengers)	9.39	9.35	9.40	9.32	9.38	9.36
Stochastic(STRAIGHT TRACK)						
passenger comfort:	Ideal	Real	Ideal	Real	Ideal	Real
-R.M.S. active (%g)	2.15	2.28	3.05	3.14	2.64	2.74

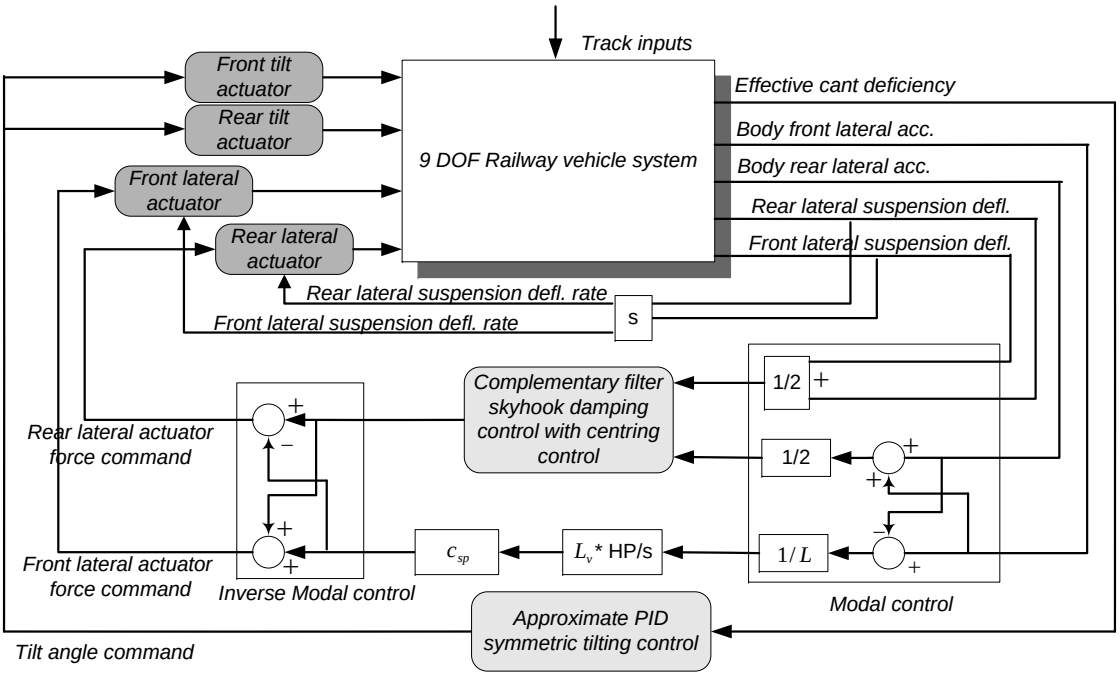

Figure 6.13: Full vehicle control with actuator dynamics

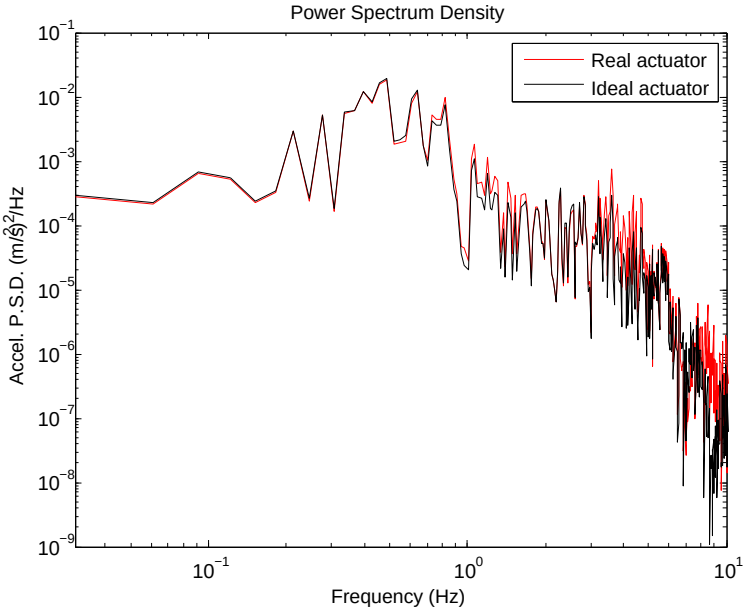

(a) Front body lateral acceleration

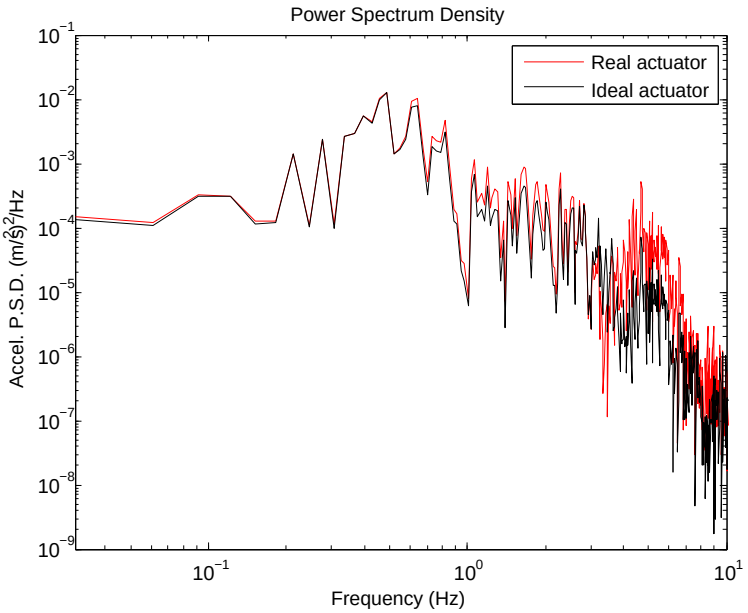

(b) Rear body lateral acceleration

Figure 6.14: The comparison between ideal actuator and real actuator

6.4 System robustness analysis

The system robustness test is based on the practical situations, i.e. the vehicle load variation. Three cases are considered here.

•$CASE$ 1: 10% decreases of vehicle body mass assuming half passengers occupied with 10% decreases in body roll inertia, and 10% decreases in body yaw inertia.
•$CASE$ 2: 10% increases of vehicle body mass assuming vehicle over load with 10% increases in body roll inertia, and 10% increases in body yaw inertia.
•$CASE$ 3: 17.5% increases of vehicle body mass assuming vehicle "crush load" with 17.5% increases in body roll inertia, and 17.5% increases in body yaw inertia.

Test results are illustrated in Figure 6.15 (Curving performance for the front vehicle body), Figure 6.16 (Curving performance for the rear vehicle body) and Figure 6.17 (on straight track). The results indicate that the overall system can accommodate the first two test cases both on straight and curved track. But in Test case 3, maximum value of suspension deflections in front and rear vehicle both exceed $60mm$ (as shown in Figure 6.16(b) and Figure 6.17(b)). The ride quality also degrades on straight track. The R.M.S. value of body centre lateral acceleration is 2.81%g, which provides an unacceptable ride quality degradation (12%). The straight track ride quality degradation in the front and rear vehicle (Test case 3) are 6.09% and -13.69% respectively. The ride quality degradations for the center, front and rear vhicle in Test case 1 and Test case 2 are all within the required limit (7%), as shown in Figure 6.17.

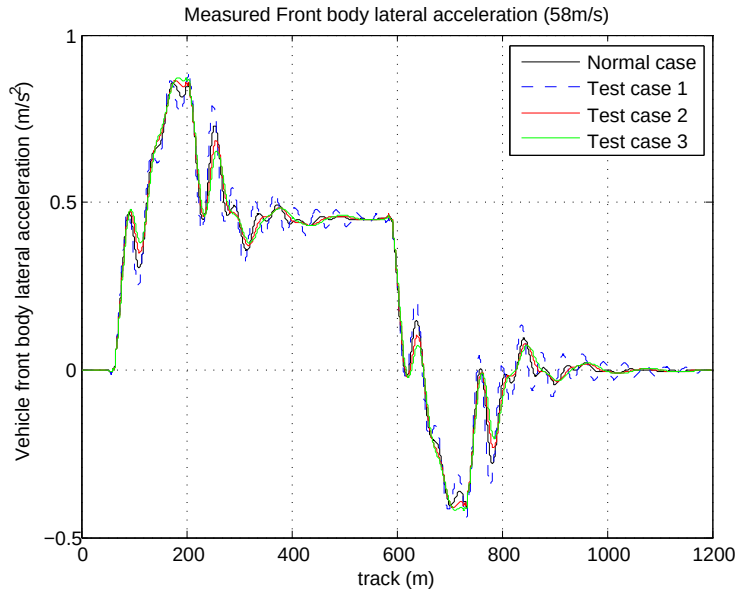

(a) Vehicle body lateral acceleration

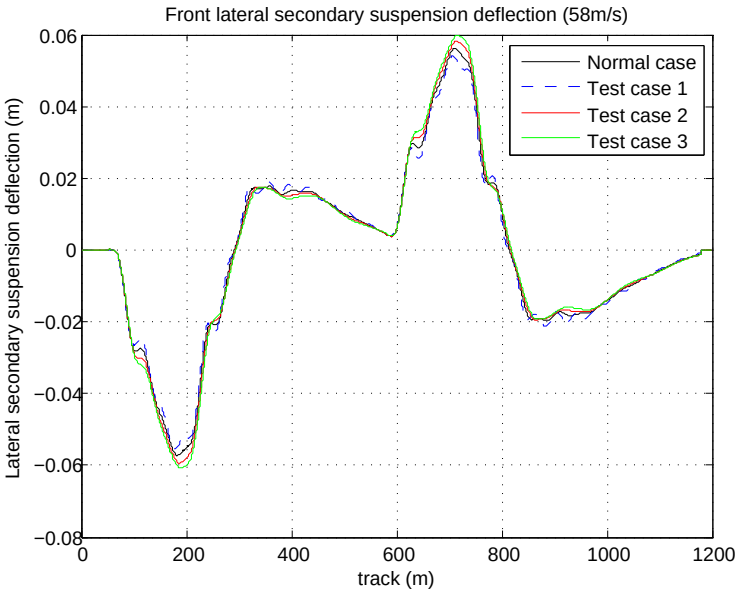

(b) Lateral secondary suspension deflection

Figure 6.15: Controller robustness test on curved track (Front vehicle)

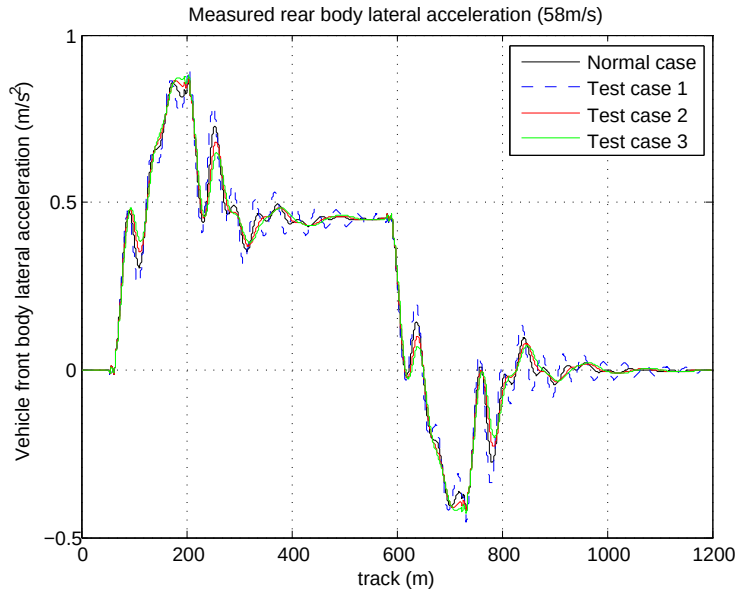

(a) Vehicle body lateral acceleration

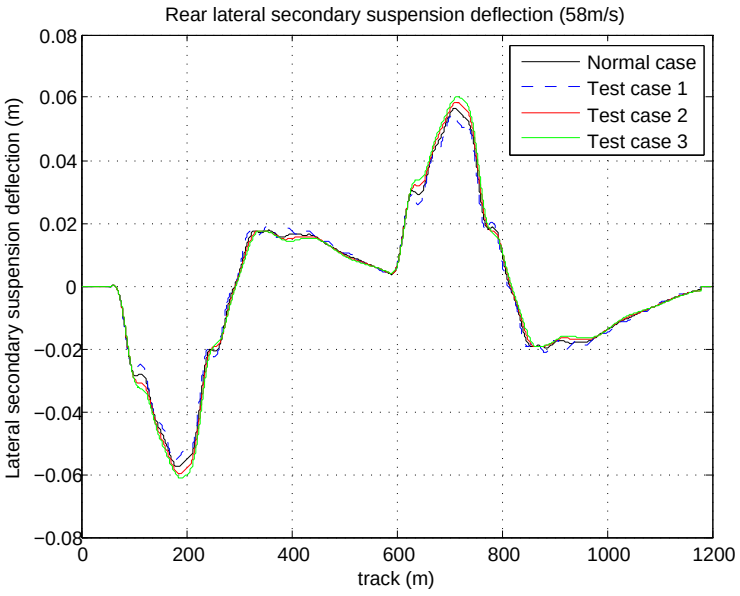

(b) Lateral secondary suspension deflection

Figure 6.16: Controller robustness test on curved track (Rear vehicle)

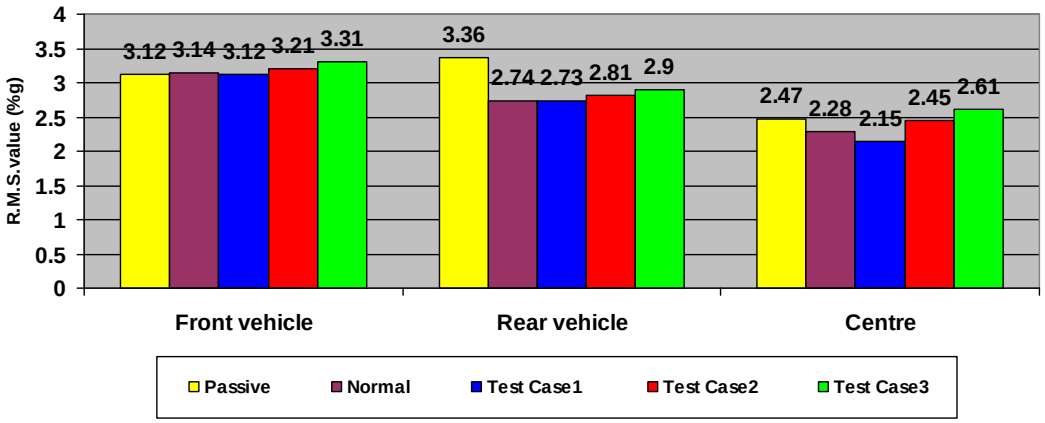

Figure 6.17: Controller robustness test on straight track

6.5 Summary

In this chapter, the 9 DOF vehicle model is presented for further investigation of integrated tilt bolster and active lateral secondary suspension control. Symmetric tilting control and lateral actuator modal control are mainly addressed. The simulation results show the efficiency of modal control on straight track ride quality improvement and the attenuation of the interaction between yaw and lateral dynamics. Electromechanical lateral actuator dynamics is discussed which slightly degrades the controller performance compared to the simulation with ideal lateral actuator. Furthermore, the overall system is well tested subject to the variation of the vehicle load.

Chapter 7

Investigation on HIL implementation

As introduced in Chapter 1, the HIL design process consists of MIL (Model-In-the-Loop), SIL (Software-In-the-Loop) and HIL. Previous chapters mainly focus on the MIL design, the vehicle model and controllers are simulated in MATLAB/SIMULINK (a non-real time environment). In this chapter, a SIL system is configured to verify controllers before their hardware implementation. In the HIL design, xPC-Target provides the real time environment for the railway vehicle model while control strategy is implemented into a FPGA-based controller. The result of 9 DOF railway vehicle control with the integrated active ARB and active lateral secondary suspension is illustrated via this HIL system, in which the combination of symetrical tilting control and lateral actuator modal control is adopted which is similar to the integrated tilting bolster and active lateral secondary suspension control.

7.1 SIL controller validation

SIL refers to the kind of testing done in a simulation environment to validate the behavior of the C code used in the controller, i.e. replacing the control algorithm in MATLAB code with C code and simulating it with the model in MATLAB/SIMULINK code. The C code mostly is generated from the code generation tools. In this section, the em-

bedded code autogeneration is introduced first followed by a SIL system configuration used in this research.

7.1.1 Embedded code auto-generation

A code generator (also automatic code generation tool or autocode tool) is essentially a compiler that translates a graphical modeling language into a high-level programming language such as from Simulink or Stateflow to C (in most cases) for the use in the embedded system. There are some commercial autocode generation tools:

- TargetLink from dSPACE (dSPACE GmbH (2010))
- Real-Time Workshop/Embedded Coder from The MathWorks (The MathWorks (2010))
- MapleSim from Maple (Maplesoft (2010))
- ASCET-SD (Advanced Simulation and Control Engineering Tool for Software Development) from ETAS (ASCET-SD (2010))
- SCADE drived by ESTEREL Technologies (ESTEREL (2010))

Most of them are used to genenrate the C code from a simulation model. These methods are also called model-based auto code generators. In this study, differing from these model-based methods, the code autogeneration from Matlab m code to embedded C code is mainly addressed. Embedded MATLAB is investigated.

Embedded MATLAB is a subset of the MATLAB language, which supports MATLAB to C translation for implementing embedded algorithms and systems (MathWorks (2010b)). By using Embedded MATLAB, the C code can be automatically generated from MATLAB m code, which provides a direct path to embedded software implementation from MATLAB. Note that the MATLAB m code should be written in a format for the Embedded MATLAB subset, but it is only slightly different compared with the normal MATLAB m code. An example of Embedded MATLAB m code for the Kalman filter is presented in Appendix G.

The standard procedures for generating C code from MATLAB m code via Embedded MATLAB are summarised below:

- Install prerequisite products (MATLAB and C Compiler)
- Set up C compiler (use command 'mex -setup') in MATLAB
- Set up the file infrastructure based on compile search paths and naming conventions
- Make the m code compliant with the Embedded MATLAB subset
- Specify properties of primary inputs by -eg/assert()
- Choose the compiler target to be Embeddable C code
- Use MATLAB command: 'emlc functionname -c -T RTW', to generate the C code
- Generate and interpret compilation reports.

Note that, the code can be generated in the fixed point data format via MATLAB fixed point toolbox functions, e.g. fi() to convert the floating point data to fixed point. But the floating point data is mainly considered here.

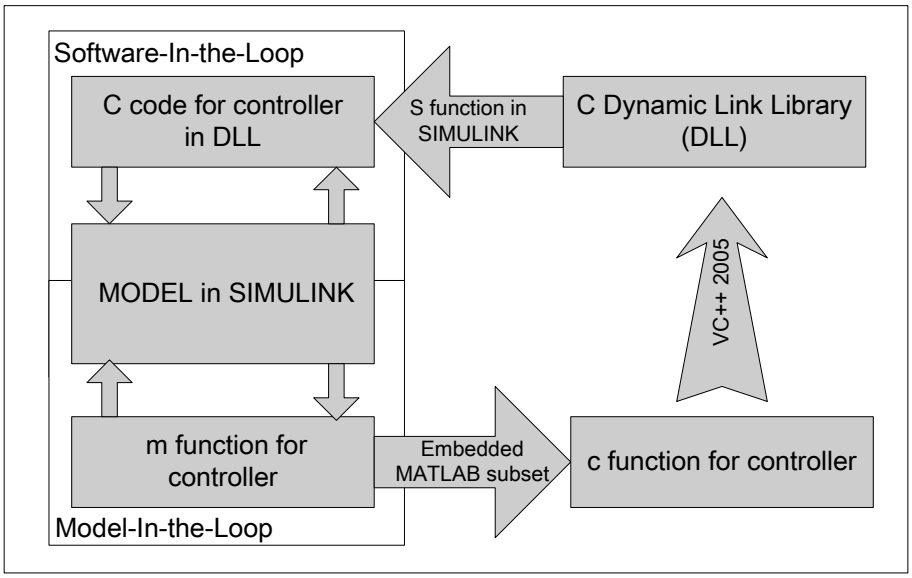

Figure 7.1: Software-In-the-Loop process

7.1.2 SIL configuration

In this study, a SIL system combining MATLAB and C together (co-simulation) is presented. Figure 7.1 shows the overall SIL process. The controller in m function is

converted into C function via the Embedded MATLAB subset. Then it is complied to C Dynamic Link Library (DLL) with VC++ 2005. S function in SIMULINK calls this DLL to provide the control signals to the SIMULINK model. The proposed SIL configuration can be used to validate the C code generated via Embedded MATLAB for the use in any engineering area.

7.2 HIL implementation

7.2.1 FPGA-based controller

Differing from the SIL, HIL has a real electronic control unit to implement the C code-based controller. The controlled model is running in a real time environment. Communication between controller and model needs to be well designed. In this research, the FPGA-based controller is investigated. There are two ways to implement the control algorithm in FPGA: Hardware direct implementation and Soft processor-based implementation.

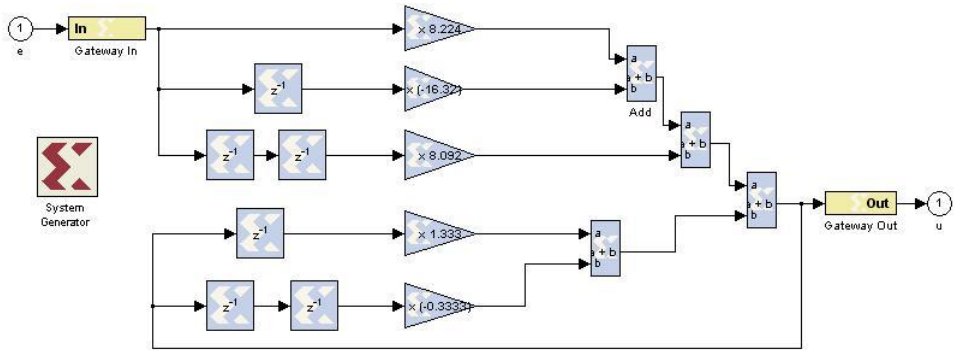

Figure 7.2: Graphical design for the PID tilting control

(1) Hardware direct implementation

It is carried out by the Hardware Description Language (HDL)/Verilog Hardware Description Language (VHDL) programming. But it also can be designed based on the graphical blocks. The well-known example is Xilinx's System Generator^{TM}. The controller is designed with special blocks in MATLAB/SIMULINK provided by the Xilinx, then the HDL code can be generated and downloaded into FPGA automatically by Xilinx's System Generator. Figure 7.2 shows the example for the approximate PID tilting

control. The blocks are similar to the tranditional blocks in SIMULINK, but the fixed point data is used in each block. The choice of the word length and fractional bit in each block greatly affects the controller performance. However, the soft processor-based implementation is mainly addressed in this research.

(2) Softprocessor-based implementation
The control algorithm can be implemented in FPGA in C code, but an embedded processor has to be configued in FPGA firstly. A typical FPGA embedded processor design consists of a processor connected via internal buses to peripherals (cores) that control various hardware interfaces. Well known embedded soft processors are: MicroBlaze, PicoBlaze from Xilinx, Nios II from Altera, LEON series from Aeroflex Gaisler, etc.. Cores have the function for the communcation interface control (i.e. Ethernet MAC, RS-232 UART), memory control (DDR SDRAM, flash, block RAM), as well as the bus structures and bus bridge control. Floating Point Unit (FPU) can be configured into the embedded processor to support floating point arithmetics. In this research, the Spartan-3E Starter Kit board (with XC3S500E Spartan-3E (Speed grade -4) FPGA) and MicroBlaze soft processor are used.

The MicroBlaze core is a 32-bit RISC Harvard architecture soft processor core with a rich instruction set optimized for embedded applications. The MicroBlaze soft processor solution integrates peripherals, memory and interface features at the lowest cost on a single FPGA (Xilinx (2010)). Also, The MicroBlaze soft processor provides an optional IEEE-754 compatible single-precision FPU. Xilinx Platform Studio and SDK provide a wizard to configure the soft processor, which facilates the design process (Xilinxedk (2010)).

7.2.2 Real time environment and communication

The easiest way to provide real time environment in SIMULINK is to use the RT-blockset, which is developed by Daga (2004) and has been realized using an S-function written in C++ language. It makes SIMULINK run with a real-time temporization. However, the main issue for the RT-blockset is the actions of the user during the simulation. Any window process (constrained to manage windows messages) can affect

the real time operation of the RT-blockset, simply because Windows Operation System (OS) is not a real time OS. RT block attempts to enhance the priority of the SIMULINK environment, which means the simulation is protected from the other processes but not from SIMULINK itself.

A more robust way for the real time environment can be provided by the xPC-Target, QNX or Vxwork. In this study, xPC-Target (MathWorks (2010a)) is adopted to provide the real time environment for the tilting railway vehicle model.

xPC-Target provides a high-performance host-target environment that enables the user to connect SIMULINK and Stateflow models to physical systems and execute them in real time on low-cost PC-compatible hardware. xPC-Target includes proven capabilities for rapid prototyping, hardware-in-the-loop testing, and application deployment in an open hardware architecture. Figure 7.3 illustrates the basic configuration for the xPC Target in this research. Railway vehicle model is developed in MATLAB/SIMULINK in the host PC. It is downloaded into the Target PC via the TCP/IP link.

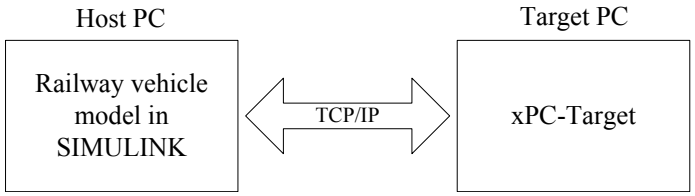

Figure 7.3: xPC Target configuration

High speed RS232 serial communication (Baud rate is configured as $115200 bit/s$) is adopted for the data transmission between xPC-Target and FPGA-based controller in this study, which is simple and easy for design. The overall HIL system configuration is shown in Figure 7.4.

7.3 HIL design for the railway vehicle control

In this section, the simulation results for the integrated active ARB and active lateral secondary suspension control (9 DOF vehicle model) are presented via the HIL system. The symetric control and modal control are adopted for the tilting and lateral actuator

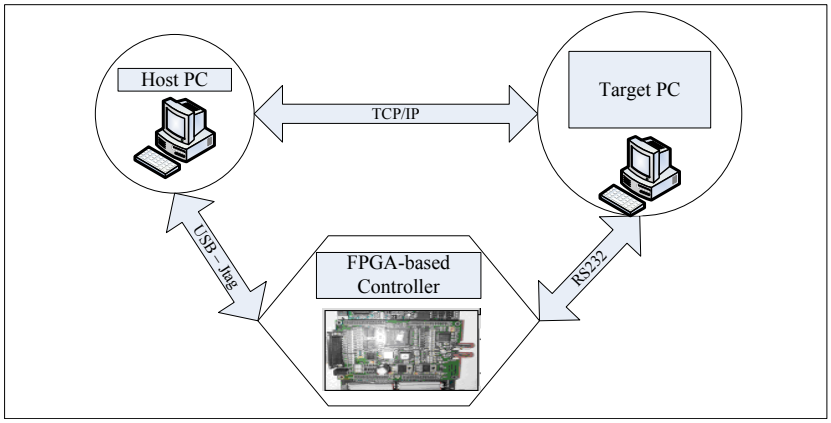

Figure 7.4: HIL system configuration

respectively. The configuration of the control system is illustrated in Figure 7.5. The parameters of the 9 DOF model for the integrated active ARB and active lateral secondary suspension are list in Appendix D, the lateral and tilt actuator dynamics are ignored here.

7.3.1 Digital controller design

The δ transformation is used to convert the control algorithm from s to δ domain. δ transformation has been proven to be very robust against coefficient sensitivity and internal variable overflow problems that are associated with the z transformation (Forsythe and Goodall (1991)). Therefore, it can provide a more robust digital controller for this study. The s operator can be converted to a δ operator using the bilinear transformation expressed as:

$$s = \frac{2\delta}{T(2+\delta)} \tag{7.1}$$

Where T is the sampling period, and δ is defined as $(z-1)$ (Forsythe and Goodall (1991)). T is set to $0.025s$ at this study, which is chosen based on the test for the best and robust HIL system performance. Using other high speed communication method, e.g. CAN bus, can further reduce the sampling period, hence improving the system overall performance.

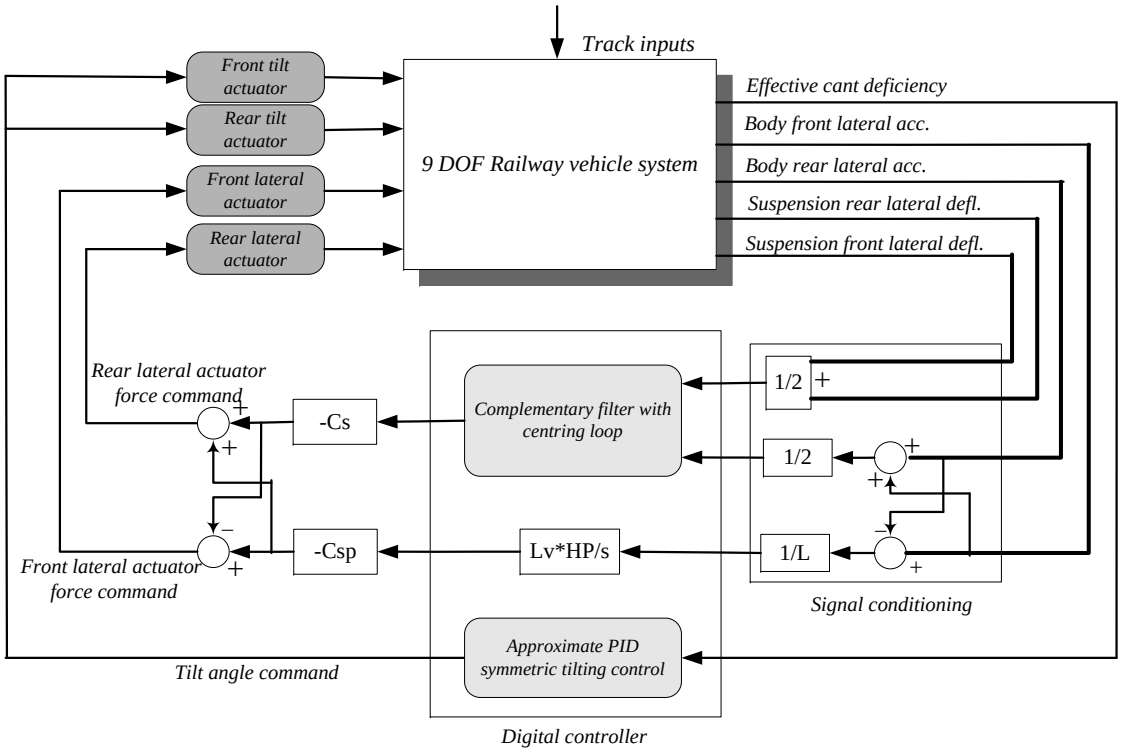

Figure 7.5: Full vehicle control (for integrated active ARB and active lateral secondary suspension)

The digital controller implementation is based on delta canonic form (Forsythe and Goodall (1991)). The structure of a second order canonic delta filter is given in Figure 7.6.

The continuous transfer function (7.2), where n_0, n_1, n_2, m_0 and m_2 are the coefficients of a second order s domain transfer function. It can be written as (7.3), where c_0, c_1, c_2, r_1 and r_2 are the coefficients of a second order discrete δ domain transfer function.

$$H(s) = \frac{n_0 + n_1 s + n_2 s^2}{1 + m_1 s + m_2 s^2}; \tag{7.2}$$

$$H(\delta) = \frac{c_0 + c_1 \delta^{-1} + c_2 \delta^{-2}}{1 + r_1 \delta^{-1} + r_2 \delta^{-2}} \tag{7.3}$$

The digital form of the controllers are list below. Note that, the values of controller parameters are the same as the parameters designed in Chapter 4, but converted to

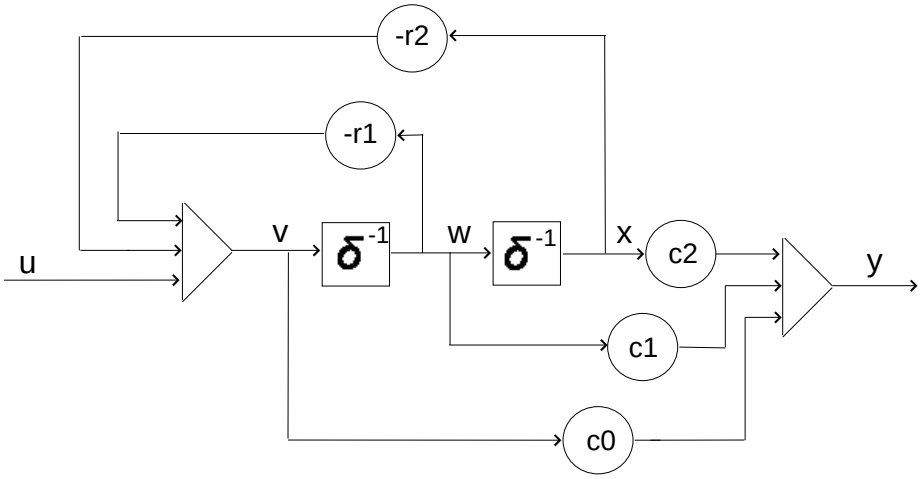

Figure 7.6: Block diagram of the second order canonic delta filter (Forsythe and Goodall (1991))

digital form here:

Approximate PID tilting control:

$$f_{A.PID}(\delta) = \frac{1.1074821 + 0.4393357 \times \delta^{-1} + 0.0744575 \times \delta^{-2}}{1 + 1.8518518 \times \delta^{-1} + 0 \times \delta^{-2}} \tag{7.4}$$

Complementary filters:

$$(HP/s)(\delta) = \frac{0.0120567 + 0.0241133 \times \delta^{-1} + 0 \times \delta^{-2}}{1 + 0.0721930 \times \delta^{-1} + 0.0025174 \times \delta^{-2}} \tag{7.5}$$

$$(LP * s)(\delta) = \frac{2.8373730 + 0.1006946 \times \delta^{-1} + 0 \times \delta^{-2}}{1 + 0.0721930 \times \delta^{-1} + 0.0025174 \times \delta^{-2}} \tag{7.6}$$

Centring control loop:

$$(k_{df}/s)(\delta) = \frac{0.036875 + 0.07375 \times \delta^{-1}}{1 + 0 \times \delta^{-1}} \tag{7.7}$$

Yaw control loop($w_y = 2 \times \pi \times 0.1$, $C_{sp} = 20000Ns/m$, $L_v = 9m$):

$$(L_v * HP/s)(\delta) = \frac{0.1174385 + 0.2348771 \times \delta^{-1} + 0 \times \delta^{-2}}{1 + 0.0222098 \times \delta^{-1} + 0.0002440 \times \delta^{-2}} \tag{7.8}$$

7.3.2 Controller implementation in HIL system

The set-up of the HIL system is illustrated in Figure 7.7. Xilinx EDK tools and MATLAB/SIMULINK are running in the Host PC. The Xilinx EDK tools are used to configure the soft processor and compile the control algorithm for FPGA. MATLAB/SIMULINK compiles the vehicle model and downloads it into Target PC. The FPGA board is connected to Target PC via RS232 cables.

The Microblaze soft processor is configured with clock frequency of $62.5MHz$, local memory of $32kB$, RS-232 UART driver (with interupt enabled) and FPU. The software design flow based on Microblaze soft processor is illustrated in Figure 7.8. The code is attached in Appendix H. Note that, the code is original generated via Embedded MATLAB, but it is modified based on the canonic delta form.

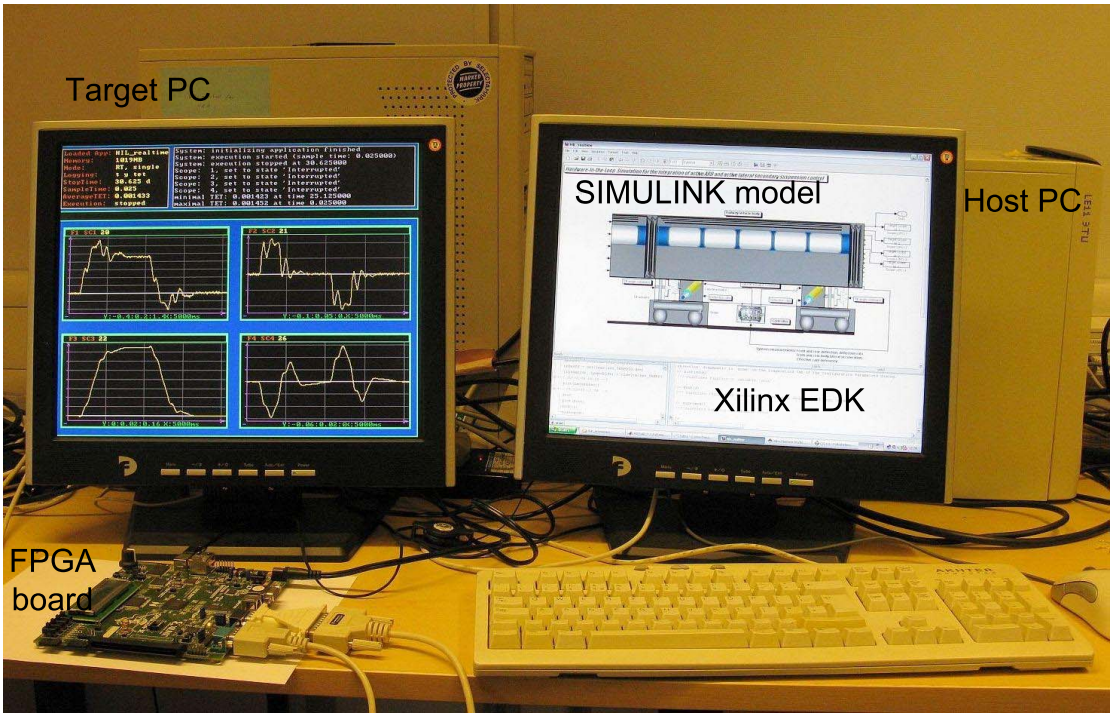

Figure 7.7: HIL system configuration for integrated tilt and active lateral secondary suspension

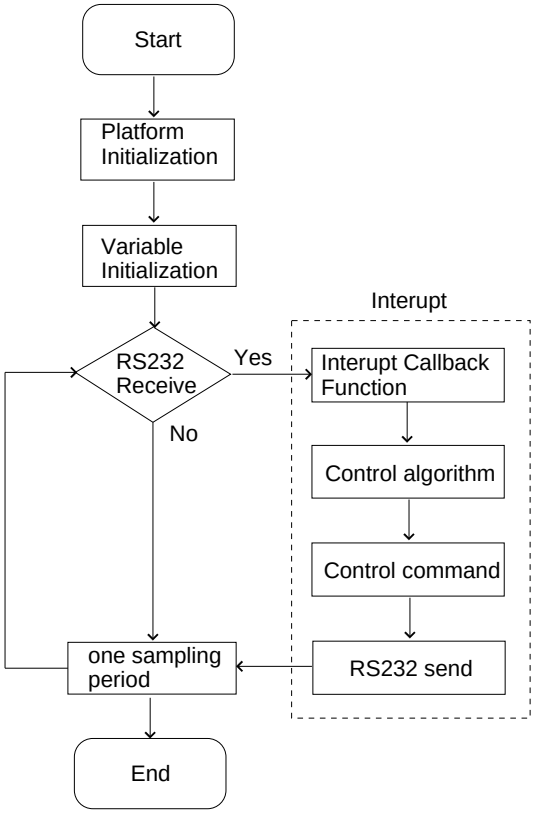

Figure 7.8: Control design flow in FPGA

7.3.3 MIL, SIL and HIL simulation results

Figure 7.9(a, b) illustrate the MIL, SIL and HIL simulation results for the vehicle body lateral acceleration (body centre) and suspension lateral deflection (body centre) on curved track. Figure 7.9(c) shows the body lateral acceleration on straight track. The results from MIL, SIL and HIL are similar to each other, but the low sampling rate results in a slight delay of the system response in HIL simulation, as shown in Figure 7.9(a). Table 7.1 gives the assessment information for the integrated active ARB and active lateral secondary suspension control with the 9 DOF model (body centre).

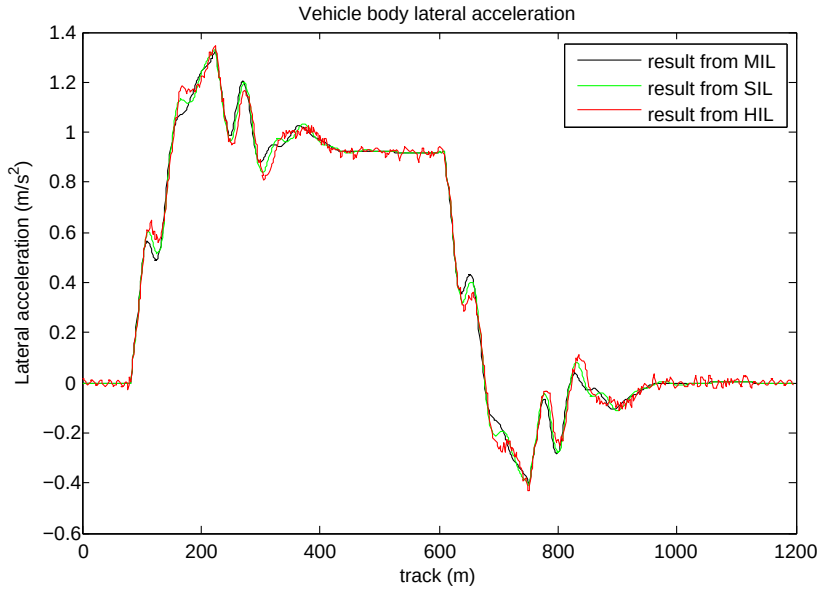

(a) Vehicle body acceleration in curved track

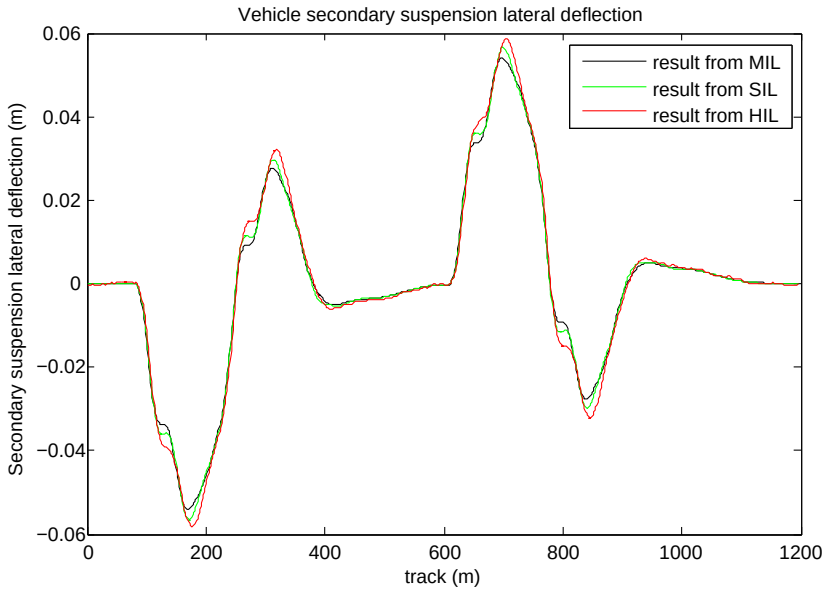

(b) Suspension deflection in curved track

Figure 7.9: A comparison of the results from MIL, SIL and HIL on curved track

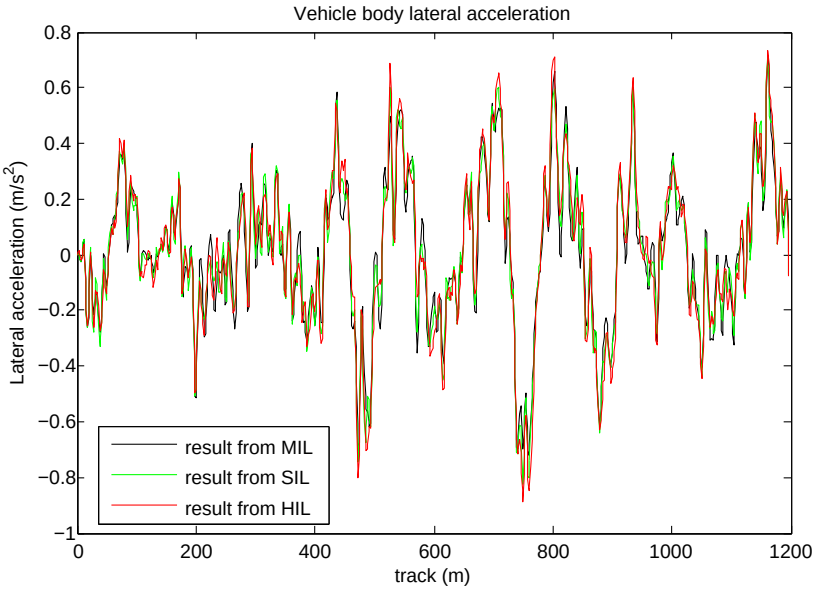

Figure 7.10: A comparison of the results from MIL, SIL and HIL on straight track

Table 7.1: Control system assessment for HIL simulation in the vehicle body centre @ 58(m/s)

Deterministic(CURVED TRACK)			
P_{ct}(P-factor):	MIL	SIL	HIL
-standing (% of pasengers)	54.1	54.2	54.5
-seated (% of pasengers)	15.6	15.5	15.4
Stochastic(STRAIGHT TRACK)			
passenger comfort:	MIL	SIL	HIL
-R.M.S. passive (%g)	2.61	2.61	3.02
-R.M.S. active (%g)	2.48	2.50	2.88
-degradation (%)	-4.5	-4.2	-4.6

7.4 Summary

In this chapter, the HIL design process is discussed. A FPGA is employed as the electronic control unit. The controller designed in MATLAB m code is compiled to C code

via Embedded MATLAB, modified to the canonical delta form and downloaed into the Microblaze soft processor in FPGA. xPC-Target is used to provide the real-time environment for the 9 DOF railway vehicle model. The communication between FPGA and xPC-Target is achieved by the RS232 cable. Results from the HIL system are similar to the results from the MATLAB simulation, which demonstrates the possiblity of future practical implementation.

The use of FPGA for control is investigated, which provides another flexible way for the C code controller implemenation. The whole system (Soft Processor, Communication Driver, System Frequency Clock, Floating Point Unit, etc.) can be configured and reconfigured for any individual design.

Chapter 8

Conclusions and Future steps

8.1 Conclusions

This thesis conducted a research on integrated tilt and active lateral secondary suspension control in high speed railway vehicles, aimed to enhance the tilting control system performance with help from active lateral secondary suspensions. Research outcomes demonstrated the efficiency of this novel idea. The trade-off for the tilting control system design between straight track ride quality and curving performance is significantly optimized by this suspension integration strategy even with classical control design, also ensuring that the suspension deflection is kept within a limit to avoid lateral bump-stop contact.

The research started with an investigation on the tilting system performance requirements and assessment methods. The control system design for tilting systems has to meet a multitude of conflicting objectives: minimization of the P_{ct} value for assessing the curving performance and the R.M.S. value (body lateral acceleration) for evaluating the straight track ride quality; keeping the suspension deflection within the limit; identifying what a tilting vehicle would ideally perform on the transition from straight to curved track and then minimizing the deviation of the actual response compared with this ideal. The conflict of these objectives is caused by a strong interaction between roll and lateral modes of the vehicle body dynamics. Current industrial practice for tilting trains is to adopt a command-driven control and put sensors in the non-tilt part (bogie)

to avoid the roll and lateral interaction. However, low pass filters are needed for attenuating the high frequency signals caused by the bogie-mounted sensors which unavoidly introduces tilting action delay. The precedence command-driven strategy is introduced later to reduce this tilting delay. The integration of tilt and active lateral secondary suspension provides another solution for the tilting railway vehicle control. Compared with the precedence command-driven control, it is simper and more straightforward in terms of detecting sensor failures.

The active anti-roll bar (ARB) tilting is used in Bombardier Talent tilting trains, where one of the vertical links between the anti-roll bar and vehicle body is replaced by an actuator. Then tilting is applied through this vertical actuator and the anti-roll bar. In this research, a lateral actuator was proposed to be installed between the vehicle body and bogie. Controllers designed for this dual-actuator system were based on local vehicle body sensors without the need for low pass filters. Classical Decentralized (CD) control was designed firstly which gave a much better performance compared with the tilt-only Nulling Tilting (PI) control. The P_{ct} value and R.M.S. value (body lateral acceleration) were both reduced to an acceptable level, 15.7% (for seated passengers) and 3.57%g respectively. Modern control approaches, such as H_∞-based Decentralised (HD) control and MIMO Linear Quadratic Gaussian (LQG) control were also investigated. The performance of the modern control was close to the industry-used Precedence Tilting control. The P_{ct} values for seated passengers were 14.2% and 12.8% for HD and LQG control respectively, R.M.S. values (lateral acceleration) were kept less than 3.78%g (the value in the passive situation). Note that, to obtain the best simulation result, Genetic Algorithm was adopted to optimize the controller parameters.

Tilting trains with tilting bolster are more common than tilting trains with active ARB, i.e. Swedish X2000, Italian Pendolino and British virgin Pendolino trains. Most use a tilt mechanism below secondary suspensions to provide the tilting action. The interaction between tilting and suspension deflection is less an issue here compared with tilting train with active ARB. In the research, a lateral actuator was assumed to be installed between the vehicle body and bolster. Classical Decentralized (CD) control and Command-Driven Decentralised (CDD) control were investigated firstly, which provided a better performance compared with the tilt-only Nulling Tilting (PI) control.

The best performance came from the precedence CDD control, the P_{ct} value indicated only 2.94% of seated passengers may feel uncomfortable during curving transition in trailing vehicles. Two modern control strategies were studied for further improvement of the leading vehicle performance: MIMO optimal and Estimator-Based Decoupling (EBD) control. In the design of EBD control, robust H_∞ filter was employed to estimate the body lateral acceleration (relative to the track) and true cant deficiency (t.c.d.), which provided a more robust estimation than Kalman filter. Relative Gain Array (RGA) was used to illustrate the efficiency of these two estimated outputs on the attenuation of the control loops interaction. EBD control gave the 4.91% P_{ct} value for curving performance assessment and provided 49.38% ride quality improvement on straight track.

9 DOF full vehicle models were developed for both mechanical integration systems. Yaw dynamics were taken into account. Symmetric configuration and modal control were used for the tilting and lateral actuator respectively. Lateral actuator dynamics were also addressed. The simulation results on the full vehicle model were similar to the results with end-view model. Moreover, the modal control for the lateral actuators attenuated the interaction between yaw and lateral dynamics of the vehicle body, hence providing a better straight track ride quality compared with the direct implemantation of lateral actuator control without yaw dynamics feedback.

Additionally, a Hardware-In-the-Loop (HIL) system was investigated with the considerations of future practical implimentation. A FPGA-based controller was studied which provides another flexible way for the digital controller implementation, i.e. softprocessor-based controller. The processor could be configured based on the individual design requirement before the C controller implementation. Moreover, xPC-Target was adopted to give a real-time environment for the 9 DOF railway vehcile model. The results from Model-In-the-Loop (MIL), Software-In-the-Loop (SIL) and Hardware-In-the-Loop (HIL) are similar to each other.

8.2 Future steps

- The study in this thesis was based on linear systems, which demonstrates the potential benifits could be obtained from the integrated tilt and active lateral secondary suspension. However, the real tilting mechanical system has some non-linear features, i.e. tilting mechanical friction and vehicle body mechanical deformation. They should be considered during both modelling and controller design stages. Using Multi-body dynamics software, i.e. SIMPACK, VAMPIRE, would be good solutions for the further modelling and controller validation. Also, non-linear control may need to be addressed as well.

- Track-vehicle interation is ignored, although the performance of the bogie is verified. The simulation results illustrate the lateral actuator generates a large force during the curving which can affect the wheel-rail contact force. It would be better to include the wheelset dynamics into the model and check the derailment criteria and stability criteria in the next step for the safty assessment.

- The FPGA-based real time optimisation for railway vehicle modelling and control would be an interesting direction for the future research. Genetic Algorithm optimisation process can be performed in a FPGA in real-time subject to the variation of the vehicle speed and rail track conditions.

- The biggest aspiration of the author is to see this work being tested on a real tilting train in the future.

References

Alstom. *http://www.transport.alstom.com/home/news/hotevents/v150/31488.EN.php?languageId=ENdir=/home/news/hotevents/v150/*, 2007. 1

Y. Arkun. Dynamic block relative gain and its connection with the performance and stability of decentralized control structures. *International Journal of Control*, 46(4): 1187 – 1193, 1987. 33

ASCET-SD. http://www.etas.com/en/products/ascet_software_products.php, 2010. 130

A. Balestrino and A. Landi. On input-output selection for multiloop control: From rga to roma. *International Symposium on Advanced Control of Chemical Processes Gramado*, Brazil - April 2-5, 2006. 32, 33

R. W. Beaven, M. T. Wright, and D. R. Seaward. Weighting function selection in h_∞ design process. *Control Engineering Practice*, 4(5):625–633, 1996. 28

A. S. Boksenbom and R. Hood. General algebraic method applied to control analysis of complex engine types. *Report NCA-TR-980, National Advisory Committee for Aeronautics*, Washington, D. C., 1949. 26

E. H. Bristol. On a new measure of interactions for multivariable process control. *IEEE Transactions on Automatic Control*, CA-11:133–134, 1966. 31, 33, 88

S. Bruni, R. M. Goodall, T. X. Mei, and H. Tsunashima. Control and monitoring for railway vehicle dynamics. *Vehicle System Dynamics*, 45:743–779, 2007. 5, 20, 23, 24

E. U. Carlos, E. L. Castro, and J. C. Castro. 2x2 individual channel design matlab toolbox. *Proceedings of the 44th IEEE conference on Decision and Control, and the European Control Conference 2005*, Sevile, Spain, 2005. 27

F. Cheli, G. Diana, and F. Resta. Numerical model of a tilting body railway vehicle compared with rig and on track tests. *Vehicle System Dynamics*, 35(6):417–442, 2001. 24

A. J. Chipperfield, P. J. Fleming, H. Pohlheim, and C. M. Fonseca. A genetic algorithm toolbox for matlab. *ICSE'94, Tenth International Conference on Systems Engineering*, pages 200–207, 1994a. 34

A. J. Chipperfield, P. J. Fleming, and C. M. Fonseca. Genetic algorithm tools for control systems engineering. *Adaptive Computing in Engineering Design and Control*, Plymouth, UK, September 21-22, 1994b. 34

M. S. Chiu and Y. Arkun. A new result on relative gain array, niederlinski index and decentralized stability condition: 2x2 plant case. *Automatica*, 27(2):419–421, 1991. 33

A. C. Coello and P. J. Fleming. An updated survey of evolutionary multiobjective optimization techniques: state of the art and future trends. *In 1999 Congress on Evolutionary Computation*, 1:1–13, 1999. DC,USA,. 34

L. Daga. http://leonardodaga.insyde.it/simulink/rtblockset.htm, 2004. 133

X. Dai and J. M. Zhang. Application of predictive control of neural network to tilting system of tilting train. *Electric drive for locomotives*, 6 2005. 21

X. Dai and J. M. Zhang. Robust h_∞ control to active tilting: An experimental research. *In Proc. Of IEEE international Vehicle Electronic Conference*, pages 290–293, 1999. 21

K. Deb. *Multi-Objective Optimization Using Evolutionary Algorithms*. John Wiley, 1 edition, 2001. 34

dSPACE. *dSPACE Catalog 2008*. 2008. 13

dSPACE GmbH. http://www.dspaceinc.com/ww/en/inc/home/products/sw/pcgs/targetli.cfm, 2010. 130

X. Du, R. Dixon, R. M. Goodall, and A. C. Zolotas. Lqg control of a high redundancy actuator. *IEEE/ASME International Conference on Advanced Intelligent Mechatronics, Switzerland*, 2007. 28

M. Enomoto, S. Kamoshita, M. Kamiyama, K. Sasaki, T. Hamada, and A. Kasato. Development of tilt control system using electrohydraulic actuators. *QR of Railway Technical Research Institute(RTRI)*, 45(4):219–224, 2005. 20

SCADE ESTEREL. http://www.esterel-technologies.com/products/scade-suite/, 2010. 130

ESW. *http://www.epicos.com/WARoot/News/ESW_presentation.pdf*, 2006. 11

C. M. Fonseca and P. J. Fleming. Genetic algorithm for multiobjective optimization: Formulation, discussion and generalization. *In Proceedings of the fifth International Conference on Genetic Algorithms*, San Mateo, CA:416–423, 1993. 34

W. Forsythe and R. M. Goodall. *Digital Control*. Macmillan New Electronics Series, 1991. x, 36, 135, 136, 137

V. Garg and R. Dukkipati. *Dynamics of Railway Vehicle Systems*. Academic Press, first edition, 1984. 101

D. E. Goldberg. *Genetic algorithm in Search, Optimization and Machine Learning*, volume Brazil - April 2-5. Addison-Wesley, USA, 1989. 34

D. E. Goldberg and J. Richardson. Genetic algorithms with sharing for multimodal function optimization. *In Second International Conference on Genetic Algorithms on Genetic algorithms and their Application*, NJ, USA:41–49, 1987. 34

R. M. Goodall. Perspectives on processing for real-time control. *Annual Reviews in Control*, 25:123–131, 2001. 36

R. M. Goodall. Active railway suspensions: Implementation status and technological trends. *Vehicle System Dynamics*, 28(2):87–117, 1997. 3, 11, 20, 23, 24, 25

R. M. Goodall. Tilting trains and beyond - the future for active railway suspensions: Part 1 improving passenger comfort. *Computing and Control Engineering Journal*, 10(4):153–160, 1999a. vii, 3, 8, 9, 15

R. M. Goodall. Tilting trains and beyond- the future for active railway suspensions, part 2 improving stability and guidance. *Computing and Control Engineering Journal*, 10: 221–230, 1999b. 4

R. M. Goodall and T. X. Mei. *Active suspensions, Chapter 11 in Handbook of Railway Vehicle Dynamics*. Taylor and Francis, 2006. 42, 116

R. M. Goodall, R. A. Williams, and A. Lawton. Railway vehicle active suspensions in theory and practice. *Proceedings of Seventh IAVSD Symposium, Cambridge, UK*, pages 301–316, 1982. 24

R. M. Goodall, J. T. Pearson, and I. Pratt. Actuator technologies for secondary active suspension on railway vehicles. *Proceedings of the International Conference on Speedup Technology for Railway and Maglev Vehicles*, pages 377–382, Nov. 1993. 13

R. M. Goodall, A. C. Zolotas, and J. Evans. Assessment of the performance of tilt system controllers. *The Railway Conference at Railtex 2000, NEC Birmingham*, Nov. 21-23 2000. 7, 42

A. Goto. Assessment of the performance of tilt system controllers. *Rolling Stock and Technology*, 24:28–34, 1997. 8

P. Grosdidier and M. Morari. Interaction measures for systems under decentralized control. *Automatica*, 22(3):309 – 320, 1986. 33

K. E. Haggblom. Partial relative gain: A new tool for control structure selection. *In: AIChE Annual Meeting*, Los Angeles, 1997. 32, 33

G. HAUSER. West coast main line trains “tilt technology”. *Railway Technology Conference*, Switzerland, 2002. 24

G. Hauser. $titlronix^{TM}$, anticipative tilt control. *Le Rail 4th Conference, Paris*, 2006. 11, 20

K. Havre and S. Skogestad. Input/output selection and partial control. *Proceedings of 13 IFAC Triennial World Congress, San Francisco*, M:181–186, 1996. 32

W. Hofbauer, P. Dolovai, H. P. Joeral, and J. Hirzinger. Lqg/ltr controller design for a gas engine. *Industrial Electronics, IEEE International Symposium*, 3:1631–1636, 2006. 28

M. Hovd and S. Skogestad. Simple frequency dependent tools for control system analysis, structure selection and design. *Automatica*, 28(5):989–996, 1992. 32, 33

D. C. Jin and K. Zhang. Experimental comparision of lateral active suspension in railway vehicles. *Journal of the China Railway Society*, 5, 1998. 25

et al. K. Kanbayashi. Development of the active vibration control system for very high speed railway vehicles. *Preprint of JSME*, 97-12:7376, 1997. 25

D. C. Karnopp. *Active and semi-active vibration control, Technical report.* Department of Mechnical and Aeronautical Engineering, University of California, 1974. 6

T. Keviczky, F. Borrelli, and G. J. Balas. Model predictive control for decoupled systems: A study on decentralized schemes. *IEEE ACC*, Boston MA, 2004. 29

S. Koizumi. An active suspension system for railway vehicles (2nd report). *Preprint of JSME*, 920-98:58, 1992. 25

S. Koizumi. An active suspension system for railway vehicles (3rd report). *Preprint of JSME*, 930-98:6164, 1993. 25

W. E. Leithead and J. O'Reilly. Multivariable control by individual channel design. *International Journal of Control*, 54:1–46, 1991. 27

W. E. Leithead and J. O'Reilly. M-input m-output feedback control by individual channel design. *International Journal of Control*, 56:1347–1397, 1992. 27

H. Li and R. M. Goodall. Linear and non-linear skyhook damping control laws for active railway suspensions. *Control Engineering Practice*, 7:843–850, 1999. 5

M. Li and M. M. Bayoumi. Adaptive decoupling control of mimo systems. *International Journal of Adaptive Control and Signal Processing*, 3(4):375–393, 2007. 29

E. Liceaga-Castro and J. Liceaga-Castro. Submarine depth control by individual channel design. *Proceedings of the 37th IEEE conference on Decision & Control*, Tampa, Florida USA,, 1998. 26

J. Liceaga-Castro, C. Verde, J. O'Reilly, and W. E. Leithead. Helicopter flight control using individual channel design. *IEE Control theory and applications*, 142(1), 1995. 26, 27

Motor Technology Ltd. http://www.motec.co.uk/, 2010. 121

W. L. Luyben. Distillation decoupling. *AIChE Journal*, 16, 1970. 26

J. M. Maciejowski. *Multivariable Feedback Design*. Reading, MA: Addison-Wesley, 1989. 33

V. Manousiouthakis, R. Savage, and Y. Arkun. Synthesis of decentralized process control structures using the concept of block relative gain. *AIChE Journal*, 32(6): 991–1003, 1986. 33

MapleSim3 Maplesoft. http://www.maplesoft.com/products/maplesim/index1.aspx, 2010. 130

MathWorks. http://www.mathworks.com/products/xpctarget/, 2010a. 134

The MathWorks. http://www.mathworks.com/products/featured/embeddedmatlab/, 2010b. 130

T. X. Mei and R. M. Goodall. Lqg and ga solution for active steering of solid axle railway vehicles. *IEE Proceedings - Control Theory and Applications*, 147(0). 34

T. X. Mei and R. M. Goodall. Robust control for independently-rotating wheelsets on a railway vehicle using practical sensors. *IEEE Transactions on Control Systems Technology*, 9(4):599–607, 2001. 4

T. X. Mei and R. M. Goodall. Multi-objective genetic algorithms optimised inter-vehicle active suspensions. *IMechE Proceedings (Part F) - Rail and Rapid Transit*, 216(0):53–63, 2002. 34

T. X. Mei and R. M. Goodall. Practical strategies for controlling railway wheelsets with independently rotating wheels. *Transactions of the ASME, Journal of Dynamic Systems, Measurement and Control*, 125(3):354–360, 2003. 4

K. Michail, A. C. Zolotas, R. M. Goodall, and J. T. Pearson. Sensor optimisation via h_∞ applied to a maglev suspension system. *WASET ICCAS 2008 International Conference on Control, Automation and Systems*, July 2008. 13, 28, 35

M. F. Miranda, R. H. C. Takahashi, and F. G. Jota. Hierarchical approach for h_∞ robust control design: S/ks mixed sensitivity with genetic algorithm. *IET Control Theory Appl.*, 1(1):18–24, 2007. 28

A. Niederlinski. A heuristic approach to the design of linear multivariable interacting control systems. *Automatica*, 7:691–701, 1971. 33

I. Okamoto. An active suspension system for railroad passenger cars. *Journal of JSME*, 53:21032109, 1987. 25

H. O'Neill. Gauge modelling of west coast main line tilting trains. *Proc. IMechE*, 222 (F):235–253, 2008. 24

H. R. O'Neill and G. D. Wale. Semi-active suspension improves rail vehicle ride. *Computing and Control Engineering Journal*, 5(4):183–188, 1994. 23

M. G. Ortega and F. R. Rubio. Systematic design of weighting matrices for the h_∞ mixed sensitivity problem. *Journal of Process Control*, 14(1):89–98, 2004. 28

J. E. Paddison. *Advanced control strategies for maglev suspension systems*. PhD thesis, Loughborough University, 1995. 41

J. T. Pearson, R. M. Goodall, and I. Pratt. Control system studies of an active anti-roll bar tilt system for railway vehicles. *Proceedings, Institution of Mechanical Engineers*, 212(F1):43–60, 1998. 21, 115

J. T. Pearson, R. M. Goodall, T. X. Mei, S. Shen, C. Kossmann, O. Polach, and G. Himmelstein. Design and experimental implementation of an active stability system for a high speed bogie. *Vehicle System Dynamics*, 41(819):43–52, 2004. 4

I. Persson and S. D. Iwnicki. Optimisation of railway profiles using a genetic algorithm. *Vehicle System Dynamics*, Supplement to Vol 41:517–527, 2004. 35

R. Persson. *Tilting trains Technology, benefits and motion sickness, Licentiate Thesis.* Railway Technology Stockholm, Sweden, 2008. 6, 15

R. Persson, R. M. Goodall, and K. Sasak. Carbody tilting - technologies and benefits. *Vehicle System Dynamics*, 47:949–981, 2009. 6, 7, 8, 20

C. L. Phillips and H. T. Nagle. *DIGITAL CONTROL SYSTEM ANALYSIS AND DESIGN (SECOND EDITION).* Prentice-Hall International, Inc., 1990. 35

I. Postlethwaite, M. C. Tsai, and D. W. Gu. Weighting function selection in h_∞ design. *In IFAC Symposia Series- Proceedings of a Triennial World Congress*, 3:127–132, 1990. 28

I. Pratt. *Active Suspension Applied to Railway Trains, Ph.D thesis.* Loughborough University of Technology, 1996. 3, 11, 13, 25, 40, 41, 120

D. E. Reeves. *A comprehensive approach to control configuration design for complex systems. PhD thesis.* Georgia Insitute of Technology, 1991. 33

H. Rosenbrock. *State-space and multivariable theory.* Wiley Interscience Division (New York), 1970. 33

B. Ruth, C. Patrizio, D. Luc, A. Frank, K. Anatolii, and S. Carsten. Trends in theory of control system design. 17th IFAC, Korea, 2008. 29

H. Schmidt. *Model based design of decentralized control configurations, Ph.D thesis.* KTH, Sweden, 2002. 32, 33

A. Seshadri. *http://www.mathworks.com/matlabcentral/fileexchange/10429-nsga-ii-a-multi-objective-optimization-algorithm*, 2009. 34

X. Shu. On the adaptive control of railway tilting coaches. *In Proceedings 14th World Congress of IFAC*, 1999. 20

D. Simon. *Optimal State Estimation: Kalman, H-Infinity, and Nonlinear Approaches, 1st ed.* Wiley Sons, 2006. 89, 90, 91

S. Skogestad and K. Havre. The use of rga and condition number as robustness measures. *Computer and Chemistry Engineering*, 20:S1005–S1010, 1996. 32

S. Skogestad and M. Morari. Variable selection for decentralized control. *In: AIChE Annual meeting, Washington DC*, 1998. 33

S. Skogestad and I. Postlethwaite. *Multivariable feedback control: Analysis and design.* Wiley, 2000, Reprinted Version, 2000. 28, 29, 32, 33

N. Srinivas and K. Deb. Multiobjective optimization using nondominated sorting in genetic algorithms. *Evolutionary computation*, 2:221–248, 1994. 34, 55

R. Streiter, M. Boller, and R. Schneider. Active lateral suspension for high speed trains-a step towards the mechatronic bogie. 2001. 25, 52, 113

A. Stribersky, H. Muller, and B. Rath. The development of an integrated suspension control technology for passenger trains. *Proceedings, Institution of Mechanical Engineers*, 212(1):33–42, 1998. 24

A. Suescun. Use of inverse dynamics in the development of tilt control strategies for rail vehicles. *Vehicle System Dynamics*, Supplement 25:655667, 1996. 21

M. Tahara, K. Watanabe, T. Endo, O. Goto, S. Negoro, and S. Koizumi. Practical use of an active suspension system for railway vehicles. *International Symposium on Speed-up and Service Technology for Railway and Maglev Systems 2003 (STECH03)*, 8, 19-22, 2003. 2, 24, 25

K. Tanifuji, S. Koizumi, and R. Shimamune. Mechatronics in japanese rail vehicles: active and semi-active suspensions. *Control Engineering Practice*, 10:4–27, 2002. 23

M. T. Tham. Multivariable control: an introduction of decoupling control. *Industrial Digital Control Systems, IEEE Control Engineering*, Series 37, Peter Peregrinus, 1998. 26

Real-Time Workshop 7.4 The MathWorks. http://www.mathworks.co.uk/products/rtw/, 2010. 130

M. van de Wal and B. de Jager. A review of methods for input/output selection. *Automatica*, 37(4):487–510, 2001. 29

T. A. Wenzel, K. J. Burnham, M. V. Blundell, and R. A. Williams. Kalman filters as a virtual sensor: applied to automotive stability systems. *Transactions of the Institue of Measurement and Control*, 29(2):95–115, 2007. 113, 114

E. Wolff. *Studies on Control of Integrated Plants, PhD thesis,*. Norwegian University of Science and Technology, Trondheim, 1994. 33

Xilinx. http://www.xilinx.com/microblaze, 2010. 133

Xilinx. Microblaze soft processor core. *http://www.xilinx.com/tools/microblaze.htm.* 37

Xilinxedk. http://www.xilinx.com/edk, 2010. 133

G. Zames. Feedback and optimal sensitivity: Model reference transformations, multiplicative seminorms, and approximate inverse. *IEEE Transactions on Automatic Control*, 26(2):301–320, 1981. 28

H. Zamzuri. *Intelligent Model-Based Robust Control for Tilting Railway Vehicles*. Ph.D thesis, Louhgborough University, 2008. 9, 22, 102

H. Zamzuri, A. C. Zolotas, and R. M. Goodall. Optimised intelligent tilt controller scheme using genetic algorithms,. *Proceedings of UKACC International Control Conference*, Glasgow, September 2006a. 22, 35

H. Zamzuri, A. C. Zolotas, and R. M. Goodall. Intelligent control approaches for tilting railway vehicles. *Vehicle System Dynamics*, 44(S1):834–843, 2006b. 22

H. Zamzuri, A. C. Zolotas, and R. M. Goodall. Lqg with fuzzy correction mechanism in tilting railway vehicle control design. *Proceedings of 3rd IFAC Workshop on Advanced Fuzzy and Neural Control (AFNC07)*, Valenciennes, France, 29-30 October 2007. 23

J. Zeng and R. Luo. Dynamic curving simulation of tilting train. *Proceedings of International Symposium on Speed-up, Safety and Service Technology for Railway and Maglev Systems 2009 (STECH09)*, 6 2009. 21

X. Zhang, J. Wang, and T. Qin. Fuzzy decoupling controller based on multi-mode control algorithm of pi-single neuron and its application. *International symposium on instrumentation and control technology*, 5253:681–685, 2003. 29

D. Zheng. *Linear System Theory (Second Edition)*. Tsinghua University, Beijing, 2002. 27

J. Zheng, G. Guo, and Y. Wang. Feedforward decouping control design for dual-actuator system in hard disk drives. *IEEE transaction magnetics*, 40(4), 2004. 26

A. C. Zolotas. *Advanced control strategies for tilting trains*. Ph.D thesis, Louhgborough University, 2002a. ix, 9, 21, 44, 46, 56, 74, 77, 80, 109, 110

A. C. Zolotas and R. M. Goodall. Modelling and control of railway vehicle suspensions. *in Mathematical Methods for Robust and Nonlinear Control, Series: Lecture Notes in Control and Information Science, Turner, Mathew C., and Bates, Declan G., Springer*, 2007a. 22, 44

A. C. Zolotas, R. M. Goodall, and G. D. Halikias. New control strategies for tilting trains. *Vehicle System Dynamics*, 37:171–182, 2002b. 22

A. C. Zolotas, R. M. Goodall, and G. D. Halikias. Recent results in tilt control design and assessment of high-speed railway vehicles. *Proceedings, Institution of Mechanical Engineers*, 212(F1):291–312, 2007b. 22, 44

Appendix

A. Evaluation for the curve transition passenger comfort

P_{ct} factor calculation:

$$P_{ct} = (Ay + By - C) \geq 0 + D(\dot{\theta})^E$$

where A, B, C, D, E are constants defined below:

Condition	A	B	C	D	E
Standing passenger	2.8	2.03	11.1	0.185	2.283
Seated passenger	0.88	0.95	5.9	0.120	1.626

P_{ct} = passenger comfor index on curve transition, representing the percentage of passenger that will feel discomfort.

y = maximum vehicle body lateral acceleration calculated between the start of curve transition and 1.6s after the end of the transition (expressed in %g)

y = maximum lateral jerk level, calculated as the maximum difference between two subsequent values of y no closer than 1 sec, in time interval between 1 sec before start of the curve transition and the end of the transition (%g/s)

$\dot{\theta}$ = maximum absolute body roll speed calculated from the beginning of the curve transition to the end of curve transition (deg/s).

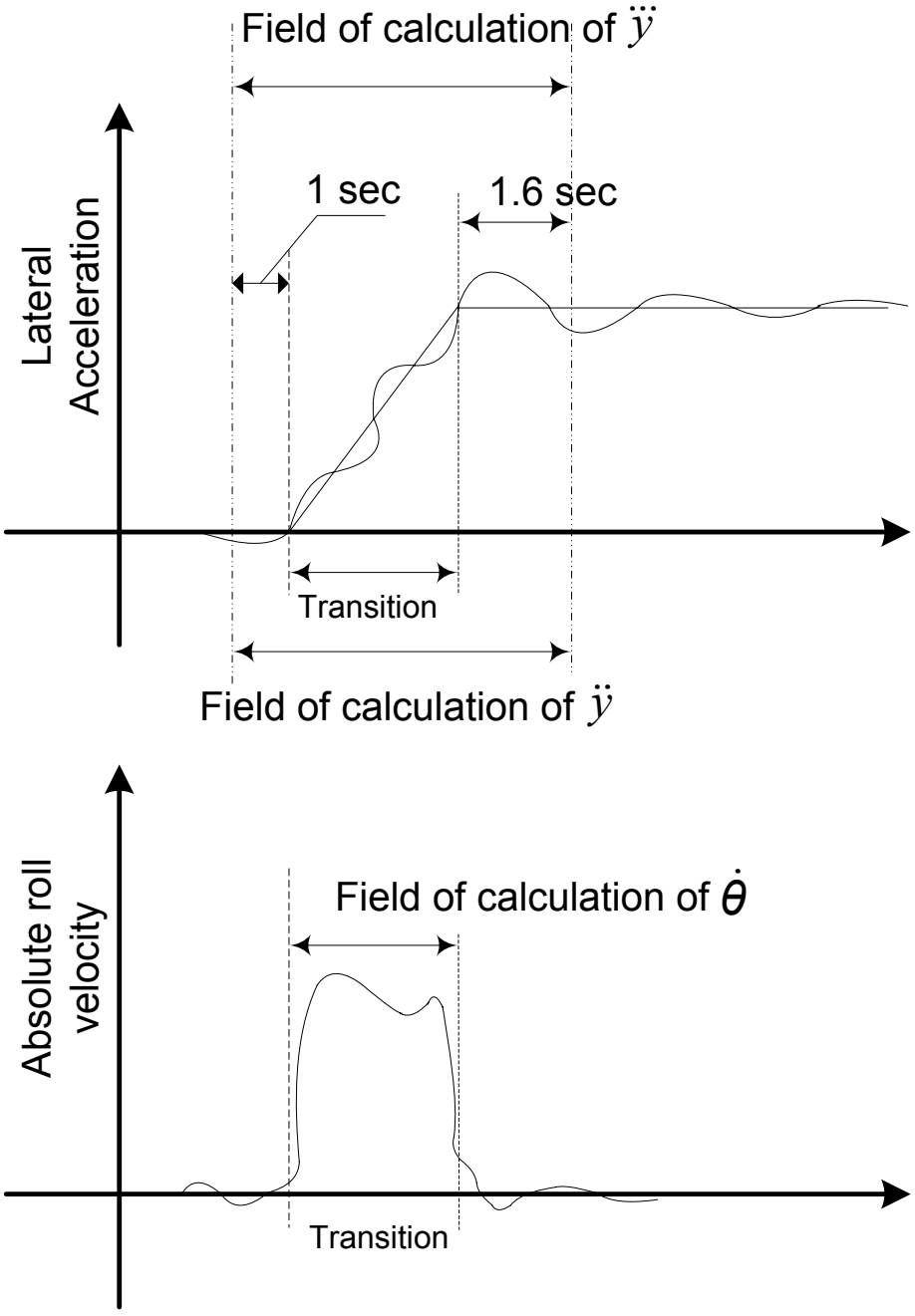

Figure A.1: Calculation of quantities y, y, $\dot{\theta}$ for P_{ct} factor

B. Airspring model

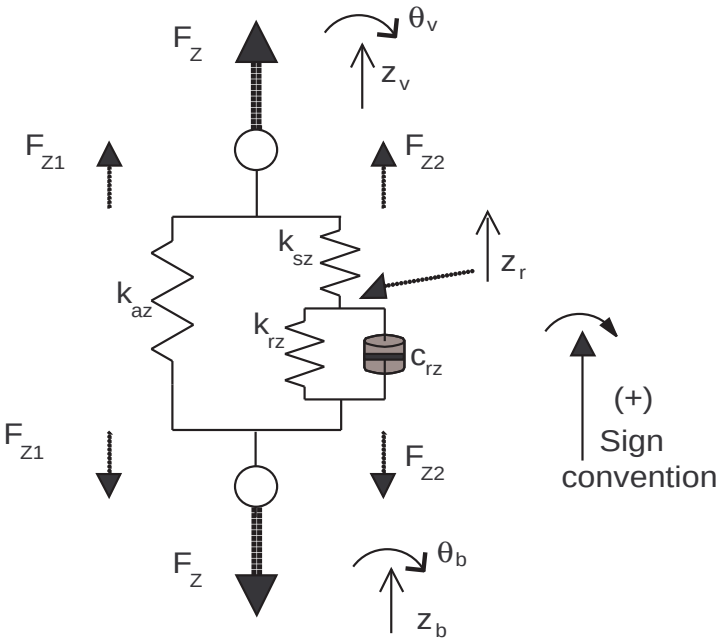

Figure B.1: Airspring Model

Disregarding vertical motions and substituting $d_1\theta_r$ for z_r:

$$F_z = -k_{az}(d_1\theta_v - d_1\theta_b) - k_{sz}(d_1\theta_v - d_1\theta_r)$$
$$\dot{\theta}_r = -\frac{(k_{sz} + k_{rz})}{c_{rz}}\theta_r + \frac{k_{sz}}{c_{rz}}\theta_v + \frac{k_{rz}}{c_{rz}}\theta_b + \dot{\theta}_b$$

C. State-Space matrices

C1. State-Space matrices for Integrated active ARB with active lateral secondary suspension

$$
A = \begin{bmatrix}
y_v & \theta_v & y_b & \theta_b & \dot{y}_v & \dot{\theta}_v \ldots \\
0 & 0 & 0 & 0 & 1 & 0 \ldots \\
0 & 0 & 0 & 0 & 0 & 1 \ldots \\
0 & 0 & 0 & 0 & 0 & 0 \ldots \\
0 & 0 & 0 & 0 & 0 & 0 \ldots \\
-\frac{2k_{sy}}{m_v} & \frac{k_{sy}h_1}{m_v} & \frac{2k_{sy}}{m_v} & \frac{2k_{sy}h_2}{m_v} & \frac{-c_{sy}}{m_v} & \frac{c_{sy}h_1}{m_v} \ldots \\
\frac{2h_1k_{sy}+m_vg}{i_{vr}} & -\frac{k_{vr}+2{h_1}^2k_{sy}+2{d_1}^2(k_{az}+k_{sz})}{i_{vr}} & -\frac{2h_1k_{sy}+m_vg}{i_{vr}} & \frac{2{d_1}^2k_{az}-2h_1h_2k_{sy}+k_{vr}}{i_{vr}} & \frac{2h_1c_{sy}}{i_{vr}} & -\frac{2h_1c_{sy}}{i_{vr}} \ldots \\
\frac{2k_{sy}}{m_b} & -\frac{2h_1k_{sy}}{m_b} & -\frac{2(k_{sy}+k_{py})}{m_b} & -\frac{2(h_2k_{sy}+h_3k_{py})}{m_b} & \frac{2c_{sy}}{m_b} & -\frac{2h_1c_{sy}}{m_b} \ldots \\
\frac{2h_2k_{sy}}{i_{br}} & \frac{k_{vr}-2h_1h_2k_{sy}+2{d_1}^2(k_{az}+k_{sz})}{i_{br}} & -\frac{2(h_2k_{sy}-h_2k_{py})}{i_{br}} & -\frac{k_{vr}+2{h_2}^2k_{sy}+2{h_3}^2k_{py}+2{d_2}^2k_{pz}+2{d_1}^2k_{az}}{i_{br}} & \frac{2h_2c_{sy}}{i_{br}} & -\frac{2h_1h_2c_{sy}}{i_{br}} \ldots \\
0 & \frac{k_{sz}}{c_{rz}} & 0 & \frac{k_{rz}}{c_{rz}} & 0 & 0 \ldots \\
0 & 0 & 0 & 0 & 0 & 0 \ldots \\
0 & 0 & 0 & 0 & 0 & 0 \ldots \\
0 & 0 & 0 & 0 & 0 & 0 \ldots
\end{bmatrix}
$$

$$
\begin{bmatrix}
\ldots\dot{y}_b & \dot{\theta}_b & \theta_r & \theta_0 & \dot{\theta}_0 & y_0 \\
\ldots 0 & 0 & 0 & 0 & 0 & 0 \\
\ldots 0 & 0 & 0 & 0 & 0 & 0 \\
\ldots 1 & 0 & 0 & 0 & 0 & 0 \\
\ldots 0 & 1 & 0 & 0 & 0 & 0 \\
\ldots \frac{2c_{sy}}{m_v} & \frac{2c_{sy}h_2}{m_v} & 0 & g & 0 & 0 \\
\ldots -\frac{2h_1c_{sy}}{i_{vr}} & \frac{2h_1h_2c_{sy}}{i_{vr}} & \frac{2k_{az}{d_1}^2}{i_{vr}} & g & 0 & 0 \\
\ldots -\frac{2(c_{sy}+c_{py})}{m_b} & -\frac{2(h_2c_{sy}-h_3c_{py})}{i_{br}} & 0 & g & 0 & \frac{2k_{py}}{m_b} \\
\ldots -\frac{2(h_2c_{sy}-h_3c_{py})}{i_{br}} & 1 & -\frac{k_{az}+k_{rz}}{c_{rz}} & 0 & 0 & 0 \\
\ldots 0 & -\frac{2{h_3}^2c_{sy}+2{h_2}^2c_{sy}+2{d_2}^2c_{pz}}{i_{br}} & -\frac{{d_1}^2k_{sz}}{i_{br}} & 0 & 0 & -\frac{2h_3k_{py}}{i_{br}} \\
\ldots 0 & 0 & 0 & 0 & 1 & 0 \\
\ldots 0 & 0 & 0 & 0 & 0 & 0 \\
\ldots 0 & 0 & 0 & 0 & 0 & 0
\end{bmatrix}
$$

$$
B = \begin{bmatrix}
\delta_a & R^{-1} & \theta_0 & \dot{y}_0 & F_a \\
0 & 0 & 0 & 0 & 0 \\
0 & 0 & 0 & 0 & 0 \\
0 & 0 & 0 & 0 & 0 \\
0 & 0 & 0 & 0 & 0 \\
0 & -v^2 & -h_{g1} & 0 & 1 \\
\frac{k_{vr}}{i_{vr}} & 0 & -1 & 0 & -h_1 \\
0 & -v^2 & -h_{g2} & \frac{2c_{py}}{m_b} & -1 \\
-\frac{k_{vr}}{i_{br}} & 0 & -1 & -\frac{2h_3c_{py}}{i_{br}} & -h_2 \\
0 & 0 & 0 & 0 & 0 \\
0 & 0 & 0 & 0 & 0 \\
0 & 0 & 1 & 0 & 0 \\
0 & 0 & 0 & 1 & 0
\end{bmatrix}
$$

C2. State-Space matrices for Integrated tilting bolster with active lateral secondary suspension

$$
A = \begin{bmatrix}
y_v & \theta_v & y_b & \theta_b & \dot{y}_v & \dot{\theta}_v & \dot{y}_b \ldots \\
0 & 0 & 0 & 0 & 1 & 0 & 0 \ldots \\
0 & 0 & 0 & 0 & 0 & 1 & 0 \ldots \\
0 & 0 & 0 & 0 & 0 & 0 & 1 \ldots \\
0 & 0 & 0 & 0 & 0 & 0 & 0 \ldots \\
-\frac{2k_{sy}}{m_v} & \frac{k_{sy}h_1}{m_v} & \frac{2k_{sy}}{m_v} & \frac{2k_{sy}h_2}{m_v} & 0 & 0 & 0 \ldots \\
\frac{2h_1k_{sy}+m_vg}{i_{vr}} & -\frac{k_{vr}+2{h_1}^2k_{sy}+2{d_1}^2(k_{az}+k_{sz})}{i_{vr}} & -\frac{2h_1k_{sy}+m_vg}{i_{vr}} & \frac{2{d_1}^2k_{az}-2h_1h_2k_{sy}+k_{vr}}{i_{vr}} & 0 & -\frac{c_{vr}}{i_{vr}} & 0 \ldots \\
\frac{2k_{sy}}{m_b} & -\frac{2h_1k_{sy}}{m_b} & -\frac{2(k_{sy}+k_{py})}{m_b} & -\frac{2(h_2k_{sy}+h_3k_{py})}{m_b} & 0 & 0 & \frac{c_{py}}{m_b} \ldots \\
\frac{2h_2k_{sy}}{i_{br}} & \frac{k_{vr}-2h_1h_2k_{sy}+2{d_1}^2(k_{az}+k_{sz})}{i_{br}} & -\frac{2(h_2k_{sy}-h_2k_{py})}{i_{br}} & -\frac{k_{vr}+2{h_2}^2k_{sy}+2{h_3}^2k_{py}+2{d_2}^2k_{pz}+2{d_1}^2k_{az}}{i_{br}} & 0 & \frac{c_{vr}}{i_{br}} & \frac{2h_3c_{py}}{i_{br}} \ldots \\
0 & \frac{k_{sz}}{c_{rz}} & 0 & \frac{k_{rz}}{c_{rz}} & 0 & 0 & 0 \ldots \\
0 & 0 & 0 & 0 & 0 & 0 & 0 \ldots \\
0 & 0 & 0 & 0 & 0 & 0 & 0 \ldots \\
0 & 0 & 0 & 0 & 0 & 0 & 0 \ldots \\
0 & 0 & 0 & 0 & 0 & 0 & 0 \ldots \\
0 & 0 & 0 & 0 & 0 & 0 & 0 \ldots \\
0 & 0 & 0 & 0 & 0 & 0 & 0 \ldots \\
0 & 0 & 0 & 0 & 0 & 0 & 0 \ldots \\
0 & 0 & 0 & 0 & 0 & 0 & 0 \ldots
\end{bmatrix}
$$

$$
\begin{array}{cccccccccccc}
\ldots\dot{\theta}_b & \theta_r & y_w & \dot{y}_w & \theta_m & \dot{\theta}_m & \theta_0 & \dot{\theta}_0 & R^{-1} & y_0 \\
\ldots 0 & 0 & 0 & 0 & 0 & 0 & 0 & 0 & 0 & 0 \\
\ldots 0 & 0 & 0 & 0 & 0 & 0 & 0 & 0 & 0 & 0 \\
\ldots 0 & 0 & 0 & 0 & 0 & 0 & 0 & 0 & 0 & 0 \\
\ldots 1 & 0 & 0 & 0 & 0 & 0 & 0 & 0 & 0 & 0 \\
\ldots 0 & 0 & 0 & 0 & -\frac{2h_{mt}k_{sy}+m_v g}{m_v} & 0 & g & 0 & -v^2 & 0 \\
\ldots \frac{c_{vr}}{i_{vr}} & \frac{2k_{sz}{d_1}^2}{i_{vr}} & 0 & 0 & -\frac{k_{vr}+2{d_1}^2 k_{az}+2k_{sy}h_1 h_{mt}}{i_v r} & \frac{c_{vr}}{i_{vr}} & 0 & 0 & 0 & 0 \\
\ldots \frac{h_3 c_{py}}{m_b} & 0 & \frac{2k_{py}}{m_b} & \frac{2c_{py}}{m_b} & \frac{2h_{mt}}{m_b} & 0 & g & 0 & -v^2 & 0 \\
\ldots -\frac{2({d_2}^2 c_{pz}+{h_3}^2 c_{py}+c_{vr})}{i_{br}} & -\frac{2k_{sz}{d_1}^2}{i_{br}} & -\frac{2h_3 k_{py}}{i_{br}} & -\frac{2h_3 c_{py}}{i_{br}} & -\frac{-k_{vr}-2{d_1}^2 k_{az}+2k_{sy}h_1 h_{mt}}{i_b r} & -\frac{c_{vr}}{i_{br}} & 0 & 0 & 0 & 0 \\
\ldots 1 & -\frac{(k_{sz}+k_{rz})}{c_{rz}} & 0 & 0 & \frac{k_{rz}}{c_{rz}} & 1 & 0 & 0 & 0 & 0 \\
\ldots 0 & 0 & 0 & 1 & 0 & 0 & 0 & 0 & 0 & 0 \\
\ldots 0 & 0 & -{w_{cm0}}^2 & -2\zeta_{m0}w_{cm0} & 0 & 0 & 0 & 0 & 0 & {w_{cm0}}^2 \\
\ldots 0 & 0 & 0 & 0 & 1 & 0 & 0 & 0 & 0 & 0 \\
\ldots 0 & 0 & 0 & 0 & -{w_{cm1}}^2 & -2\zeta_{m1}w_{cm1} & 0 & 0 & 0 & {w_{cm1}}^2 \\
\ldots 0 & 0 & 0 & 0 & 0 & 0 & 0 & 1 & 0 & 0 \\
\ldots 0 & 0 & 0 & 0 & 0 & 0 & 0 & 0 & 0 & 0 \\
\ldots 0 & 0 & 0 & 0 & 0 & 0 & 0 & 0 & 0 & 0 \\
\ldots 0 & 0 & 0 & 0 & 0 & 0 & 0 & 0 & 0 & 0
\end{array}
\quad]
$$

$$
B = \begin{array}{c}
\begin{array}{ccccccc}
\theta_{mi} & \dot{R}^{-1} & \theta_0 & \dot{y}_0 & F_a \\
\end{array} \\
\left[\begin{array}{ccccccc}
0 & 0 & 0 & 0 & 0 \\
0 & 0 & 0 & 0 & 0 \\
0 & 0 & 0 & 0 & 0 \\
0 & 0 & 0 & 0 & 0 \\
0 & 0 & -h_{g1} & 0 & 1 \\
0 & 0 & -1 & 0 & -h_1 \\
0 & 0 & -h_{g2} & 0 & -1 \\
0 & 0 & -1 & 0 & -h_2 \\
0 & 0 & 0 & 0 & 0 \\
0 & 0 & 0 & 0 & 0 \\
0 & 0 & 0 & 0 & 0 \\
0 & 0 & 0 & 0 & 0 \\
0 & 0 & 0 & 0 & 0 \\
{w_{cm1}}^2 & 0 & 0 & 0 & 0 \\
0 & 0 & 0 & 0 & 0 \\
0 & 0 & 1 & 0 & 0 \\
0 & 1 & 0 & 0 & 0 \\
0 & 0 & 0 & 1 & 0
\end{array}\right]
\end{array}
$$

D. Vehicle parameter values

D1. Integrated active ARB with active lateral secondary suspension

Parameters for 4 DOF Model

m_v	Half body mass, 19,000kg
i_{br}	Bogie roll inertia, 1,500kgm^2
k_{az}	Airspring area stiff., 210,000N/m
k_{sz}	Airspring series stiff., 620,000N/m
k_{rz}	Airspring reserv. stiff., 244,000N/m
c_{rz}	Airspring reserv. damp., 33,000$(Ns)/m$
k_{sy}	Secondary lateral stiff., 260,000N/m
k_{vr}	Anti-roll bar stiff./bogie, 2,000,000$(Nm)/rad$
k_{pz}	Primary vertical stiff., 2,000,000N/m
c_{pz}	Primary vertical damp., 20,000$(Ns)/m$
k_{py}	Primary lateral stiff., 35,000,000N/m
c_{py}	Primary lateral damp., 16,000$(Ns)/m$
d_1	Airspring semi-spacing, 0.90m
d_2	Prim. vert. suspen. semi-spacing, 1.00m
h_1	2ndary later. suspen. height(body cog), 0.9m
h_2	2ndary later. suspen. height(bogie cog), 0.25m
h_3	Primary later. suspen. height(bogie cog), 0.09m
h_{g1}	Bogie cog height(rail level), 0.37m
h_{g2}	Body cog height(rail level), 1.52m
i_{vr}	Half body roll inertia, 25,000 kgm^2
m_b	Bogie mass, 2,500kg

Parameters for 9 DOF Model

m_v	Full body mass, 38,000kg
i_{vr}	Full body roll inertia, 50,000kgm^2
i_{vy}	Full body yaw inertia, 2,310,000kgm^2
m_b	Bogie mass, 2,500kg
i_{br}	Bogie roll inertia, 1,500kgm^2
i_{by}	Bogie roll inertia, 3,100kgm^2
k_{az}	Airspring area stiff., 210,000N/m
k_{sz}	Airspring series stiff., 620,000N/m
k_{rz}	Airspring reserv. stiff., 244,000N/m
c_{rz}	Airspring reserv. damp., 33,000$(Ns)/m$
k_{sy}	Secondary lateral stiff., 260,000N/m
c_{sy}	Secondary lateral damp., 20,000Ns/m
k_{xp}	Secondary yaw stiff., 20,000N/m
c_{xp}	Secondary yaw damp., 2Ns/m
k_{vr}	Anti-roll bar stiff./bogie, 2,000,000$(Nm)/rad$
k_{pz}	Primary vertical stiff., 1,000,000N/m
c_{pz}	Primary vertical damp., 10,000$(Ns)/m$
k_{py}	Primary lateral stiff., 17,500,000N/m
c_{py}	Primary lateral damp., 8,000$(Ns)/m$
d_1	Airspring semi-spacing, 0.90m
d_2	Prim. vert. suspen. semi-spacing, 1.00m
h_1	2ndary later. suspen. height(body cog), 0.9m
h_2	2ndary later. suspen. height(bogie cog), 0.25m
h_3	Primary later. suspen. height(bogie cog), 0.09m
h_{g1}	Bogie cog height(rail level), 0.37m
h_{g2}	Body cog height(rail level), 1.52m
L_v	Semi bogie to bogie length, 9.5m
L	Full vehicle length, 19m
b	Bogie center to axle, 1.25m
I_r	Semi wheel to wheel spacing, 1.25m

(D2. Integrated tilting bloster with active lateral secondary suspension)

Parameters for 4 DOF Model

m_v	Half body mass, 16,000kg
m_b	Bogie mass, 3,680kg
i_{vr}	Half body roll inertia, 20,000kgm^2
i_{br}	Bogie roll inertia, 2,500kgm^2
k_{az}	Airspring area stiff., 210,500N/m
k_{sz}	Airspring series stiff., 300,000N/m
k_{rz}	Airspring reserv. stiff., 201,000N/m
c_{rz}	Airspring reserv. damp., 20,000$(Ns)/m$
k_{sy}	Secondary lateral stiff., 100,000N/m
k_{vr}	Anti-roll bar stiff./bogie, 1,500,000$(Nm)/rad$
c_{vr}	Primary vertical damp., 18,200$(Ns)/m$
k_{pz}	Primary vertical stiff., 1,600,000N/m
c_{pz}	Primary vertical damp., 20,000$(Ns)/m$
k_{py}	Primary lateral stiff., 18,000,000N/m
c_{py}	Primary lateral damp., 20,000$(Ns)/m$
d_1	Airspring semi-spacing, 0.835m
d_2	Prim. vert. suspen. semi-spacing, 1.00m
h_1	2ndary later. suspen. height(body cog), 0.844m
h_2	2ndary later. suspen. height(bogie cog), 0.252m
h_3	Primary later. suspen. height(bogie cog), 0.194m
h_{g1}	Bogie cog height(rail level), 1.696m
h_{g2}	Body cog height(rail level), 0.60m
h_{mt}	Mechanism c.o.g. vertical separation from effective tilt centre, 0.60m

Parameters for 9 DOF Model

m_v/m_b	Full body/bogie mass, 32,000/3,680kg
i_{vr}	Full body roll inertia, 40,000kgm^2
i_{vy}	Full body yaw inertia, 3,110,000kgm^2
i_{br}	Bogie roll inertia, 2,500kgm^2
i_{by}	Bogie roll inertia, 3,800kgm^2
k_{az}	Airspring area stiff., 210,500N/m
k_{sz}	Airspring series stiff., 300,000N/m
k_{rz}	Airspring reserv. stiff., 201,000N/m
c_{rz}	Airspring reserv. damp., 20,000$(Ns)/m$
k_{sy}	Secondary lateral stiff., 100,000N/m
c_{sy}	Secondary lateral damp., 22,000Ns/m
k_{xp}	Secondary yaw stiff., 20,000N/m
c_{xp}	Secondary yaw damp., 20Ns/m
k_{vr}	Anti-roll bar stiff./bogie, 1,500,000$(Nm)/rad$
c_{vr}	Anti-roll bar damp./bogie, 18,200$(Ns)/m$
k_{pz}	Primary vertical stiff., 800,000N/m
c_{pz}	Primary vertical damp., 10,000$(Ns)/m$
k_{py}	Primary lateral stiff., 9,000,000N/m
c_{py}	Primary lateral damp., 10,000$(Ns)/m$
d_1	Airspring semi-spacing, 0.835m
d_2	Prim. vert. suspen. semi-spacing, 1.00m
h_1	2ndary later. suspen. height(body cog), 0.844m
h_2	2ndary later. suspen. height(bogie cog), 0.252m
h_3	Primary later. suspen. height(bogie cog), 0.194m
h_{g1}	Bogie cog height(rail level), 1.696m
h_{g2}	Body cog height(rail level), 0.60m
h_{mt}	Mechanism c.o.g. vertical separation from effective tilt centre, 0.60m
L_v	Semi bogie to bogie length, 9.5m
L	Full vehicle length, 19m
b	Bogie center to axle, 1.25m
I_r	Semi wheel to wheel spacing, 1.25m

E. Internal stability of feedback control systems

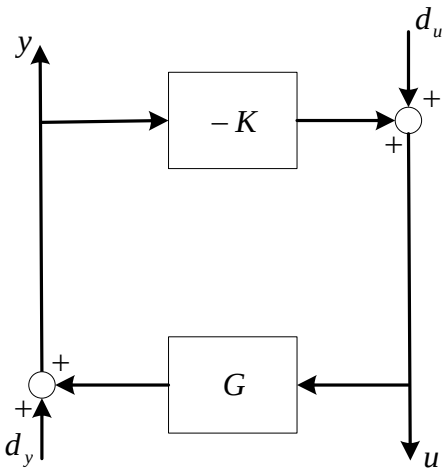

Figure E.1: Block diagram used to check internal stability of feedback system

The feedback system in Figure E.1 is internally stable if and only if all four closed-loop transfer matrices in equations below are stable.

$$u = (I + KG)^{-1}d_u - K(I + GK)^{-1}d_y$$
$$y = G(I + KG)^{-1}d_u + (I + GK)^{-1}d_y$$

where G is the system model, K is the controller, u is the system input, y is the measurement. d_u and d_y are the system inputs disturbance and measurement disturbance respectively.

The decentralised control in Section 4.2 has the controller K:

$$K = \begin{bmatrix} K_{tilting} & 0 & 0 \\ 0 & HP * s * cs & LP * 1/s * cs \end{bmatrix}$$

F. 9 DOF numerical model for integrated active ARB with active lateral secondary suspension

The full numerical equations for the 9 DOF railway vehicle integrating active ARB with active lateral secondary suspension are as follows:

Body lateral:

$$\begin{aligned} m_v\ddot{y}_v &= -4k_{sy}y_v - 4c_{sy}\dot{y}_v + 4k_{sy}h_1\theta_v + 4c_{sy}h_1\dot{\theta}_v + 2k_{sy}y_{bf} + 2c_{sy}\dot{y}_{bf} + 2k_{sy}h_2\theta_{bf} \\ &\quad +2c_{sy}h_2\dot{\theta}_{bf} + 2k_{sy}y_{br} + 2c_{sy}\dot{y}_{br} + 2k_{sy}h_2\theta_{br} + 2c_{sy}h_2\dot{\theta}_{br} \\ &\quad -\frac{m_v v^2}{R_c} + m_v g\theta_0 - h_{g1}m_v\ddot{\theta}_{0c} + F_{ar} + F_{af} \end{aligned}$$

Body roll:

$$\begin{aligned} i_{vr}\ddot{\theta}_v &= (4h_1k_{sy} + m_v g)y_v + 4h_1c_{sy}\dot{y}_v - (4h_1k_{sy} + 4{d_1}^2k_{az} + 4d_1k_{sz} - 2k_{vr})\theta_v \\ &\quad -4h_1c_{sy}\dot{\theta}_v - (2h_1k_{sy} + \frac{m_v g}{2})y_{bf} - 2h_1c_{sy}\dot{y}_{bf} - (2h_1h_2k_{sy} \\ &\quad -2{d_1}^2k_{az} + k_{vf})\theta_{bf} - 2h_1h_2c_{sy}\dot{\theta}_{bf} - (2h_1k_{sy} + \frac{m_v g}{2})y_{br} - 2h_1c_{sy}\dot{y}_{br} \\ &\quad -(2h_1h_2k_{sy} - 2{d_1}^2k_{az} + k_{vr})\theta_{br} - 2h_1h_2c_{sy}\dot{\theta}_{br} \\ &\quad +k_{vr}\delta_f + k_{vr}\delta_r - i_{vr}\ddot{\theta}_{0c} - F_{af}h_1 - F_{ar}h_1 \end{aligned}$$

Body yaw:

$$\begin{aligned} i_{vy}\ddot{\psi}_v &= -2L_vk_{sy}y_{bf} - 2L_vc_{sy}\dot{y}_{bf} - 2L_vh_2k_{sy}\theta_{bf} - 2L_vc_{sy}h_2\dot{\theta}_{bf} \\ &\quad +2L_vy_{br} + 2L_vc_{sy}\dot{y}_{br} + 2L_vh_2k_{sy}\theta_{br} + 2L_vc_{sy}h_2\dot{\theta}_{br} + k_{xt}\psi_{bf} \\ &\quad +k_{xt}\psi_{br} - 2k_{xt}\psi_v + c_{xt}\dot{\psi}_{bf} + c_{xt}\dot{\psi}_{br} - 2c_{xt}\dot{\psi}_v + i_{vy}\dot{\gamma}_c \\ &\quad +F_{af}L_v - F_{ar}L_v \end{aligned}$$

Front bogie lateral:

$$\begin{aligned} m_b\ddot{y}_{bf} &= 2k_{sy}y_v + 2c_{sy}\dot{y}_v - 2k_{sy}h_1\theta_v - 2c_{sy}h_1\dot{\theta}_v - 2k_{sy}L_v\psi_v \\ &\quad -2c_{sy}L_v\dot{\psi}_v - (2k_{sy} + 4k_{py})y_{bf} - (2c_{sy} - 2c_{py})\dot{y}_{bf} \\ &\quad -(2k_{sy}h_2 - 4k_{py}h_3)\theta_{bf} - (2c_{sy}h_2 - 4c_{py}h_3)\dot{\theta}_{bf} \\ &\quad +2k_{py}y_{yof1} + 2k_{py}y_{yof2} + 2c_{py}\dot{y}_{yof1} + 2c_{py}\dot{y}_{yof2} \\ &\quad -\frac{m_b v^2}{R_f} + m_b g\theta_{of} + m_b h_{g2}\ddot{\theta}_{of} + F_{af} \end{aligned}$$

Front bogie roll:

$$\begin{aligned} i_{vr}\ddot{\theta}_{bf} &= 2h_2k_{sy}y_v + 2h_2c_{sy}\dot{y}_v - (2h_1h_2k_{sy} - k_{vr} - 2k_{az}{d_1}^2 - 2k_{sz}{d_1}^2)\theta_v \\ &\quad -2h_1h_2c_{sy}\dot{\theta}_v - 2h_2k_{sy}L_v\psi_v - 2h_2c_{sy}L_v\dot{\psi}_v - (2h_2k_{sy} + 4h_3k_{py})y_{bf} \\ &\quad -(2h_2c_{sy} + 4h_3c_{py})\dot{y}_{bf} - (2{h_2}^2k_{sy} - 4{h_3}^2k_{py} + 2{d_2}^2k_{pz} \\ &\quad +2{d_1}^2k_{az} + k_{vr})\theta_{bf} - (2{h_2}^2c_{sy} - 4{h_3}^2c_{py} - 2{d_2}^2c_{pz})\dot{\theta}_{bf} \\ &\quad +k_{vr}\delta_f + 2k_{sz}{d_1}^2\theta_{rf} - i_{bf}\ddot{\theta}_{of} - F_{af}h_2 \end{aligned}$$

Front bogie yaw:

$$\begin{aligned} i_{by}\ddot{\psi}_{bf} &= -(4b^2k_{py} + k_{xt})\psi_{bf} - (4b^2c_{py} + c_{xt})\dot{\psi}_{bf} - 2bk_{py}y_{of1} - 2bc_{py}\dot{y}_{of1} \\ &\quad +2bk_{py}y_{of2} - 2bc_{py}\dot{y}_{of2} - i_{by}\dot{\gamma}_f \end{aligned}$$

Rear bogie lateral:

$$\begin{aligned} m_b\ddot{y}_{br} &= 2k_{sy}y_v + 2c_{sy}\dot{y}_v - 2k_{sy}h_1\theta_v - 2c_{sy}h_1\dot{\theta}_v + 2k_{sy}L_v\psi_v \\ &\quad +2c_{sy}L_v\dot{\psi}_v - (2k_{sy} + 4k_{py})y_{br} - (2c_{sy} - 2c_{py})\dot{y}_{br} \\ &\quad -(2k_{sy}h_2 - 4k_{py}h_3)\theta_{br} - (2c_{sy}h_2 - 4c_{py}h_3)\dot{\theta}_{br} \\ &\quad +2k_{py}y_{yor1} + 2k_{py}y_{yor2} + 2c_{py}\dot{y}_{yor1} + 2c_{py}\dot{y}_{yor2} \\ &\quad -\frac{m_bv^2}{R_f} + m_bg\theta_{or} + m_bh_{g2}\ddot{\theta}_{or} + F_{ar} \end{aligned}$$

Rear bogie roll:

$$\begin{aligned} i_{vr}\ddot{\theta}_{br} &= 2h_2k_{sy}y_v + 2h_2c_{sy}\dot{y}_v - (2h_1h_2k_{sy} - k_{vr} - 2k_{az}{d_1}^2 - 2k_{sz}{d_1}^2)\theta_v \\ &\quad -2h_1h_2c_{sy}\dot{\theta}_v + 2h_2k_{sy}L_v\psi_v + 2h_2c_{sy}L_v\dot{\psi}_v - (2h_2k_{sy} + 4h_3k_{py})y_{br} \\ &\quad -(2h_2c_{sy} + 4h_3c_{py})\dot{y}_{br} - 2{h_2}^2k_{sy} - 4{h_3}^2k_{py} + 2{d_2}^2k_{pz} \\ &\quad +2{d_1}^2k_{az} + k_{vr})\theta_{br} - (2{h_2}^2c_{sy} - 4{h_3}^2c_{py} - 2{d_2}^2c_{pz})\dot{\theta}_{br} \\ &\quad +k_{vr}\delta_f + 2k_{sz}{d_1}^2\theta_{rr} - i_{bf}\ddot{\theta}_{or} - F_{ar}h_2 \end{aligned}$$

Rear bogie yaw:

$$\begin{aligned} i_{by}\ddot{\psi}_{br} &= -(4b^2k_{py} + k_{xt})\psi_{br} - (4b^2c_{py} + c_{xt})\dot{\psi}_{br} - 2bk_{py}y_{of1} - 2bc_{py}\dot{y}_{or1} \\ &\quad +2bk_{py}y_{or2} - 2bc_{py}\dot{y}_{of2} - i_{by}\dot{\gamma}_r \end{aligned}$$

G. Embedded MATLAB code for Kalman filter

%Kalman filter for the state estimation in LQG control for 4 DOF integrated active ARB with active lateral secondary suspension

function [x_esti,Pout] = KalEstimator(Ad, Bd, Cd, Dd, u, y, x, P, R, Q) %eml

% To declear the size of the inputs

assert(all(size(Ad) == [12 12]));

assert(all(size(Bd) == [12 2]));

assert(all(size(Cd) == [3 12]));

assert(all(size(Dd) == [3 2]));

assert(all(size(u) == [2 1]));

assert(all(size(y) == [3 1]));

assert(all(size(R) == [3 3]));

assert(all(size(Q) == [12 12]));

assert(all(size(x) == [12 1]));

assert(all(size(P) == [12 12]));

% Prediction for state vector and covariance:

x = Ad*x + Bd(:,1:2)*u;

P = Ad*P*Ad'+ Q;

% Compute Kalman gain factor:

K = P*Cd'*inv(Cd*P*Cd'+R);

% Correction based on observation:

x = x + K*(y-Cd*x-Dd(:,1:2)*u);

P = P - K*Cd*P;

% Function outputs

x_esti = x;

Pout = P;

%***

%This function can be converted to C code via the MATLAB command:

$$emlc\ KalEstimator\ -c\ -T\ RTW$$

%***

H. C code for the tilt and lateral actuator control in FPGA

```
****************************************************************
/*Appromate PID tilting control*/
float TiltController(float eml_e)
{
    //Canonic delta operator
    v0 = (eml_e - 1.851851*v1 + 0*v2);
    TiltComd = (1.107482*v0 + 0.439336*v1 + 0.074458*v2);

    v2 = v2 + v1;
    v1 = v1 + v0;

    return TiltComd;
}
****************************************************************
/* Complimentary filters with Centering control */
float LateralController(float eml_uai, float eml_udi)
{
    //Canonic delta operator
    wh0 = eml_uai - 0.0721930*wh1 - 0.0025174*wh2;
    eml_Hpout = 0.0120567*wh0 + 0.0241133*wh1 + 0*wh2;
    wh2 = wh2 + wh1;
    wh1 = wh1 + wh0;

    wl0 = eml_udi - 0.0721930*wl1 - 0.0025174*wl2;
    eml_Lpout = 2.8373730*wl0 + 0.1006946*wl1 + 0*wl2;
    wl2 = wl2 + wl1;
    wl1 = wl1 + wl0;

    wd0 = eml_udi - 0.0000222*wd1 - 0.00000000025 * wd2;
```

```
    eml_DIpout = 0.0369*wd0 + 0.0738*wd1 + 0* wd2;
    wd2 = wd2 + wd1;
    wd1 = wd1 + wd0;

    eml_SKYout = eml_Hpout + eml_Lpout + eml_DIpout;
    return eml_SKYout;
}
*****************************************************************
/*Yaw cotrol*/
float YawController(float yaw_i)
{
    float yawcontrol = 0;

    yaw0 = (yaw_i - 0.022210*yaw1 - 0.000244*yaw2);
    yawcontrol = (0.117439 *yaw0 + 0.234877*yaw1 + 0*yaw2);
    yaw2 = yaw2 + yaw1;
    yaw1 = yaw1 + yaw0 ;

    return yawcontrol;
}
```